INSTITUTE OF PHYSICS PUBLISHING REPORTS ON PROGRESS IN PHYSICS

Rep. Prog. Phys. **68** (2005) 449–521 doi:10.1088/0034-4885/68/2/R06

Physics of negative refractive index materials

S Anantha Ramakrishna

Department of Physics, Indian Institute of Technology, Kanpur 208 016, India

E-mail: sar@iitk.ac.in

Received 3 September 2004
Published 18 January 2005
Online at stacks.iop.org/RoPP/68/449

Abstract

In the past few years, new developments in structured electromagnetic materials have given rise to negative refractive index materials which have both negative dielectric permittivity and negative magnetic permeability in some frequency ranges. The idea of a negative refractive index opens up new conceptual frontiers in photonics. One much-debated example is the concept of a *perfect lens* that enables imaging with sub-wavelength image resolution. Here we review the fundamental concepts and ideas of negative refractive index materials.

First we present the ideas of structured materials or *meta-materials* that enable the design of new materials with a negative dielectric permittivity, negative magnetic permeability and negative refractive index. We discuss how a variety of resonance phenomena can be utilized to obtain these materials in various frequency ranges over the electromagnetic spectrum. The choice of the wave-vector in negative refractive index materials and the issues of dispersion, causality and energy transport are analysed. Various issues of wave propagation including nonlinear effects and surface modes in negative refractive materials (NRMs) are discussed. In the latter part of the review, we discuss the concept of a perfect lens consisting of a slab of a NRM. This perfect lens can image the far-field radiative components as well as the near-field evanescent components, and is *not* subject to the traditional diffraction limit. Different aspects of this lens such as the surface modes acting as the mechanism for the imaging of the evanescent waves, the limitations imposed by dissipation and dispersion in the negative refractive media, the generalization of this lens to *optically complementary media* and the possibility of magnification of the near-field images are discussed. Recent experimental developments verifying these ideas are briefly covered.

(Some figures in this article are in colour only in the electronic version)

 © 2005 IOP Publishing Ltd Printed in the UK

Contents

1. Introduction

In optics, the refractive index of a material is conventionally taken to be a measure of the 'optical density' and is defined as

$$n = \frac{c}{v}, \tag{1.1}$$

where c is the speed of light in vacuum and v is the speed of an electromagnetic plane wave in the medium. From Maxwell's equations the refractive index is given by the Maxwell relation,

$$n^2 = \varepsilon\mu, \tag{1.2}$$

where ε is the relative dielectric permittivity and μ is the relative magnetic permeability of the medium. Usual optical materials have a positive ε and μ, and n could easily be taken as $\sqrt{\varepsilon\mu}$ without any problems. Although it was realized that the refractive index would have to be a complex quantity to account for absorption and even a tensor to describe anisotropic materials, the question of the sign of the refractive index did not arise. In 1967, Veselago [1] first considered the case of a medium that had both negative dielectric permittivity and negative magnetic permeability at a given frequency and concluded that the medium should then be considered to have a negative refractive index (i.e. the negative square root, $n = -\sqrt{\varepsilon\mu}$, had to be chosen). Although Veselago went on to point out several interesting effects in NRMs, such as a modified Snell's law of refraction, a reversed Doppler shift and an obtuse angle for Cerenkov radiation, in such media, his result remained an academic curiosity for a long time as real materials with simultaneously negative ε and μ were not available. However, in the last few years, theoretical proposals [2, 3] for structured photonic media whose ε and μ could become negative in certain frequency ranges were developed experimentally [4, 5], and this has brought Veselago's result into the limelight. The striking demonstration by Pendry [6] that NRMs can be used to make perfect lenses with resolution capabilities not limited by the conventional diffraction limit has given an enormous boost to the interest in NRMs. This field has become a hot topic of scientific research and debate over the past four years.

1.1. Objectives

The physics of NRMs can be extremely counter-intuitive. 'Standard' notions and intuitions of electromagnetic theory can be misleading, and unexpected situations arise with NRMs. This has mostly (for example the problems of the perfect lens) been responsible for the initial severe criticism and debate [7–9] as well as the later explosion of research in this area. It is imperative now to develop new intuitions and understanding to deal with these materials. Although many of the developments are only recent, the basic conceptual issues have now been widely debated and reasonably clarified. At the time of writing the theoretical foundations have been laid and several experiments verifying the concepts have been performed, placing the field on a sound footing. Thus it appears to be the correct moment to review the conceptual issues of negative refractive index materials.

Shorter reviews have been published elsewhere [10–12] which cover certain aspects of the topic, or are at a semi-popular level [13, 14]. Thus this will not be the first review nor do we expect it to be the last, given the rapid developments in this field. But the hope is that it will serve as a good reference point for the conceptual ideas involving negative refractive index materials and the problem of the perfect lens, and as a good starting point for a newcomer to get into this area of research. Given the exponentially rising number of publications, it will not be possible to review or cite all of them. We will only concentrate here on the main developments.

1.2. Basic concepts and definitions

The dielectric constant (ε) and the magnetic permeability (μ) characterize the macroscopic response of a homogeneous medium to applied electric and magnetic fields. These are macroscopic parameters because one usually only seeks time-averaged and spatially-averaged responses averaged over sufficiently long times and sufficiently large spatial volumes. All that survive the averaging in macroscopic measurements are the frequency components of the individual (atomic or molecular) oscillators driven by the external fields. This idea can now be extended to a higher class of inhomogeneous materials where the inhomogeneities are on length-scales much smaller than a wavelength of the radiation but can be large compared with atomic or molecular length-scales. The radiation then does not resolve these individual meso-structures, but responds to the (atomically) macroscopic resonances of the structure. Such materials have been termed meta-materials [13, 15] and can be characterized by macroscopic parameters such as ε and μ that define their response to applied electromagnetic fields, much like homogeneous materials. Meta-materials, in some sense, can be strictly distinguished from other structured photonic materials, i.e. photonic crystals or photonic band-gap materials [16, 17]. In the photonic crystals or band-gap materials the stops bands or band-gaps arise as a result of multiple Bragg scattering in a periodic array of dielectric scatterers. In fact, the periodicity of the structure here is of the order of the wavelength, and hence homogenization in this sense cannot be carried out. In meta-materials the periodicity is by comparison far less important and all the properties mainly depend on the single scatterer resonances.

All causal materials are dispersive, i.e. the dielectric permittivity and the magnetic permeability are, in general, complex functions of the frequency. This is because the polarizations in such media do not respond instantaneously to the applied fields but depend on the history of the applied fields. This becomes particularly visible when the applied fields have frequencies close to a resonant frequency of the material oscillators. In fact, the real parts and the imaginary parts of the material parameters ($\varepsilon(\omega)$ and $\mu(\omega)$) are related to each other by the famous Kramers–Kronig relations [18]. Noting that the imaginary parts of ε and μ relate directly to the absorption of electromagnetic radiation in the material, we realize that dispersion and dissipation in thermodynamic media always accompany each other. As with any resonance, the response follows the applied field at frequencies below the resonance, and above the resonance the response is anti-phased with respect to the applied field. If now the resonance can be made sharp enough, it will be possible to drive the real parts of the effective ε or μ negative. This under-damped, over-screened response is responsible for the negative material parameters. There is no fundamental objection to the real parts of the ε and μ being negative [19]. In media at thermodynamic equilibrium, there is, however, a restriction that the imaginary parts of the corresponding ε or μ are not to be negative. This is so that the total absorbed energy in a volume V of the medium,

$$\int_V \mathrm{d}^3 r \int_{-\infty}^{\infty} \omega[\mathrm{Im}(\varepsilon(\omega))|\vec{E}(\vec{r},\omega)|^2 + \mathrm{Im}(\mu(\omega))|\vec{H}(\vec{r},\omega)|^2]\frac{\mathrm{d}\omega}{2\pi}, \tag{1.3}$$

is positive definite [19]. Thus, media with negative ε and μ are causal, but necessarily dispersive and dissipative.

Although most materials exhibiting a good electric response can be found at almost any frequency from radio-frequencies to the ultraviolet frequencies, the magnetic response of most materials is limited to low microwave frequencies. Magnetic polarization usually results from either unpaired electron spins or orbital electron currents, and the collective excitations of these usually tend to occur at low frequencies. Some ferromagnetic, ferrimagnetic and antiferromagnetic materials exhibit some magnetic activity at even frequencies of hundreds of gigahertz [20]. But these are rare and usually have narrow bandwidths. But now the possibility

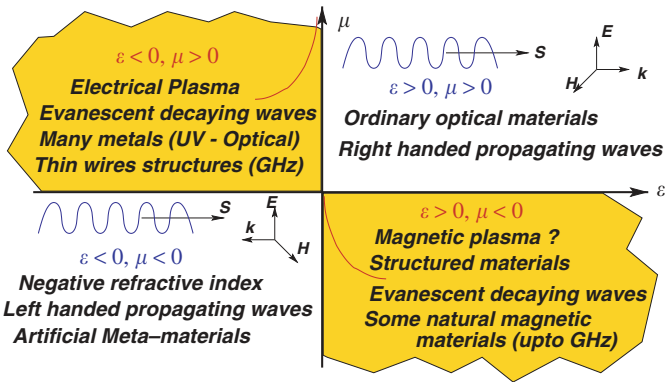

Figure 1. A schematic showing the classification of materials based on the dielectric and magnetic properties. The wavy lines represent materials that allow propagating waves, and the axes set in quadrants 1 and 3 show the right- and left-handed nature of $\boldsymbol{E}$, $\boldsymbol{H}$ and $\boldsymbol{k}$ vectors. The waves in quadrants 2 and 4 decay evanescently inside the materials, which is depicted schematically. $\boldsymbol{S}$ is the Poynting vector.

of artificially structuring materials at micro- and nano-scales can enable us to generate a variety of meta-materials with magnetic activity at almost any frequency we wish—from a few hertz [21] to near-infrared frequencies [22] including the radio frequencies [3, 23, 24], the microwave frequencies [3, 4, 25] and the terahertz frequencies [27, 28] in between. Thus even magnetic activity, let alone negative magnetic permeability, is special at high frequencies.

Consider the Maxwell's equation for a plane harmonic wave $\exp[\mathrm{i}(\boldsymbol{k}\cdot\boldsymbol{r}-\omega t)]$:

$$\boldsymbol{k}\times\boldsymbol{E}=\omega\mu_0\mu\boldsymbol{H}, \tag{1.4}$$

$$\boldsymbol{k}\times\boldsymbol{H}=-\omega\varepsilon_0\varepsilon\boldsymbol{E}, \tag{1.5}$$

where $\boldsymbol{E}$ and $\boldsymbol{H}$ are the electric and magnetic fields. If we take a medium with negative real parts of ε and μ with the imaginary parts being small (negligibly small for the time being) at some frequency (ω), then we realize that the vectors $\boldsymbol{E}$, $\boldsymbol{H}$ and $\boldsymbol{k}$ will now form a left-handed triad. It is for this reason that such materials are also popularly termed *left-handed materials*, although this does risk a confusion with the terminology of chiral optical materials. Using the definition that the wave-vector $\boldsymbol{k}=n\omega/c\hat{n}$, where $\hat{n}$ is the unit vector along $\boldsymbol{E}\times\boldsymbol{H}$, it appears that the refractive index in such media with $\mathrm{Re}(\varepsilon)<0$ and $\mathrm{Re}(\mu)<0$ is also negative. Such materials permit propagating waves with a reversed phase vector ($\boldsymbol{k}$)[1] compared with media with only one of $\mathrm{Re}(\varepsilon)$ or $\mathrm{Re}(\mu)$ negative which do not allow any propagating modes (all waves decay evanescently in such media from the point of injection as $k^2<0$). Note that in the case of the NRMs, the Poynting vector ($\boldsymbol{S}=\boldsymbol{E}\times\boldsymbol{H}$) and the phase vector, $\boldsymbol{k}$, are anti-parallel. In figure 1, we show the four quadrants in the $\mathrm{Re}(\varepsilon)$–$\mathrm{Re}(\mu)$ plane into which we can conveniently classify electromagnetic materials. The behaviour of the waves in each of the quadrants is qualitatively different: materials that fall in the first quadrant allow the usual right-handed electromagnetic propagating waves, the materials that fall in the second and fourth quadrants do not allow any propagating waves inside them (all electromagnetic radiation is evanescently damped in these media) and the NRMs that fall in the third quadrant allow left-handed propagating waves inside them. This follows from the dispersion for the wave-vector

$$\boldsymbol{k}\cdot\boldsymbol{k}=\varepsilon\mu\frac{\omega^2}{c^2}. \tag{1.6}$$

[1] This has prompted some authors to call these *backward wave media* [29] or *negative phase velocity media* [10]. Some authors have preferred to term such media *double negative media*, referring to the negative ε and μ [30].

Making $\mathrm{Re}(\varepsilon)$ or $\mathrm{Re}(\mu)$ negative not only makes electromagnetic radiation decay exponentially inside them, but also renders the materials rather very special. For example, we know that metals whose dielectric permittivity is dominated by the plasma-like response of the free electron gas,

$$\varepsilon(\omega) = 1 - \frac{\omega_{\mathrm{p}}^2}{\omega(\omega + \mathrm{i}\gamma)}, \tag{1.7}$$

where ω_{p} is the bulk plasma frequency and γ is the damping constant, have negative dielectric permittivity at UV–optical frequencies. These materials can support a host of resonant states localized at their surfaces, known as the surface plasmons [31, 32]. These surface plasmons can resonantly interact with radiation on structured surfaces, giving rise to a wide variety of novel optical phenomena [33] and have given rise to the new field of plasmonics [34]. This is a generic effect of having a negative dielectric permittivity, and materials with negative magnetic permeability can also be expected to support the analogous surface plasmons of a magnetic nature!

These resonant states can affect the propagation of the electromagnetic radiation in a very profound manner and are deeply involved in the mechanism of the perfect lens [6] made of an NRM. Such a lens is not limited in its resolution to super-wavelength length-scales according to the standard principles of diffraction theory [35]. In fact this has been one of the most fundamental new effects associated with NRMs thus far and has been a topic of intense debate [8, 30] and much activity. This issue will be treated in detail in the latter sections of this review.

We will now proceed to examine all these concepts in detail. The review can be broadly split into two parts: sections 2 and 3, dealing with the general properties of negative refractive index media, and sections 4 and 5, dealing with the specific problem of the perfect lens that can be formed from negative refractive index media. The experimental efforts in this area are covered in section 6.

2. Materials with negative refractive index

There is nothing fundamentally objectionable about negative material parameters such as the dielectric permittivity and the magnetic permeability. But finding a material that has these properties is a more difficult task and it was because of the lack of a material that exhibited negative values of these parameters at a common frequency band that Veselago's early result did not arouse much interest for a long time. Pendry's seminal work on structured materials which display negative dielectric permittivity [2, 43] and magnetic permeability [3], along with the technological capability to make structures at microscopic length-scales, has made it possible and interesting to create experimentally such materials at a variety of wavelengths. All the NRMs that have been developed today are obtained by putting together two structured materials that show separately a negative dielectric permittivity and negative magnetic permeability. Although it is not immediately obvious, the resulting composite structure possesses a negative refractive index. In this section, we will first separately discuss the negative dielectric materials and the negative magnetic materials before we discuss the composite that behaves as an NRM. We will then address the issues of homogenization and causality that confront us in the context of such materials. In general, we will strictly not consider photonic band-gap materials, which can display some of the effects of negative refraction [36] at wavelengths which are of the same order of the length-scales of the structures in the meta-materials, as negative refractive index materials. There are significant problems of homogenization that are involved here.

2.1. Negative dielectric materials

2.1.1. Metals and plasmons at optical frequencies. At optical frequencies many metals have a negative dielectric permittivity when the conduction electrons in the metals can be assumed to be reasonably free in a background of static positive ion cores, the overall system being charge neutral. It is this plasma-like behaviour that is responsible for a negative dielectric permittivity at frequencies less than the plasma frequency. Consider the equation of motion for an electron in an applied time harmonic electromagnetic field with angular frequency ω_0,

$$m\ddot{\boldsymbol{r}} + m\gamma\dot{\boldsymbol{r}} = -e\boldsymbol{E}\exp(-\mathrm{i}\omega_0 t), \tag{2.1}$$

where m is the mass of the electron and $m\gamma$ is a phenomenogical damping (viscous) force on the electron due to all inelastic processes. It is assumed that the wavelength of light is large compared with the distance travelled by the electron, so that it effectively sees a spatially constant field and the velocities involved are sufficiently low so that the magnetic field can be neglected. This yields a polarization per volume in the medium of

$$\boldsymbol{P} = (\varepsilon - 1)\varepsilon_0\boldsymbol{E} = -ne\boldsymbol{r} = -\frac{ne^2/m\boldsymbol{E}}{\omega(\omega + \mathrm{i}\gamma)}, \tag{2.2}$$

where n is the number density of the conduction electrons and each electron is assumed to contribute independently to the polarization. From this we obtain the relative dielectric constant of equation (1.7), where $\omega_\mathrm{p} = ne^2/\varepsilon_0 m$ is the plasma frequency. The dielectric permittivity is negative up to ω_p and the plasma shields the interior from electromagnetic radiation. Above ω_p the medium behaves as an ordinary positive dielectric. This is the theory of Drude and Lorentz for the dispersion characteristics of a plasma [18, 35]. Substituting the expression for the dielectric constant into Maxwell's equation, we obtain the dispersion for light in a metal:

$$k^2c^2 + \omega_\mathrm{p}^2 = \omega^2. \tag{2.3}$$

Thus, the waves below the plasma frequency correspond to the negative energy solutions, and above the plasma frequency, it appears as if the transverse modes of light had a finite rest mass of $m_0 = \hbar\omega_\mathrm{p}/c^2$.

The plasma frequency also has a physical manifestation as a collective excitation of the electron gas. If the electron gas is displaced by a small distance in a finite metal, the excess negative (electronic) charge and the positive (background) charge that accumulate at the edges provide a restoring force proportional to the displacement and cause the entire electron gas to oscillate at frequency ω_p [37]. Hence ω_p is known as the plasmon frequency. This is the dispersionless plasmon mode that occurs at $\omega = \omega_\mathrm{p}$.

As mentioned before, rendering the dielectric constant negative makes it possible for the surface to support resonances called the surface plasmons [32]. Consider the interface ($z = 0$ plane) between a metal with a dielectric constant ε_- and a positive dielectric medium (vacuum) with dielectric permittivity ε_+ (=+1) as shown in figure 2. Now the fields for a p-polarized light are

$$\boldsymbol{E} = \boldsymbol{E}_0\exp[\mathrm{i}(k_x x + k_y y - \omega t) - \kappa_{z+}z] \qquad \forall z > 0, \tag{2.4}$$

$$\boldsymbol{E} = \boldsymbol{E}_0\exp[\mathrm{i}(k_x x + k_y y - \omega t) + \kappa_{z-}z] \qquad \forall z < 0, \tag{2.5}$$

where $k_x^2 + k_y^2 - \kappa_{z\pm}^2 = \varepsilon_\pm\mu\omega^2/c^2$ are good solutions to the Maxwell equations when

$$\frac{\kappa_{z+}}{\varepsilon_+} + \frac{\kappa_{z-}}{\varepsilon_-} = 0. \tag{2.6}$$

These are collective excitations of electrons with the charges displaced parallel to the (real part of the) wave-vector. Thus we have a mode with longitudinal components whose fields

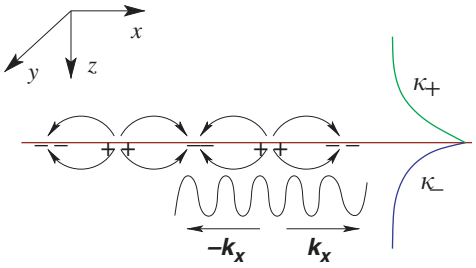

Figure 2. A schematic showing the surface plasmon on an interface between a negative and a positive dielectric media and the associated charge density fluctuations. The exponential decay of the fields normal to the surface and the propagating nature along the surface are depicted schematically.

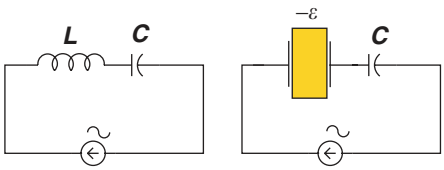

Figure 3. A capacitor and an inductor form a resonant circuit that can oscillate at $\omega_0 = 1/\sqrt{LC}$. A capacitor filled with a negative dielectric has negative capacitance, acts as an inductor and can resonate with another usual capacitor.

decay exponentially into the metal and the dielectric on either side of the interface. This charge density wave thus lives on the surface of the metal and is called a *surface plasmon*. Equation (2.6) yields the dispersion

$$k_x = \frac{\omega}{c}\left[\frac{\varepsilon_+\varepsilon_-}{\varepsilon_+ + \varepsilon_-}\right]^{1/2}. \tag{2.7}$$

For a metal with $\varepsilon_-(\omega)$ given by equation (1.7) and setting $\varepsilon_+ = 1$ for vacuum, we note that $k_x > \omega/c$ for the surface plasmon (see figure 22). Thus it will not be possible to excite the surface plasmon on a perfectly flat surface using propagating modes of light, and a coupling mechanism will have to be provided by mechanisms such as the surface roughness, a grating structure or a dielectric coupler to vacuum such as a hemisphere or a prism. Complicated surface structures can generate a variety of surface plasmon dispersions, and this has given rise to new optical phenomena such as the extraordinary transmission of light through sub-wavelength sized holes [38]. Next note that for reasonably large wave-vectors the surface plasmons are nearly degenerate with a frequency of $\omega_p/\sqrt{2}$. This is the reason why the interaction of the radiation with the resonant surface plasmons is very rich and difficult to model: the radiation couples with the metal surface at all length-scales. This remains true down to a nanometre or so when non-local dispersive effects kick in due to inadequate electronic screening inside the metal.

The negative dielectric constant is central to the nature of resonant interactions of structured metal surfaces with radiation. Pendry [33] provides a very insightful explanation for this. We know that a capacitor can be formed by two parallel conducting plates with an insulating dielectric placed in between. Filling up the gap with a negative dielectric material instead would now lead to a capacitor with negative capacitance, which is the same as being an inductor. Thus two capacitors in a circuit, one filled with a positive dielectric and the other filled with a negative dielectric material, can become resonant (see figure 3). It is as if in a structured

metallic structure the metal pieces form the capacitors filled by the negative dielectric material and the holes in between form the capacitors filled with the positive dielectric material. The resulting system is a very complicated circuit with many L–C resonances.

For many metals, the plasma frequency is at ultraviolet frequencies and γ is small compared with ω_p (see [32]). Thus we have many examples of materials with a negative dielectric constant at optical frequencies. However, the dissipation in most metals is large, and we have trouble when we try to extend this behaviour to lower frequencies where $\omega \sim \gamma$. Then it can hardly be claimed that the dielectric constant is an almost real and negative number. The dissipation dominates all phenomena and we no longer have the behaviour of a good plasma.

It must be pointed out that negative dielectric permittivity can also be obtained in more ordinary dielectric media with bound charges, within a frequency band above a resonance frequency. Consider a medium in which the electrons are bound to positive nuclei and its response to an applied electromagnetic field. For small displacements of the electrons there is a restoring force on the electron, $-m\omega_0^2\boldsymbol{r}$. Including this term in equation (2.1), one obtains the resonant Lorentz dielectric permittivity,

$$\varepsilon = 1 + \frac{ne^2/(\varepsilon_0 m)}{\omega_0^2 - \omega^2 - \mathrm{i}\gamma\omega}, \tag{2.8}$$

where n is now the total density of bound electrons (here it is assumed simplistically that all the electrons are bound with the same strength). Setting $\omega_0 = 0$, we immediately obtain the Drude form for ε for a good plasma. Note now that the dielectric constant can be negative in a small frequency range above ω_0 if the resonance is sharp enough. In fact, one can make use of resonant effects such as electromagnetically induced transparency or similar effects based on atomic coherences [39, 40] to drive the dielectric constant negative over selected small frequency ranges.

2.1.2. Wire-mesh structures as low frequency negative dielectrics. Metal-dielectric composites have long been studied for their rich electrodynamic response (see [41] and references therein). For example, composites of randomly oriented long conducting fibres have been known to exhibit very high values of permittivity even at low concentrations [42]. Effective medium theories have been developed to describe these systems when the wavelength of the incident radiation is much larger than the intrinsic length-scales of the structure. However, the radiation usually only probes the end surfaces of the metallic structures, and it is hard to make it penetrate well into the bulk of the structure for the appearance of a three-dimensional effective medium to hold true in many cases. Pendry *et al* [2,43] and Sievenpiper *et al* [44] independently demonstrated that metallic wire-mesh structures have a low frequency stop band from zero frequency up to a cutoff frequency which they attributed to the motion of electrons in the metal wires. The meta-material of Pendry *et al*, consisting of very thin wires, is structured on truly sub-wavelength length-scales and can be effectively homogenized, while it is not clear that this holds for the structure of Sievenpiper. The low frequency stop band can be attributed to an effective negative dielectric permittivity and provides us with a way of obtaining negative dielectrics at even microwave frequencies. The idea is to obtain negative permittivity materials at low frequencies by literally doping the vacuum with metal.

Consider an array of infinitely long, parallel and very thin metallic wires of radius r placed periodically at a distance a in a square lattice with $a \gg r$ as shown in figure 4. The electric field is considered to be applied parallel to the wires (along the Z axis) and we will work in the quasi-static limit when the wavelength of the radiation $\lambda \gg a \gg r$. The electrons are confined to move within the wires only, which has the first effect of reducing the effective electron density as the radiation cannot sense the individual wire structure but only the average

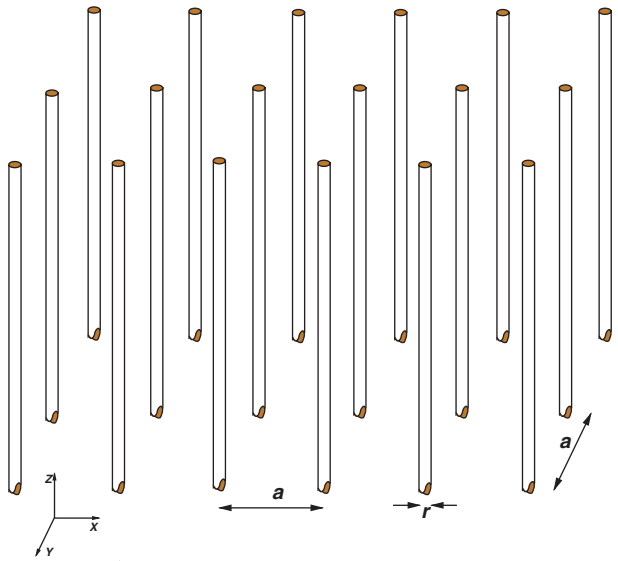

Figure 4. An array of infinitely long thin metal wires of radius r and a lattice period of a behaves as a low frequency plasma for the electric field oriented along the wires.

charge density. The effective electron density is immediately seen to be

$$n_{\text{eff}} = \frac{\pi r^2}{a^2} n, \tag{2.9}$$

where n is the actual density of conduction electrons in the metal.

There is a second equally important effect to be considered. The thin wires have a large inductance, and it is not easy to change the currents flowing in these wires. Thus, it appears as if the charge carriers, namely the electrons, have acquired a tremendously large mass. To see this, consider the magnetic field at a distance ρ from a wire. On an average we can assume a uniform $\boldsymbol{D}$ field within the unit cell. But the current density is not uniform, leading to a non-zero non-uniform magnetic field that is large close to the wires which contributes to most of the flux. By symmetry there is a point of zero field in between the wires and hence we can estimate the magnetic field along the line between two wires as

$$\boldsymbol{H}(\rho) = \frac{\hat{\phi} I}{2\pi} \left(\frac{1}{\rho} - \frac{1}{a - \rho} \right). \tag{2.10}$$

The vector potential associated with the field of a single infinitely long current-carrying conductor is non-unique unless the boundary conditions are specified at definite points. In our case, we have a periodic medium that sets a critical length of $a/2$. We can assume that the vector potential associated with a single wire is

$$\boldsymbol{A}(\rho) = \frac{\hat{z} I}{2\pi} \ln \left[\frac{a^2}{4\rho(a - \rho)} \right] \qquad \forall \rho < \frac{a}{2}, \tag{2.11}$$

$$= 0 \qquad \forall \rho > \frac{a}{2}. \tag{2.12}$$

This choice avoids the vector potential of one wire overlapping with another wire and thus the mutual induction between the adjacent wires is addressed to some extent. Noting that $r \ll a$

by about three orders of magnitude in our model and that the current $I = \pi r^2 nev$, where v is the mean electron velocity, we can write the vector potential as

$$\boldsymbol{A}(\rho) = \frac{\mu_0 \pi r^2 nev}{2\pi} \ln\left(\frac{a}{\rho}\right)\hat{z}. \tag{2.13}$$

This is a very good approximation in the mean field limit. We have considered only two wires, and the lattice actually has four-fold symmetry. The actual deviations from this expression are much smaller than in our case. We note that the canonical momentum of an electron in an electromagnetic field is $\boldsymbol{p} + e\boldsymbol{A}$. Thus assuming that the electrons flow on the surface of the wire (assuming a perfect conductor), we can associate a momentum per unit length of the wire of

$$\boldsymbol{p} = \pi r^2 ne\boldsymbol{A}(r) = \frac{\mu_0 \pi^2 r^4 n^2 e^2 v}{2\pi} \ln\left(\frac{a}{r}\right) = m_{\text{eff}} \pi r^2 nv \tag{2.14}$$

and thus an effective mass of

$$m_{\text{eff}} = \frac{\mu_0 \pi r^2 ne^2}{2\pi} \ln\left(\frac{a}{r}\right), \tag{2.15}$$

for the electron.

Thus, assuming a longitudinal plasmonic mode for the system, we have

$$\omega_{\text{p}} = \frac{n_{\text{eff}} e^2}{\varepsilon_0 m_{\text{eff}}} = \frac{2\pi c^2}{a^2 \ln(a/r)} \tag{2.16}$$

for the plasmon frequency. We note that a reduced effective electron density and a tremendously increased effective electronic mass would immediately reduce the plasmon frequency for this system. Typically one can choose $r = 1\,\mu$m, $a = 10$ mm and aluminium wires ($n = 10^{29}\,\text{m}^{-3}$), which gives an effective mass of

$$m_{\text{eff}} = 2.67 \times 10^{-26}\,\text{kg}, \tag{2.17}$$

that is almost 15 times that of a proton, and a plasma frequency of about 2 GHz! Thus, we have succeeded in obtaining a negative dielectric material at microwave frequencies.

Note that the final expression for the plasma frequency in equation (2.16) is independent of the microscopic quantities such as the electron density and the mean drift velocity. It only depends on the radius of the wires and the spacing, suggesting that the entire problem can be recast in terms of the capacitances and inductances of the problem. This approach has been taken [45, 46] and we present it below for the sake of completeness. Consider the current induced by the electric field along the wires, related by the total inductance (self and mutual) per unit length (L):

$$E_z = +\text{i}\omega LI = \text{i}\omega L\pi r^2 nev, \tag{2.18}$$

noting that the polarization per unit volume in the homogenized medium is

$$P = -n_{\text{eff}} er = \frac{n_{\text{eff}} ev}{\text{i}\omega} = -\frac{E_z}{\omega^2 a^2 L}, \tag{2.19}$$

where $n_{\text{eff}} = \pi r^2 n/a^2$ as before. We can estimate the inductance, L, by calculating the magnetic flux per unit length passing through a plane between the wire and the point of symmetry between itself and the next wire where the field is zero:

$$\phi = \mu_0 \int_r^{a/2} H(\rho)\,\text{d}\rho = \frac{\mu_0 I}{2\pi} \ln\left[\frac{a^2}{4r(a-r)}\right]. \tag{2.20}$$

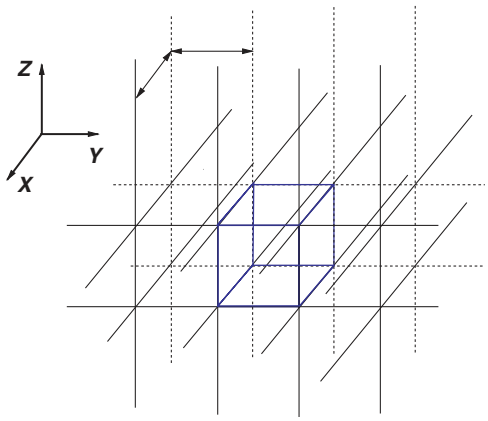

Figure 5. A three-dimensional lattice of thin conducting wires behaves like an isotropic low frequency plasma.

Noting $\Phi = LI$, and the polarization $P = (\varepsilon - 1)\varepsilon_0 E_z$, where ε is the effective permittivity, we obtain in the limit $r \ll a$,

$$\varepsilon(\omega) = 1 - \frac{2\pi c^2}{\omega^2 a^2 \ln(a/r)}, \tag{2.21}$$

which is identical to the relation obtained in the plasmon picture. However, we lose the physical interpretation of a low frequency plasmonic excitation here.

It is simple to add the effects of finite conductivity in the wires which had been neglected in the above discussion. The electric field and the current would now be related by

$$E_z = \mathrm{i}\omega LI + \sigma\pi r^2 I, \tag{2.22}$$

where σ is the conductivity, which modifies the expression for the dielectric permittivity to

$$\varepsilon = 1 - \frac{\omega_\mathrm{p}^2}{\omega(\omega + \mathrm{i}(\varepsilon_0 a^2 \omega_\mathrm{p}^2/\pi r^2 \sigma))}. \tag{2.23}$$

Thus the finite conductivity of the wires contributes to the dissipation, showing up in the imaginary part of ε. For aluminium, the conductivity is $\sigma = 3.65 \times 10^7\ \Omega^{-1}\,\mathrm{m}^{-1}$ that yields a values of $\gamma = 0.1\omega_\mathrm{p}$ which is comparable to the values in real metals [32]. Thus the low frequency plasmon is sufficiently stable against absorption to be observable.

In our above discussion, we considered only wires pointing in the z-direction. This makes the medium anisotropic with negative ε only for waves with the electric field along the z-direction. The medium can be made to have a reasonably isotropic response by considering a lattice of wires oriented along the three orthogonal directions as shown in figure 5. In the limit of large wavelengths, the effective medium appears to be isotropic as the radiation fails to resolve the underlying cubic symmetry yielding a truly three-dimensional low frequency plasma. For very thin wires, the polarization in the direction orthogonal to the wires is small and can be neglected. Thus the waves only sense the wires parallel to the electric field and correspondingly have a longitudinal mode. The effects of the connectivity of the wires along different directions at the edges of the unit cell have also been examined [43]. A wire mesh with non-intersecting wires was also shown to have a negative ε at low frequencies below the plasma frequency, but had strong spatial dispersion for the transverse modes above the plasma frequency. This issue of spatial dispersion has been studied more recently by Belov *et al* [46].

Some objections were raised to Pendry's original propositions. Mikhailov [47] assumed the results for a one-dimensional plasmon polarition on a metal wire and neglected the essential

three-dimensional nature of the problem [48]. Walser *et al* [49] incorrectly assumed the Drude form of the dielectric constant of the metal for the dielectric response of a single metallic wire as well and claimed that dissipation would damp out all phenomena. They also opined that the interpretation of a heavy electronic effective mass was due to the gauge dependent vector potential which could be changed at will. However, their results completely neglect the fact that there are two length-scales of the problem and that the wires are very thin compared with the wavelength. Thus no homogenization could be carried out. Further, the claim that any gauge term could be added to the vector potential without affecting the problem is incorrect as that would change the electric field and the plasmon would appear to have a position dependent mass [50]. The use of the Coulomb gauge does spoil the manifest covariance, but insofaras the velocities of the charges involved are small compared with c, the speed of light in vacuum, it is the most suitable gauge.

The effects of having continuous metal wires have been studied in [43], where it was shown that the response of wires systems with periodic sections of the wires removed was more akin to that of periodically placed interacting dipoles [51]. Low frequency transverse modes appear well below the effective plasma frequency for the corresponding continuous wire structure, but propagating modes appeared above them. The additional capacitance between the edges of the wires and the self-capacitance of the edges can be considered easily in our model as a term additional to the impedance in equation (2.22). The additional capacitance gives rise to a L–C resonance at a finite frequency, and one has a resonant Lorentz form of the dispersion for the dielectric permittivity. For a sufficiently sharp resonance and low wire resistivity, one can again obtain a negative dielectric permittivity within a frequency band above the resonant frequency. This response for periodic finite wire strips has also been considered by Koschny *et al* in [52], where it was also shown that the corresponding magnetic permeability, however, showed an anti-resonant dispersion with a negative imaginary part of μ when the real part of ε was negative. We will discuss this latter aspect later. Makhnovskiy and Panina [53] have considered the possibility of using the magneto-impedance effect to change the surface impedance of thin ferromagnetic wires using an applied magnetic field to generate negative dielectric media whose plasma frequency can be tuned by the magnetic field. Again the response of short wires gave rise to a resonant effective permittivity, with a finite frequency band for negative permittivity. Simovsky and He [54] considered the response of an array of Ω-shaped particles and found that the array showed the resonant dielectric response of periodically cut wires.

Dense wire media have been of interest in the electrical engineering community for a long time for artificial impedance surfaces [55, 56]. But they were usually considered when the wavelength was comparable with the period of the lattice and the radius of the wires. A transmission line model [57] gives a result of

$$\varepsilon = \frac{\varepsilon_0}{(ka)^2}\left\{\cos^{-1}\left[\cos(ka) + \frac{\pi}{ka\ln(a/(2\pi r))}\sin(ka)\right]\right\}^2, \tag{2.24}$$

which was shown to agree with our expression for a low frequency plasmonic medium in the limit of very thin wires [45]. Pitarke *et al* [58] have considered the photonic response of metallic cylinders embedded in a dielectric host and have agreement with the classical Maxwell–Garnet result when the wavelength is at least twice as large as the spacing between the cylinders. However, these cases do not ideally fall in the category of effective media. The scattering turns out to be quite important at higher frequencies.

The photonic response of superconducting cylinders made of high T_c materials has been considered [59], and it was shown that the system has a low frequency cutoff that is much smaller than that of the bulk superconductor. The role of a plasmon in a superconductor as

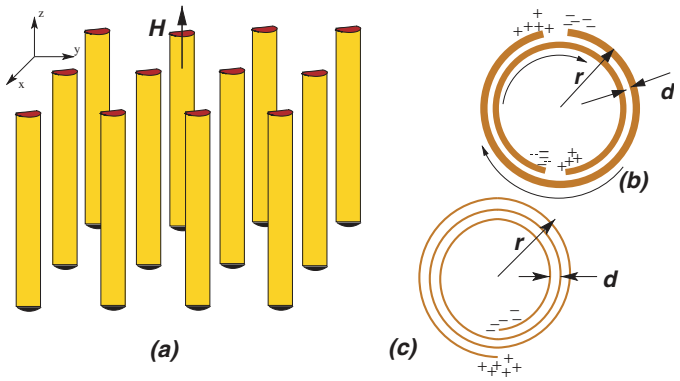

Figure 6. (*a*) An applied magnetic field along the axes of a stack of conducting cylinders induces circumferential currents that shield the interior. The resulting effective medium is diamagnetic. (*b*) The split-ring structure: the capacitance across the rings now causes the structure to be resonant. (*c*) The Swiss roll structure: more capacitance for lower frequency operation.

a massive *Higgs boson* has been stressed by Anderson [60]. Pendry [2, 43] has pointed out the importance of the fact that in such thin wire superconductor structures, the frequency of the plasmon could well be smaller than the superconducting gap, making such media of great interest in a fundamental manner.

2.2. Materials with negative magnetic permeability

As mentioned before, the magnetic activity in most materials tends to tail off at high frequencies of even a few gigahertz. So it is indeed a challenge even to obtain magnetic activity, let alone negative magnetic permeability, at microwave frequencies and beyond. In fact, Landau and Lifschitz [19] give a very general argument as to how the magnetic activity arising from atomic orbital currents should be negligible at optical frequencies if one could neglect the polarization currents. In the case of nano-metallic structures, the magnetic moments of induced real and displacement current distributions can actually contribute to an effective magnetization if the electric polarizability of the corresponding medium is small.

2.2.1. A stack of metal cylinders. Most materials have a natural tendency to be diamagnetic as a consequence of Lenz's law. Consider the response of a stack of metallic cylinders to an incident electromagnetic wave with the magnetic field along the axis of the cylinders as shown in figure 6. The cylinders have a radius r and are placed in a square lattice with period a. The oscillating magnetic field along the cylinders induces circumferential surface currents which tend to generate a magnetization opposing the applied field. The axial magnetic field inside the cylinders is

$$H = H_0 + j - \frac{\pi r^2}{a^2} j, \tag{2.25}$$

where H_0 is the applied magnetic field and j is the induced current per unit length of the cylinder. The third term is due to the depolarizing field which is assumed to be uniform as the cylinders are infinitely long. The emf around the cylinder can be calculated from Lenz's law and is balanced by the Ohmic drop in potential:

$$\mathrm{i}\omega\mu_0\pi r^2 \left(H_0 + j - \frac{\pi r^2}{a^2} j \right) = 2\pi r \rho j, \tag{2.26}$$

where time harmonic fields are assumed and ρ is the resistance per unit length of the cylinder surface. The frequencies are assumed to be sufficiently low so as to have only a small skin effect. Now we homogenize the system of cylinders by adopting an averaging procedure (discussed in section 2.4) that consists of averaging the magnetic induction, B, over the area of the unit cell while averaging the magnetic field, H, over a line along the edge of the unit cell. The averaged magnetic field is

$$B_{\text{eff}} = \mu_0 H_0, \tag{2.27}$$

while the averaged H field outside the cylinders is

$$H_{\text{eff}} = H_0 - \frac{\pi r^2}{a^2} j. \tag{2.28}$$

Using the above, we obtain the effective relative magnetic permeability:

$$\mu_{\text{eff}} = \frac{B_{\text{eff}}}{\mu_0 H_{\text{eff}}} = 1 - \frac{\pi r^2/a^2}{1 + \mathrm{i}2\rho/(\mu_0 \omega r)}. \tag{2.29}$$

Thus, the real part of μ_{eff} is always less than 1 (diamagnetic) and greater than 0 here. This diamagnetic screening effect has been known for some time for superconducting cylindrical shells [61], and a diamagnetic effective medium is also obtained with percolation metallo-dielectric composites [41].

2.2.2. The split ring resonator. In the case of the cylinders, the induced currents made it appear as if magnetic monopoles were flowing up and down the cylinders. But the problem was that the system only had an inductive response (the monopoles equivalently had no inertia). By introducing capacitive elements into the system, a rich resonant response can be induced [3]. Consider an array of concentric cylindrical metallic shells with a gap in them as shown in figure 6(*b*). This has become well known subsequently as the split ring resonator—SRR for short. The SRRs are the basis of most of the meta-materials exhibiting negative magnetic permeability today [4, 5, 25–27, 62–64].

The SRR works on the principle that the magnetic field of the electromagnetic radiation can drive a resonant L–C circuit through the inductance, and this results in a dispersive effective magnetic permeability. The induced currents flow in the directions indicated in figure 6, with charges accumulating at the gaps in the rings. The large gap in each ring prevents the current from flowing around in a single ring, and the circuit is completed across the small capacitive gap between the two rings. Assuming that the gap (d) is very small compared with the radius (r) and that the capacitance due to the large gaps in any single ring is negligible, we balance the emf around the circuit as

$$-\mathrm{i}\omega\mu_0\pi r^2 \left(H_0 + j - \frac{\pi r^2}{a^2} j \right) = 2\pi r \rho j - \frac{j}{\mathrm{i}\omega C}, \tag{2.30}$$

where the effective capacitance $C = \varepsilon_0 \varepsilon \pi r/(3d)$ and ε is the relative dielectric permittivity of the material in the gap. It is assumed that the potential varies linearly with the azimuthal angle around the ring. Proceeding as before, we obtain the effective permeability as

$$\mu_{\text{eff}} = 1 - \frac{\pi r^2/a^2}{1 - (3d/\mu_0\varepsilon_0\varepsilon\pi^2\omega^2 r^3) + \mathrm{i}(2\rho/\mu_0\omega r)} = 1 + \frac{f\omega^2}{\omega_0^2 - \omega^2 - \mathrm{i}\Gamma\omega} \tag{2.31}$$

and thus we have a resonant form of the permittivity with a resonant frequency of

$$\omega_0 = \left(\frac{3d}{\mu_0\varepsilon_0\varepsilon\pi^2 r^3} \right)^{1/2} \tag{2.32}$$

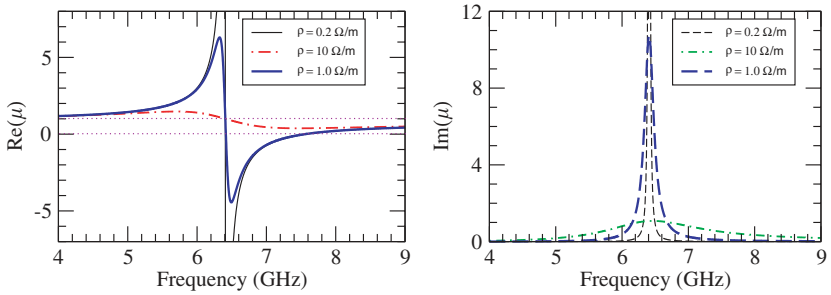

Figure 7. The behaviour of (*a*) the real and (*b*) the imaginary parts of the effective magnetic permeability for a system of split cylinders with $r = 1.5\,\mathrm{mm}$, $d = 0.2\,\mathrm{mm}$ and the magnetic field along the axis for different values of ρ. The system has negative magnetic permeability for $6.41 < \omega < 7.56\,\mathrm{GHz}$. As the resistance increases, the response of the system tends to tail off.

that arises from the L–C resonance of the system. The factor $f = \pi r^2/a^2$ is the filling fraction of the material. For frequencies larger than ω_0, the response is out of phase with the driving magnetic field and μ_{eff} is negative up to the 'magnetic plasma' frequency of

$$\omega_{\mathrm{m}} = \left(\frac{3d}{(1-f)\mu_0\varepsilon_0\varepsilon\pi^2 r^3}\right)^{1/2}, \tag{2.33}$$

assuming the resistivity of the material is negligible, and it is seen that the filling fraction plays a fundamental role in the bandwidth over which $\mu < 0$. The dielectric permittivity of the embedding medium, ε, can be used to tune the resonant frequency, which is also borne out in the numerical calculations of [65]. A finite resistivity, in general, broadens the peak, and in the case of very resistive materials the resonance is so highly damped that the region of negative μ can disappear altogether as shown in figure 7.

The resonance frequency and the negative μ band can be varied by changing the inductance (area) of the loop and the capacitance (the gap width, d, or the dielectric permittivity, ε, of the material in the capacitive gap) of the system. For typical sizes of $r = 1.5\,\mathrm{mm}$, $a = 5\,\mathrm{mm}$, $d = 0.2\,\mathrm{mm}$, we have a resonance frequency of $\omega_0 = 6.41\,\mathrm{GHz}$, and a 'magnetic plasma frequency' $\omega_{\mathrm{m}} = 7.56\,\mathrm{GHz}$. The dispersion in μ_{eff} is shown in figure 7. We note that $\mu_{\mathrm{eff}} \simeq 1 - \pi r^2/a^2$ asymptotically at large frequencies. This is due to the assumption of a perfect conductor in our analyses. Let us also note that μ_{eff} can attain very large values on the low frequency side of the resonance. Thus, the effective medium of SRR is going to have a very large surface impedance $Z = \sqrt{\mu_{\mathrm{eff}}/\varepsilon_{\mathrm{eff}}}$. Such large impedances have also been obtained by capacitively loaded structured surfaces [67, 68].

2.2.3. Isotropic negative magnetic media. In our discussion till now, we assumed a medium of infinitely long split cylinders which shows magnetic properties when the magnetic field is along the axes of the cylinders. Obviously the system does not show any magnetic activity when the magnetic field is oriented perpendicular to the cylinders, rendering the medium uniaxial. To overcome this limitation, a three-dimensional photonic material was proposed [3] which would have a reasonably isotropic response. The essential building blocks of this system are shown in figure 8(*a*) which consists of interleaved orthogonal planes of planar SRRs. Assuming that the magnetic flux through the stacked split rings remains the same as for a cylinder, this system would have the same magnetic response in all the orthogonal directions, and the effective magnetic permeability has been calculated as

$$\mu_{\mathrm{eff}}(\omega) = \frac{\pi r^2/a^2}{1 - (3l/\mu_0\varepsilon_0\pi^2\omega^2 r^3 C) + \mathrm{i}(2l\rho/\mu_0\omega r)}, \tag{2.34}$$

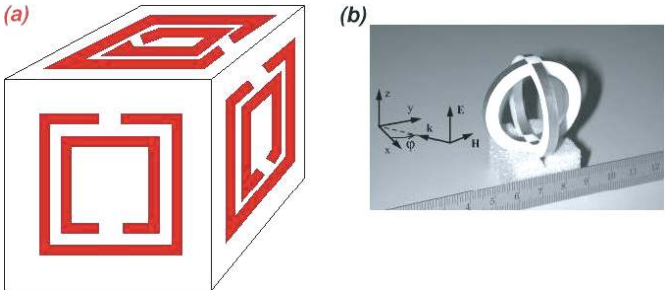

Figure 8. (*a*) The unit cell of a three-dimensional SRR medium with isotropic magnetic response. (*b*) The three-dimensional SRR scatterer proposed in [63] (reprinted with permission from [63]. Copyright 2002 American Institute of Physics).

where $C = \varepsilon_0/\pi \ln(2\tau_c/d)$ is the capacitance between two parallel sections of planar rings of thickness τ_c. Obviously if the rings are very thin, the capacitance across the ends of the single rings (which we neglect) can become comparably large. In the limit of an effective medium, the response of this medium would be very isotropic. For this assumption of no flux leakage to hold, the stacking distance, l, of the rings have to be much smaller than the radius, r, of the ring itself, which is not satisfied in the actual medium. Hence the actual resonant frequency when the flux leakage is accounted for (which is non-trivial) can be expected to differ somewhat from this expression, but it is not otherwise expected to give rise to large differences in the functioning.

Balmaz and Martin [63] have introduced a novel magnetic scatterer which consists of two orthogonal intersecting SRRs as shown in figure 8(*b*). This has an isotropic response for any wave incident on it normal to the plane of the rings. Balmaz and Martin discuss the various orientations of the rings and conclude that the rings can only intersect along symmetric points for an isotropic response. Three orthogonal non-intersecting SRRs is a possible candidate as an isotropic scatterer, but unfortunately the SRRs then tend to have non-degenerate resonant frequencies or different Q factors. An array of two-dimensional isotropic scatterers with random orientations can be expected to behave reasonably as an effective medium with isotropic response.

2.2.4. Wave dispersion in a resonant magnetic medium. Given the generic form of the dispersion in a SRR medium (or any of the resonant magnetic media to be discussed below), one can obtain the dispersion relation between k, the wave-vector, and ω, the frequency, for a wave. We show schematically this generic relationship in figure 9. One can see that the medium allows two degenerate waves (polarizations) with a gap for frequencies $\omega_0 < \omega < \omega_m$, where ω_0 is the resonance frequency and ω_m is the *magnetic plasma* frequency. This is the region where the magnetic permeability is negative and all waves in the medium are evanescent. This also gives rise to the idea that a band-gap (say in a photonic crystal) can be ascribed to negative μ just as one can ascribe it to an imaginary refractive index or negative ε [69]. Of course, the origin of the gap would depend on the symmetries of the fields in question.

One also notes that the effective medium can support a longitudinal bulk *magnetic plasma* mode at ω_m. The induced currents in the system give the appearance of magnetic monopoles sloshing up and down the cylinders. Interestingly the system should also be able to sustain the magnetic equivalent of surface plasmon modes at an interface with vacuum (say) when $\mathrm{Re}(\mu) = -1$ just like for the usual surface plasmons at an interface between positive and negative dielectric media. These will couple to s-polarized light with a non-zero component of the magnetic field normal to the surface.

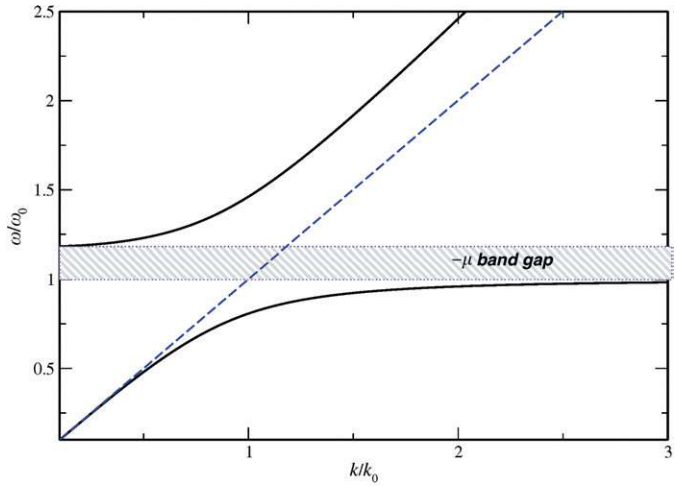

Figure 9. The dispersion for a wave in an SRR medium. The frequency and wave-vector are scaled with respect to the resonance frequency, ω_0, and $k_0 = \omega_0/c$. Propagation is not possible in the frequency gap where $\mu < 0$ as shown.

2.2.5. The Swiss roll structure at radio-frequencies. For lower radio-frequencies, the capacitance of the system can be made large instead of increasing the size of the loop (inductance). This is both convenient and increases the validity of our assumption of an effective medium as well. This can be achieved by rolling up a metal sheet in the form of a cylinder with each coil separated by an insulator of thickness d as shown in figure 6(c). This structure has also been popularly called the *Swiss roll* structure. The current loop is now completed through the differential capacitance across the space between the metal sheets as shown. As before, the effective magnetic permeability for a system of such structures can be calculated as

$$\mu_{\text{eff}} = 1 - \frac{\pi r^2/a^2}{1 - (dc^2/2\pi^2 r^3(N-1)\omega^2) + \mathrm{i}(2\rho/\mu_0\omega r(N-1))}, \tag{2.35}$$

where N is the number of coils in the structure and it is assumed that the total thickness of the wound layers $Nd \ll r$ the cylinder radius. This system also has the same generic resonance form of the permeability with frequency as the SRR structures, but now the resonance frequency occurs at a much smaller frequency owing to the larger capacitance of the structure. This has seen application in magnetic resonance imaging (MRI) at radio-frequencies as magnetic flux tubes in the region where the effective magnetic permeability assumes very large values on the lower frequency side of the resonance [23, 24].

2.2.6. Scaling to high frequencies. Maxwell's equations appear to suggest that one can scale the phenomena to higher frequencies by simply scaling down the corresponding length-scales. Terahartz operation of SRRs has been demonstrated experimentally [27]. However, the main problem in scaling to higher infrared and optical frequencies is that metals no longer behave as perfect conductors and electromagnetic fields penetrate considerably into the metal. This means that the dispersive nature of the metals must be taken into account for scaling to higher frequencies. Another cause of concern is the technological ability to make the resonant structures necessary at the small length-scales.

Keeping this in mind, a single ring with two symmetric splits providing a capacitive gap and suitable for operation in the terahertz region was proposed [28] and is shown in figure 10(a).

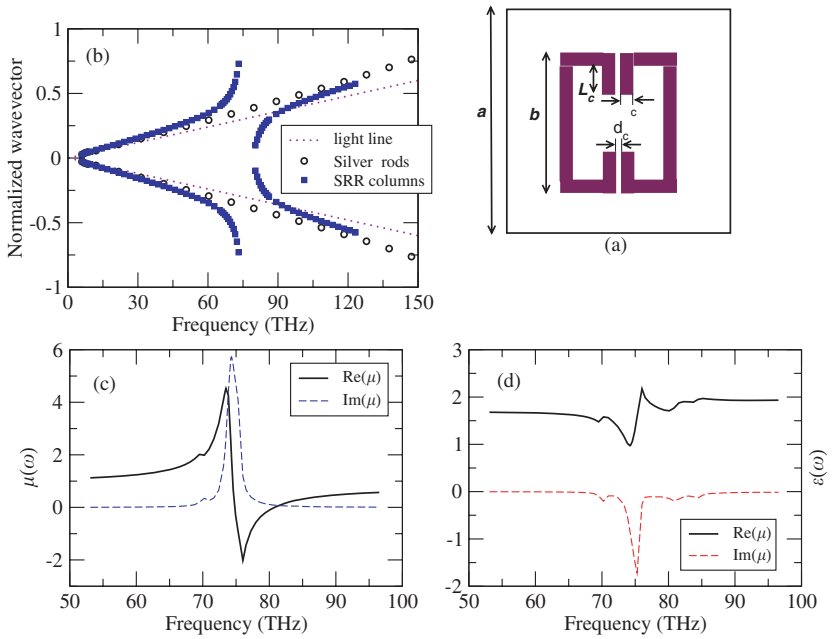

Figure 10. (*a*) The single ring with a double split with $a = 600\,\text{nm}$, $b = 312\,\text{nm}$, $\tau_c = 24\,\text{nm}$, $d_c = 24\,\text{nm}$ and $L_c = 144\,\text{nm}$ used for the calculations. (*b*) The photonic band structure of this system of columns for the s-polarization (with $\boldsymbol{H}$ along the cylindrical axes). The light line (· · · · · ·) and the bands for silver columns with the dame filling fraction are shown for comparison. The band-gap at about 75 THz arises due to a negative μ. (*c*) The real and imaginary parts of μ and (*d*) the real and imaginary part of ε. All the data are taken from [28].

The band structure and the transmission for infinitely long split cylinders of silver obtained using a photonic band-structure calculation using the transfer matrix method [70] is shown in figure 10(*b*). The magnetic field is assumed to be along the axis of the split cylinders. A plasma form for the dielectric function of silver, $\varepsilon(\omega) = \varepsilon_\infty - \omega_p^2/[\omega(\omega + i\gamma)]$, was used with the empirical values [71] of $\hbar\omega_p = 9.013\,\text{eV}$, $\gamma = 0.018\,\text{eV}$ and $\varepsilon_\infty = 5.7$. Note the presence of a frequency gap that arises due to the negative effective μ of the structure at about 75–80 THz, while a simple circuit theory predicts a resonance frequency of 104 THz for the L–C resonance. Clearly the assumptions of a perfect conductor cannot be made at these high frequencies. Using the method of Smith *et al* [72], the effective ε and μ were recovered from the emergent quantities, viz, the complex transmission and reflection coefficients, and are shown in figure 10. Clearly there is a frequency band with $\text{Re}(\mu) < 0$, although surprisingly $\text{Im}(\varepsilon) < 0$ near the resonance and $\text{Re}(\varepsilon)$ disperse the other way around. This behaviour, analogous to the case of the cut-wire system discussed before, was also found by Koschny *et al* [52], who call it *anti-resonant* behaviour, and seems to be generic to meta-materials with one negative material parameter.

Let us analyse this system to gain an insight into the high frequency scaling properties. Assuming a strong skin effect, i.e. that the thickness, τ_c, of the metal shells is smaller than the skin depth (∼20 nm at 100 THz), we can write the displacement current per unit length $j_\phi = -i\omega\varepsilon_0\varepsilon_m E_\phi$. Thus the potential drop across each half of the ring is

$$V_r = \int_0^\pi E_\phi r \, d\phi = \frac{\pi r j_\phi}{-i\omega\varepsilon_0\varepsilon_m} \tag{2.36}$$

and the potential drop across each capacitive gap (of arm length L_c) is

$$V_c = \frac{1}{C}\int I(t)\,dt = \frac{j_\phi \tau_c d_c}{-i\omega\varepsilon_0\varepsilon L_c}. \tag{2.37}$$

Using the fact that the total emf induced around the loop is $\oint E_\phi\,dl = i\omega\mu_0 H_{int}\,ds$, we can equate the potentials as

$$2V_r + 2V_c = i\omega\mu_0\pi r^2 H_{int}. \tag{2.38}$$

Using Ampere's law, the magnetic fields inside and outside the split cylinders can be related as

$$H_{int} - H_{ext} = j_\phi\tau_c, \tag{2.39}$$

yielding the relation that

$$\frac{H_{ext}}{H_{int}} = 1 - \frac{\mu_0\varepsilon_0\omega^2\pi r^2\tau_c}{[2\pi r/\varepsilon_m + 2\tau_c d_c/(\varepsilon L_c)]}. \tag{2.40}$$

The averaged magnetic induction is $B_{eff} = (1-f)\mu_0 H_{ext} + f\mu_0 H_{int}$, where $f = \pi r^2/a^2$ is the filling factor. Averaging over a line lying entirely outside the cylinders for the magnetic field $H_{eff} = H_{ext}$, we obtain the effective magnetic permeability as

$$\mu_{eff} = \frac{B_{eff}}{\mu_0 H_{eff}} = 1 + \frac{f\varepsilon_0\mu_0\omega^2\pi r^2}{[(2\pi r/(\varepsilon_m\tau_c) + 2d_c/(\varepsilon L_c)] - \varepsilon_0\mu_0\omega^2\pi r^2\tau_c}. \tag{2.41}$$

Assuming that $\varepsilon_m \simeq -\omega_p^2/[\omega(\omega + i\gamma)]$ for frequencies in the infrared and optical regions, we obtain the same generic form for the effective permeability,

$$\mu_{eff}(\omega) = 1 + \frac{f'\omega^2}{\omega_0^2 - \omega^2 - i\Gamma\omega}, \tag{2.42}$$

with the resonant frequency, effective damping and the effective filling fraction

$$\omega_0^2 = \frac{1}{(L_i + L_g)C}, \qquad \Gamma = \frac{L_i}{L_g + L_i}\gamma, \qquad f' = \frac{L_g}{L_g + L_i}f, \tag{2.43}$$

where $C = \varepsilon_0\varepsilon L_c/2d_c$ is the effective capacitance of the structure, $L_g = \mu_0\pi r^2$ is the geometrical inductance and $L_i = 2\pi r/(\varepsilon_0\tau_c\omega_p^2)$ is an additional inductance that shows up. Noting that the plasma frequency is $\omega_p^2 = ne^2/(\varepsilon_0 m)$, we see that the additional inductance is entirely due to the electronic mass and L_i can hence be termed the *inertial inductance*.

The presence of this additional inductance can be explained by noting that at high frequencies the currents are hardly diffusive and almost ballistic because the distance through which the electron moves within a period of the wave becomes comparable with the mean free path in the metal. This means that if the frequencies are too high, the electrons can hardly be accelerated and the response falls. The mass of the electron contributes additionally to the inductance[2]. The effective damping factor also becomes much larger as the size of the ring is reduced. This is due to the fact that the proportion of energy in the ballistic motion of the electrons increases as the size is reduced and the resistive losses are then very effective indeed.

Thus even if the size of the ring were negligible, the inertial inductance would still be present, preventing scaling to higher frequencies. This effect has also been discussed in connection with using superconducting SRRs in the microwave region [73]. The large increase in the damping as the dimensions are scaled down broadens the resonance and the permeability does not disperse violently now, and the region of negative permeability vanishes altogether. The increase in damping is a matter of great concern for operation at optical

[2] The current $j = nev \sim ne(-i\omega eE/m)$, where E is the applied field. Then the potential drop is $V \sim m\ell/(ne^2)\partial j/\partial t$, implying an inductance that is proportional to the electronic mass.

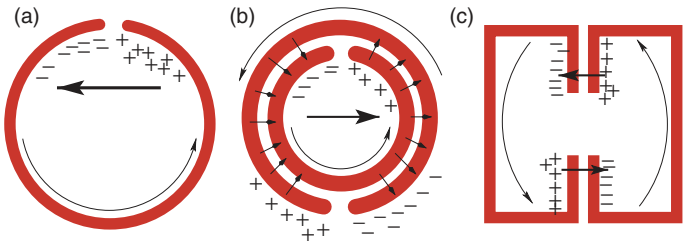

Figure 11. The SRRs develop an electric polarization too although driven by a magnetic field. This bianisotropic behaviour is maximal for (*a*) a single split ring which develops a large dipole moment. (*b*) The original SRR with two splits is also bianisotropic as it develops an electric dipole. The field lines due to the charges are also shown by thin lines. (*c*) The single ring with two symmetric splits only develops a quadrupole moment and is hardly bianisotropic.

frequencies [74]. It has been shown that the response of the SRR with two splits tends to tail off in the infrared region ($\lambda \sim 5\,\mu$m) [28]. By adding more capacitive gaps to lower the net capacitance and adjusting the dielectric constant of the embedding medium, it has been numerically demonstrated that a medium of SRR with four splits can have a negative μ at a telecommunications wavelength of about $1.5\,\mu$m [22]. Panoiu and Osgood [75] have shown that the original SRR, suitably scaled down, can also operate at infrared frequencies. Panina *et al* [76] have proposed the use of pairs of parallel metal sticks (with lengths $\sim$100 nm) periodically embedded in a dielectric medium as an effective medium with negative magnetism at infrared frequencies. Hsu *et al* [64] have claimed resonance with the original SRR at a wavelength of $10.6\,\mu$m. But the size of the SSR was $10.48\,\mu$m and the assumption of an effective medium would hardly be valid.

2.2.7. Other approaches. One might ask then if the main ingredients of a resonant magnetic medium are just a capacitance and an inductance, then why a single capacitive gap cannot work as well. In fact, SRR media of rings with a single split [76–78], Ω-shaped particles [54], a double ring with a single split in one ring [79] and deformed split rings [66] have been proposed as candidates for a resonant magnetic medium. The point is that we would like to have as low an electrical polarizability as possible. With a single split ring, a large electric dipole moment would be generated across the capacitive gap (see figure 11(*a*)) and this could well dominate over the weaker magnetic dipole moment generated in the ring. When there are two splits present, the dipole moments across opposite ends cancel each other and one only gets a weak electric quadrupole moment (see figure 11(*c*)) whose effects would be expected to be much weaker than those of the magnetic dipole moment. Most of the magnetic media that simultaneously generate an electric dipole moment are bianisotropic media [80], i.e. the constitutive relations are

$$\boldsymbol{D} = \varepsilon \boldsymbol{E} + \alpha \boldsymbol{H}, \qquad \boldsymbol{B} = \beta \boldsymbol{E} + \mu \boldsymbol{H}, \tag{2.44}$$

where α and β are the bianisotropy coefficients. The Ω–shaped particles, first introduced as the components of a bianaisotropic medium [81], when arranged in a periodic lattice also have a resonant ε and μ and can behave as negative magnetic materials [54]. Even the original SRR medium [3] is bianisotropic [82] as there is an electric dipole moment that develops across the capacitive gaps (see figure 11(*b*)), and this can also be driven by an electric field [62]. Thus the SRR is oriented such that the magnetic field is normal to the plane of the SRR and the electric field is along the SRR and can be driven by the electric field and the magnetic and electric resonances can overlap. This can be effectively resolved, of course, by rotating adjacent

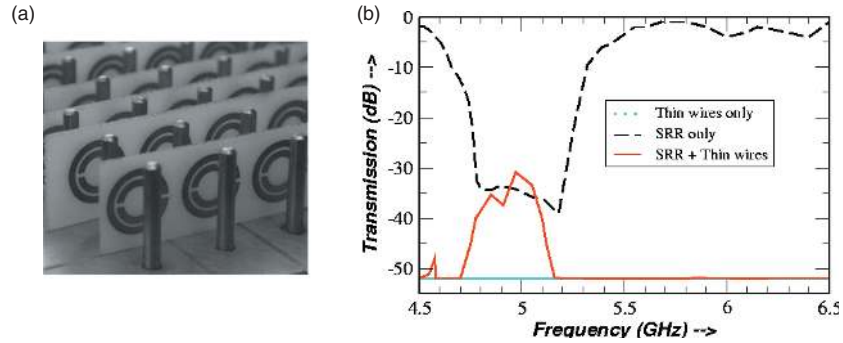

Figure 12. The left panel shows a photograph of the composite of thin wire arrays and SRRs that shows a negative refractive index made by the San Diego group (courtesy D R Smith). The right panel shows the transmission across a sample of thin wire arrays (· · · · · ·), SRRs (- - - -) and a composite of thin wire arrays and SRRs (——) as measured by the San Diego group (adapted from the data of [4]). The enhanced transmission in the latter case within the negative μ band is interpreted as evidence of a negative refractive index.

SRRs in the plane by 180° and the corresponding electric dipole moments would cancel. The symmetry of the single ring with two symmetrically placed capacitive gaps renders this less bianisotropic and electrically less active.

In fact, any resonance that can be driven by the magnetic field of radiation can be used. The use of the magnetic Mie scattering resonances of a dielectric cylinder for generating a negative magnetic medium has also been proposed [83]. Only the first monopolar magnetic Mie resonance (with the applied magnetic field along the cylinders) can contribute to the effective magnetic polarizability upon homogenization, and the dielectric constant of the cylinders needs to be large to reduce the resonant frequencies to within the first Bragg band. The use of ferroelectric cylinders with very large values of ε at gigahertz frequencies has been proposed. The possibility of a medium with a very low frequency (∼50 Hz) negative magnetic metamaterial has also been proposed [21]. This consists of a periodic lattice of current carrying wires, with alternate wires carrying currents in opposite directions. Displacements of these wires magnetize the medium. The tension in the wires and the mutual repulsion between them give a restoring force, causing them to oscillate at low frequencies. In a process very similar to that in an electrical resonant dipole medium, the dispersive μ can become negative in a band of frequencies above the resonance frequency where the system mimics a plasma of magnetic monopoles.

2.3. Negative refractive index materials

We will follow the rule that any medium with $\mathrm{Re}(\varepsilon) < 0$ and $\mathrm{Re}(\mu) < 0$ simultaneously will be considered to have a negative refractive index. A rigorous justification of this is presented in section 3.1. Smith *et al* [4] proposed that combining in a composite the thin wire medium with $\varepsilon < 0$, and the SRR medium with $\mu < 0$ would yield an effective medium with $n < 0$. Admittedly it is not obvious that the media would have a negative n. But the calculations and experimental measurements of Smith *et al* [4, 84] were very suggestive of it. Their uniaxial composite shown in figure 12(*a*) consisted of wires of 0.8 mm thickness and SRRs with $\omega_0 = 4.845$ GHz. Their numerical calculations showed that if thin wires were introduced into a SRR medium, a pass-band occurs within the band-gap of negative μ for radiation with the electric field along the wires and the magnetic field normal to the plane of the SRR. Combining

the dispersions for the plasma-like dielectric medium and a resonant magnetic medium, we get

$$k^2 = \frac{\varepsilon\mu\omega^2}{c^2} = \frac{(\omega^2 - \omega_{\rm p}^2)(\omega^2 - \omega_{\rm m}^2)}{c^2(\omega^2 - \omega_0^2)}, \tag{2.45}$$

where $\omega_{\rm p}$ and $\omega_{\rm m}$ are the electric and magnetic plasma frequencies, respectively, and ω_0 is the magnetic resonance frequency ($\omega_{\rm m} = \omega_0/\sqrt{(1-f)}$). If $\omega_{\rm p}$ is the largest of them, then we obtain a pass-band in the region $\omega_0 < \omega < \omega_{\rm m}$. The numerical calculations suggested that the thin wires and the SRRs functioned independently and the composite had a pass-band with a negative refractive index. The experimental results on transmission through waveguides filled with a medium of thin wires, a medium of SRRs only and a composite medium with both thin wires and SRRs is shown in figure 12(*b*). The transmission is in the stop-band due to the negative μ for SRRs and there is enhanced transmission within this bandwidth when thin wires are introduced into the SRR medium. This was taken as proof that the medium was a NRM. The San Diego group went on to show [5] that a prism made of such a composite NRM refracted microwaves in the direction opposite to the normal direction compared with a prism of a positive refractive material such as Teflon[3].

The samples in the original San Diego experiments had a small transmission, and it was claimed that the observed effects could be due to just absorption [9]. Numerical photonic calculations [65, 85] showed that there was indeed a negative index band which overlapped reasonably with the negative μ frequency band, but indicated that there was considerable absorption in these media due to Ohmic losses and dissipation in the dielectric board. Other calculations [26] showed that the losses were primarily due to Ohmic losses in the metal rings and showed that the losses were somewhat smaller. The San Diego experiments also met with criticism as they were conducted in a waveguide and there was speculation about leaky waveguide modes. Now these experiments have been repeated with large samples in free space [25, 26] where both the transmission and reflection were measured, and the absorption was found to be sufficiently small to unambiguously demonstrate the negative refraction effect and to be consistent with calculations. These experiments have unequivocally demonstrated the existence of a negative refractive index.

Although there is both experimental and numerical evidence that the composite of thin wires and SRRs has a negative refractive index band, it is not a straightforward conclusion. That the two structures do not interact and interfere with each other's functioning is questionable. Pokrovsky and Efros [86] showed that embedding a thin wire array in a homogeneous medium with $\mu < 0$ does not produce an NRM and the system has no propagating modes. First, in a meta-material, one cannot assume a homogeneous ε or μ due to the other parts of the composite structure. Second, as long as the thin wires are not placed in regions where the highly inhomogeneous magnetic fields associated with the SRRs are present (along the axis of the SRR) and the SRR planes are placed such that they are at the points of symmetry between the wires (where the magnetic fields associated with the wires are minimal), the interference can be reduced greatly [87]. Third, we note that the magnetic fields due to the wires fall off rather rapidly with distance from the wires and should not affect the SRRs badly. Then the quasi-static responses derived here for ε and μ would be valid in the negative refractive index band, and the SRRs and the thin wires would function independently as if in vacuum. Thus the relative placement of the components could be crucial and might account for the differences reported in numerical and experimental data. A clear demonstration that the fields due to the two structures do not interfere with the functioning of each other is yet to be made. It has been shown that although the quasi-static interaction between the SRR and the thin

[3] This is due to the fact that radiation refracts to the other side of the normal at the interface between positive and negative media (see section 3.2.1).

wire array is small, there are residual interactions between the two sub-systems which lead to both a shift in the resonant frequency [88] and an increased dissipation in the structure [89]. Further there are problems associated with a simplistic approach to homogenization of the composite at sub-resonance frequencies where μ is positive and large, and ε due to the thin wires is negative. Then the wave is highly evanescent and homogenization may not be easily possible [88].

Alternative proposals for NRMs using other systems have been put forward. The use of alternatively oriented Ω-shaped particles, where the magnetic resonance frequency (for the magnetic field normal to the loop) and the electric dipole resonance (for the electric field along the legs) coincide, has been proposed [54]. Panina *et al* [76] have proposed the use of oriented paired parallel metal sticks as the constituents of the NRM. Deformed SRRs have similarly been used to simultaneously generate an electric and a magnetic resonance for orthogonal magnetic and electric fields [66]. Marqués *et al* [90] have demonstrated that a waveguide filled with a negative μ medium behaves as an NRM for frequencies below the cutoff frequency. It is well known that a waveguide below the cutoff behaves as a one-dimensional plasma and the split rings when placed within it make it behave as an NRM.

2.4. Homogenization and effective macroscopic material parameters

In our discussion, it was assumed that media with highly inhomogeneous inclusions could be described by only two complex parameters, ε and μ insofaras the electromagnetic interactions are concerned. Central to this assumption was the fact that the size or length-scales of the inclusions are very small compared with the free space wavelength of the radiation. Then the radiation encounters a coarse-grained spatial average of the polarizabilities of the constituent structures of the medium. In fact, there are two levels of averaging involved here. The structural units of the meta-material are assumed to be sufficiently large on a molecular scale, i.e. microscopically large, to be described by the bulk dielectric permittivity and magnetic permeability of the constituent materials. Thus we have the Maxwell's equations

$$\nabla \cdot \boldsymbol{D} = 0, \qquad \nabla \times \boldsymbol{E} = -\frac{\partial B}{\partial t}, \tag{2.46}$$

$$\nabla \cdot \boldsymbol{B} = 0, \qquad \nabla \times \boldsymbol{H} = \frac{\partial D}{\partial t}, \tag{2.47}$$

where $\boldsymbol{D} = \varepsilon_0 \varepsilon(\boldsymbol{r})\boldsymbol{E}$ and $\boldsymbol{B} = \mu_0 \mu(\boldsymbol{r})\boldsymbol{H}$, and ε and μ are the material parameters of the constituent materials. This is the first level of homogenization. However, the structures in question are sufficiently small compared with the length-scale over which the applied fields vary for only the fields due to the first few multipoles of the charge and current distributions induced in the structures to contribute to the polarization. In other words, the fine structure of the charge and current distributions is not discernible, but only a few averages such as the corresponding dipolar fields or (rarely) the quadrupolar fields can be resolved. Thus we have the averaged fields,

$$\langle \boldsymbol{D} \rangle = \varepsilon_0 \tilde{\varepsilon}_{\text{eff}} \cdot \langle \boldsymbol{E} \rangle, \qquad \langle \boldsymbol{B} \rangle = \mu_0 \tilde{\mu}_{\text{eff}} \cdot \langle \boldsymbol{H} \rangle, \tag{2.48}$$

that determine the effective dielectric permittivity and the magnetic permeability of the bulk meta-material which are second ranked tensors in general.

The Maxwell–Garnett approximation, which is essentially the quasi-static generalization of the Clausius Mossotti electrostatic approximation, has been used widely to calculate the bulk electromagnetic properties of inhomogeneous materials [91]. The component with the largest filling factor is considered to be a host in which other components are embedded, and the field induced in the uniform host by a single inclusion (assumed to be spherical or

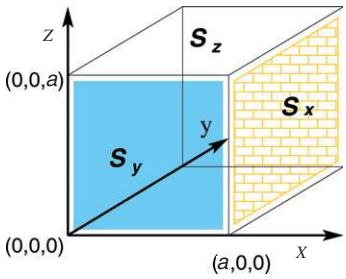

Figure 13. The procedure for averaging the internal microscopic fields consists of averaging the $\boldsymbol{E}$ and $\boldsymbol{H}$ fields over the edges of the unit cell of the simple cubic lattice, while the $\boldsymbol{D}$ and $\boldsymbol{B}$ fields are averaged over a face S_x for the x-component and so on.

elliptical) is calculated and the distortion of this field due to the other inclusions is calculated approximately. The Maxwell–Garnett approach incorporates the distortions due to the dipole field on an average and has been very successful in describing the properties of dilute random inhomogeneous materials. In our treatment we have in some sense used the Maxwell–Garnett type approximation but, however, assumed uniform depolarizing fields that simplified the calculations. There are other effective medium theories [92, 93] for high filling fractions that include more residual interactions or higher multipole effects. We should also note that there are more mathematically rigorous homogenization theories [94], which analyse the fields in an asymptotic expansion in terms of the microscopic length-scale associated with the inhomogeneities, which is however beyond the scope of this review.

In the case of periodically structured materials, the periodicity, first of all, implies that the averaging need not be over orientational and density fluctuations. We will now discuss an averaging procedure of Pendry [3] that was first used to discretize Maxwell's equations on a lattice [17]. Consider the unit cell of the lattice (assumed to be simple cubic) shown in figure 13. The Maxwell equations can be recast in their integral form:

$$\oint_C \boldsymbol{H}\cdot \mathrm{d}\boldsymbol{l} = -\int_S \boldsymbol{D}\cdot \mathrm{d}\boldsymbol{\sigma}, \tag{2.49}$$

$$\oint_C \boldsymbol{E}\cdot \mathrm{d}\boldsymbol{l} = -\int_S \boldsymbol{B}\cdot \mathrm{d}\boldsymbol{\sigma}, \tag{2.50}$$

where the curve C encloses the surface S, which itself suggests an averaging procedure. The averaged fields, $\boldsymbol{E}_{\mathrm{eff}}$ and $\boldsymbol{H}_{\mathrm{eff}}$, are defined by averaging $\boldsymbol{E}$ and $\boldsymbol{H}$ along the sides of the unit cell:

$$E_{\mathrm{eff}}^{(x)} = \frac{1}{a}\int_{(0,0,0)}^{(a,0,0)} E_x\,\mathrm{d}x, \quad E_{\mathrm{eff}}^{(y)} = \frac{1}{a}\int_{(0,0,0)}^{(0,a,0)} E_y\,\mathrm{d}y, \quad E_{\mathrm{eff}}^{(z)} = \frac{1}{a}\int_{(0,0,0)}^{(0,0,a)} E_z\,\mathrm{d}z, \tag{2.51}$$

$$H_{\mathrm{eff}}^{(x)} = \frac{1}{a}\int_{(0,0,0)}^{(a,0,0)} H_x\,\mathrm{d}x, \quad H_{\mathrm{eff}}^{(y)} = \frac{1}{a}\int_{(0,0,0)}^{(0,a,0)} H_y\,\mathrm{d}y, \quad H_{\mathrm{eff}}^{(z)} = \frac{1}{a}\int_{(0,0,0)}^{(0,0,a)} H_z\,\mathrm{d}z. \tag{2.52}$$

Similarly, $\boldsymbol{D}_{\mathrm{eff}}$ and $\boldsymbol{B}_{\mathrm{eff}}$ are defined by averaging them over the faces of the unit cell:

$$D_{\mathrm{eff}}^{(x)} = \frac{1}{a}\int_{S_x} D_x\,\mathrm{d}\sigma_x, \quad D_{\mathrm{eff}}^{(y)} = \frac{1}{a}\int_{S_y} D_y\,\mathrm{d}\sigma_y, \quad D_{\mathrm{eff}}^{(z)} = \frac{1}{a}\int_{S_z} D_z\,\mathrm{d}\sigma_z, \tag{2.53}$$

$$B_{\mathrm{eff}}^{(x)} = \frac{1}{a}\int_{S_x} B_x\,\mathrm{d}\sigma_x, \quad B_{\mathrm{eff}}^{(y)} = \frac{1}{a}\int_{S_y} B_y\,\mathrm{d}\sigma_y, \quad B_{\mathrm{eff}}^{(z)} = \frac{1}{a}\int_{S_z} B_z\,\mathrm{d}\sigma_z, \tag{2.54}$$

where S_x is the face in the Y–Z plane, S_y is the face lying in the Z–X plane and S_z is the face along the X–Y plane. The averaged fields enable us to determine $\varepsilon_{\mathrm{eff}}$ and μ_{eff} component-wise.

There is only one restriction in this procedure: that the unit cell should not intersect any of the structures contained within, so that the continuity of the parallel components of $\boldsymbol{E}_{\rm eff}$ and $\boldsymbol{H}_{\rm eff}$ across the surfaces is maintained. This procedure was adopted in section 2.2 to determine the effective magnetic permeability.

The effective medium parameters determined from any such averaging process should be unique and independent of the manner of the averaging process. Likewise, it should give unique medium responses to applied fields, and it should be possible to uniquely determine the scattered fields for the meta-material. In fact, experiments usually access only the emergent quantities such as the reflection and transmission through (say) a slab of the effective medium and not the internal microscopic fields. Smith *et al* [72] inverted the classical relations for the reflection and transmission coefficients from a slab of homogeneous material of thickness d,

$$T = \left[\cos(nk_z d) - \frac{\mathrm{i}}{2}\left(Z + \frac{1}{Z}\right)\sin(nk_z d)\right]^{-1} \mathrm{e}^{-\mathrm{i}k_z d}, \tag{2.55}$$

$$R = \frac{-\mathrm{i}}{2}\left(Z - \frac{1}{Z}\right)\sin(nk_z d)T\,\mathrm{e}^{\mathrm{i}k_z d}, \tag{2.56}$$

for the refractive index, n, and the impedance, Z, as

$$n = \pm\cos^{-1}\left(\frac{1 - r^2 - t^2}{2t}\right), \tag{2.57}$$

$$Z = \pm\left[\frac{(1+r)^2 - t^2}{(1-r)^2 - t^2}\right]^{1/2}, \tag{2.58}$$

where $r = R$ and $t = T\,\mathrm{e}^{\mathrm{i}k_z d}$, from which one obtains the dielectric permittivity $\varepsilon = n/Z$ and the magnetic permeability $\mu = nZ$. The multi-valued nature of the trigonometric functions gives rise to an ambiguity in n and Z which, however, can be resolved by determining them for several thicknesses, d, of the slab and requiring that $\mathrm{Re}(Z) > 0$ and $\mathrm{Im}(n) > 0$ for causal and absorptive media (see section 3.1). It is then a matter of great reassurance that the effective medium parameters derived from the emergent quantities coincide with the effective medium parameters obtained from a homogenization of the microscopic internal fields [28, 72]. In these processes, there is always an inbuilt ambiguity in the phase of the wave corresponding to the unit cell size which would always affect the effective medium parameters to a small extent. That would be negligible in the limit of a very small unit cell size.

As has been pointed out, the meta-material of cut wires with $\mathrm{Re}(\varepsilon) < 0$ has a counter-intuitive $\mathrm{Im}(\mu) < 0$ [52]. Similarly, meta-materials with $\mathrm{Re}(\mu) < 0$ have $\mathrm{Im}(\varepsilon) < 0$ for both an SRR medium [28,52] and a medium of dielectric cylinders [83]. Although surprising, this does not violate any fundamental requirement as long as the passive meta-material is only dissipative, i.e. the right-hand side of equation (1.3) is positive definite. These negative imaginary parts of ε and μ have been explained in part as a result of the finiteness of the unit cell [52]. One should, however, note that many of the meta-materials are intrinsically bianisotropic, at least weakly, and a simple interpretation of the reflection and transmission of the meta-material slab in terms of an isotropic or anisotropic material is not strictly correct. The reasons for this effect are yet to be completely understood.

It should be noted here that we do not consider a photonic crystal or a band-gap material to be a meta-material at high frequencies when the lattice period is comparable with or smaller than the wavelength in free space. In this limit, the radiation can discern the individual structures and scattering dominates—there is a splitting of the wave with large phase shifts. In the meta-material limit of low frequencies, the scattered fields corresponding to the small scatterers have very large wave-vectors, implying that the scattered fields are evanescent and

do not propagate. This is not true in the case of photonic band-structure materials, where momentum can be transferred between the propagating modes of the radiation and the crystal.

2.5. Causality and energy density in negative refractive media

It must be noted that dispersionless material parameters $\varepsilon < 0$ or a $\mu < 0$ cannot exist. Negative ε or μ for static fields would, for example, imply that the energy density for static fields,

$$\mathcal{E}_{\text{static}} = \frac{\varepsilon_0 \varepsilon}{2} \boldsymbol{E}_s^2 + \frac{\mu_0 \mu}{2} \boldsymbol{H}_s^2 < 0, \tag{2.59}$$

is negative, which is clearly not possible. Negative ε and μ are resonant effects and they are necessarily dispersive and dissipative. A non-dispersive NRM would imply, for example, that time runs backwards for light in the medium [110].

The material parameters of a causal medium should satisfy the Kramers–Kronig (KK) relations [18, 95]. These are relations between the real and imaginary parts of the response functions:

$$\text{Re}(\varepsilon(\omega)) - 1 = \frac{1}{\pi} P \int_{-\infty}^{\infty} \frac{\text{Im}(\varepsilon(\omega'))\, \text{d}\omega'}{\omega' - \omega}, \tag{2.60}$$

$$\text{Im}(\varepsilon(\omega)) = -\frac{1}{\pi} P \int_{-\infty}^{\infty} \frac{[\text{Re}(\varepsilon(\omega')) - 1]\, \text{d}\omega'}{\omega' - \omega}, \tag{2.61}$$

$$\text{Re}(\mu(\omega)) - 1 = -\frac{1}{\pi} P \int_{-\infty}^{\infty} \frac{\text{Im}(\mu(\omega'))\, \text{d}\omega'}{\omega' - \omega}, \tag{2.62}$$

$$\text{Im}(\mu(\omega)) = \frac{1}{\pi} P \int_{-\infty}^{\infty} \frac{[\text{Re}(\mu(\omega')) - 1]\, \text{d}\omega'}{\omega' - \omega}, \tag{2.63}$$

where P is the Cauchy principal value, i.e. the real and imaginary parts are Hilbert transforms of each other. These relations hold as long as the response functions are analytic in the upper half plane and poles of the functions are in the lower half plane. If the poles occur only in the upper half frequency plane, for example an amplifying medium or for nonlinear four-wave mixing, then too the Hilbert transforms hold, but the sign of the transform becomes negative [96]. The case of meromorphic response functions when poles occur in both the upper and lower plane [97] has been discussed in [98], which is important for meta-materials with negative material parameters.

The generic forms of the dispersion for a resonant dielectric and magnetic media satisfy the KK relations, and they are causal insofaras the homogenization is valid. For the plasma of equation (1.7) a term of $4\pi\sigma/\omega$ should be added to the right-hand side of equation (2.61) due to the pole at zero frequency. However, note that the integrals in the KK relations involve frequencies all the way up to infinity and it is clear that the effective medium theories will break down at high frequencies. This never really affects us in the case of common optical media where the macroscopic material response functions hold almost down to the level of a few atomic distances. Thus the very high frequency limit is never really probed. In the case of meta-materials, usually the wavelength is larger than the periodicity by only one or two orders of magnitude, and this high frequency cutoff, when the homogenization becomes invalid, is easily accessed. Thus the KK relations should be applied cautiously to meta-materials keeping this in mind. Further, due to the finiteness of the structures the metamaterials have highly non-local responses, implying that the dielectric permittivity and the magnetic permeability also disperse spatially at high frequencies (before the breakdown of homogenization). Generalized KK relations for the spatially dispersive materials are available [99] and may be made use of.

It is non-trivial to identify a positive definite quantity as the electromagnetic energy density in dispersive media [19,100,101]. The dissipation in the medium depends on the time histories of the fields and the medium polarizations. Assuming narrow band radiation and making a Taylor series expansion about the carrier frequency and retaining only the linear term, it is possible to write down an expression for the energy density as [18, 19]

$$\mathcal{E} = \frac{1}{2}\left[\frac{\partial(\omega\varepsilon)}{\partial\omega}\varepsilon_0\boldsymbol{E}^2 + \frac{\partial(\omega\mu)}{\partial\omega}\mu_0\boldsymbol{H}^2\right] \tag{2.64}$$

in the so-called transparency regions, for frequencies far enough away from a resonance where absorption is small. Thus a sufficient condition for a positive energy density under these approximations is $\partial(\omega\varepsilon)/\partial\omega > 0$ and $\partial(\omega\mu)/\partial\omega$. This is satisfied in the regions of normal dispersion far from the resonances. A general and exact expression for the energy density has been derived in [101],

$$\mathcal{E}(t) = \frac{\varepsilon_0}{2|\boldsymbol{E}(t)|^2} + \frac{\mu_0}{2|\boldsymbol{H}(t)|^2} + \int_{-\infty}^{+\infty} \mathrm{d}\omega \left[\left|\alpha_E(\omega)\int_{-\infty}^{t} \mathrm{d}\tau\, \mathrm{e}^{\mathrm{i}\omega\tau}\boldsymbol{E}(\tau) + \alpha_H(\omega)\int_{-\infty}^{t} \mathrm{d}\tau\, \mathrm{e}^{\mathrm{i}\omega\tau}\boldsymbol{H}(\tau)\right|^2\right], \tag{2.65}$$

where $\alpha_E^*(\omega)\alpha_E(\omega) = \omega\,\mathrm{Im}\varepsilon(\omega)$ and $\alpha_H^*(\omega)\alpha_H(\omega) = \omega\,\mathrm{Im}\mu(\omega)$. This is positive definite and applicable to the case where ε and μ can become negative as well. Although important from a fundamental point of view, this expression is rather difficult to use due to integrals over the time history of the fields. Again it is emphasized that the KK relations have been used to obtain this energy density and it is valid only for the low frequency regime when the effective medium parameters themselves are valid.

3. Propagation of radiation in negative refractive media

3.1. Choice of the wave-vector

As discussed in section 1.2, the reversal of the signs of both ε and μ in Maxwell's equations,

$$\boldsymbol{k}\times\boldsymbol{E} = \omega\mu_0\mu\boldsymbol{H}, \tag{3.1}$$

$$\boldsymbol{k}\times\boldsymbol{H} = -\omega\varepsilon_0\varepsilon\boldsymbol{E}, \tag{3.2}$$

implies that the phase vector $\boldsymbol{k}$ has a reversed sign, i.e. it is opposite to the Poynting vector $\boldsymbol{S} = \boldsymbol{E}\times\boldsymbol{H}$. We can take this to imply that the refractive index $n = \sqrt{\varepsilon\mu}$ is negative. Thus, the phase accumulated in propagating a distance Δ is $\Delta\phi = -n\omega\Delta/c$.

Writing $\varepsilon = \varepsilon' + \mathrm{i}\varepsilon''$, and $\mu = \mu' + \mathrm{i}\mu''$, we note that the medium is absorbing if $\varepsilon'' > 0$, $\mu'' > 0$ and amplifying if $\varepsilon'' < 0$, $\mu'' < 0$. Let us consider a plane wave $\exp(\mathrm{i}nk_0x)$ in an absorbing NRM where the refractive index $n = \pm[(\varepsilon'\mu' - \varepsilon''\mu'') + \mathrm{i}(\varepsilon'\mu'' + \mu'\varepsilon'')]^{(1/2)} \simeq \pm[\varepsilon'\mu' + \mathrm{i}/2(\varepsilon'\mu'' + \mu'\varepsilon'')/(\varepsilon'\mu')]$ for small absorption. Now the wave should decay in amplitude as it propagates in the dissipative medium and that is governed by the sign of $\mathrm{Im}(k_z)$. For the case $\varepsilon' < 0$ and $\mu' < 0$, this condition demands that the negative sign of the square root be chosen. Smith and Kroll [102] considered the problem of a radiating current sheet in a NRM and found that power is radiated away from the current sheet if the impedance

$$Z = \sqrt{\frac{\mu(\omega)}{\varepsilon(\omega)}} = \frac{\mu}{n} \tag{3.3}$$

was positive. For positive media, $\mu > 0$ and $n > 0$ and the power is radiated away. But if $\mu < 0$ in an NRM, then $n < 0$. This has been contested by some authors [7, 103]. Walser

and co-workers [7] claimed that the wave propagation in NRMs was *very inhomogeneous* and a negative refractive index could not be claimed. Pokrovsky and Efros [103] argued that the refractive index is ambiguous as it does not enter the Maxwell equations and that only the group velocity is negative in NRMs. For complex ε, μ and $\vec{k}$, the wave of course becomes inhomogeneous. However, there does exist a very general problem of choosing the sign of the square root for determining the wave-vector,

$$|\boldsymbol{k}|^2 = k_x^2 + k_y^2 + k_z^2 = \varepsilon\mu\frac{\omega^2}{c^2}, \tag{3.4}$$

in such homogeneous media.

This problem can be formally treated [104] by considering the most general properties of the wave-vector in the complex plane. Without loss of generality, we consider an electromagnetic wave with a wave-vector $[k_x,\ 0,\ k_z]$ to be incident from vacuum on the left ($-\infty < z < 0$) on a semi-infinite medium ($\infty > z > 0$) with an arbitrary value of ε and μ. Due to x-invariance, k_x is preserved across the interface. The z-component of the wave-vector, k_z, however, has to be obtained from the dispersion relation,

$$k_z = \pm\sqrt{\varepsilon\mu\frac{\omega^2}{c^2} - k_x^2}, \tag{3.5}$$

where a physical choice has to be made for the sign of the square root. Now the waves in medium 2 could be propagating [$k_x^2 < \mathrm{Re}(\varepsilon\mu\omega^2/c^2)$] or evanescent [$k_x^2 > \mathrm{Re}(\varepsilon\mu\omega^2/c^2)$]. Further the media could be absorbing or amplifying, depending on the sign of $\mathrm{Im}(\varepsilon\mu)$ in equation (3.5). This enables us to divide the complex plane for $Z = k_z^2$ into the four quadrants shown in figure 14. The waves corresponding to quadrants 1 and 4 have a propagating nature, and the waves corresponding to quadrants 2 and 3 are evanescent. Crucially, we note that there is a branch cut in the complex plane for $\sqrt{Z} = k_z$ and one cannot analytically continue the behaviour of the waves across this branch cut. This branch cut divides the Riemann surface into two sheets in which the two different signs for the square root will have to be taken. The different regions in the $Z = k_z^2$ plane are mapped into the different physical regions of the $\sqrt{Z}$ plane, depending on k_x, ε and μ. For absorbing media, the wave amplitude at the infinities has to obviously disappear. For amplifying media, one has to be more careful. The only conditions are that evanescently decaying waves remain decaying, propagating ones remain propagating and no information can flow in from the infinities. This ensures that the near-field features of a source cannot be probed at large distances merely by embedding the source in an amplifying medium. Due to the above reasons we will inconveniently choose the branch cut along the negative imaginary axis as shown in figure 14. Hence our range for the argument θ of k_z^2 becomes $-\pi/2 < \theta < 3\pi/2$ for the first Riemann sheet and $3\pi/2 < \theta < 7\pi/2$ for the second Riemann sheet, corresponding to the two signs of the square root, $k_z = \pm\sqrt{Z} = |Z|^{1/2}\,\mathrm{e}^{\mathrm{i}\theta/2}$ and $|Z|^{1/2}\,\mathrm{e}^{\mathrm{i}\pi+\mathrm{i}\theta/2}$, respectively. The complex plane for $k_z = \sqrt{Z}$ with the corresponding eight regions in the two Riemann sheets is shown in figure 14. Note that although the position of the branch cut in the k_z^2 plane is only a convenient choice, the final regions in k_z for various media is fixed by causality.

Regions 1 and 8 correspond to propagating waves in conventional positive media that are absorptive or amplifying, respectively. Regions 6 and 7 correspond to growing evanescent waves that blow up at the infinities, which are unphysical in a semi-infinite medium. Decaying evanescent waves fall within region 2 if $\varepsilon'\mu'' + \varepsilon''\mu' > 0$ and in region 3 if $\varepsilon'\mu'' + \varepsilon''\mu' < 0$, regardless of ε' and μ'. Note that the Poynting vector points away from the source (interface) if the medium is absorptive overall, and actually towards the source if the medium is overall amplifying, $\varepsilon' < 0$ and $\mu' < 0$. For the case of evanescent waves in amplifying media, our choice results in a Poynting vector that points towards the source (interface in this case). This,

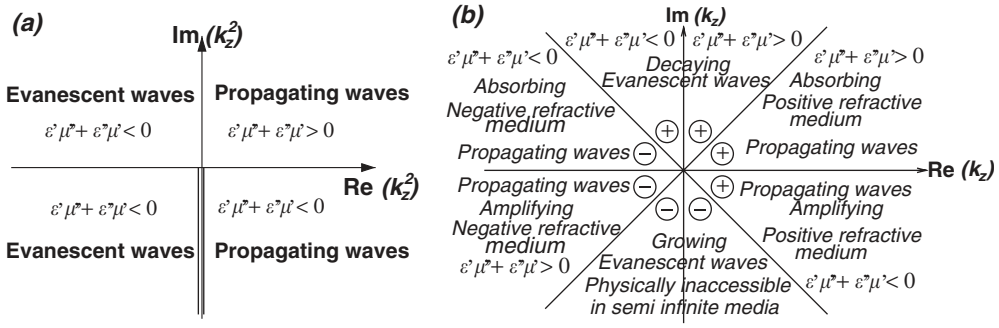

Figure 14. (*a*) The complex plane for k_z^2 showing the different regions for the propagating and evanescent waves. The branch cut along the negative imaginary axis for the square root is shown. (*b*) The complex plane for $k_z = \sqrt{Z}$ with the corresponding eight regions in the two Riemann sheets for k_z^2. The evanescent regions could be absorbing or amplifying as explained in the text, depending on the sign of ε' and μ'. The sign of the square root for the region is shown enclosed in a small circle.

however, does not violate causality as the Poynting vector/energy flow decays exponentially to zero at infinity and no information flows in from the infinities. This counter-intuitive behaviour does not imply that source has turned into a sink—rather it indicates that there would be a large (infinitely large for unsaturated linear gain) accumulation of energy density (intense local field enhancements) near a source. Now propagating waves in media with $\varepsilon' < 0$ and $\mu' < 0$ simultaneously are included in regions 4 and 5, depending on whether $\varepsilon'\mu'' + \varepsilon''\mu' < 0$ or $\varepsilon'\mu'' + \varepsilon''\mu' > 0$, respectively, corresponding to absorbing or amplifying media. In both cases, the negative sign of the square root needs to be chosen, justifying calling these media with both $\varepsilon < 0$ and $\mu < 0$ negative refractive index media. In the case of normal incidence, the sign of the wave-vector and the sign of the refractive index are the same. The quantity $\varepsilon'\mu'' + \varepsilon''\mu'$ determines the energy flow which has also been recently noted by Depine and Lakhtakia [105]. In dissipative media $\mathrm{Im}(k_z) < 0$ for propagating waves, which reduces to $\mathrm{Im}(n) > 0$ for normal incidence as noted in [106]. Thus, one can more reasonably talk of NRMs as media in which radiation has a *negative phase velocity* rather than a negative group velocity.

3.2. Some effects of a reversed wave-vector

Now let us look at some of the effects of a reversed wave-vector in some detail. Veselago [1] has discussed some of these effects in his original paper[4].

3.2.1. The modified Snell's law of refraction. The refraction of radiation at the interface of a positive medium and a negative medium has been one of the most discussed issues. Consider the electromagnetic plane wave incident on an NRM from a positive medium with a wave-vector $(k_x, 0, k_{z+})$. From the discussion in section 3.1, it is clear that the continuity of the fields and Maxwell's equations require the transmitted wave-vector to be $(k_x, 0, k_{z-})$, where k_{z-} is the negative square root in equation (3.5). Noting that Poynting vector is oriented exactly opposite to the phase vector, $\boldsymbol{k}$, in the NRM, we realize that the ray representing the energy

[4] In addition to the effect discussed here, Veselago has also suggested a reversed radiation pressure in NRMs. The problem of radiation pressure even in ordinary dispersive media is controversial [107] and we will not discuss this problem in structured NRMs and meta-materials here.

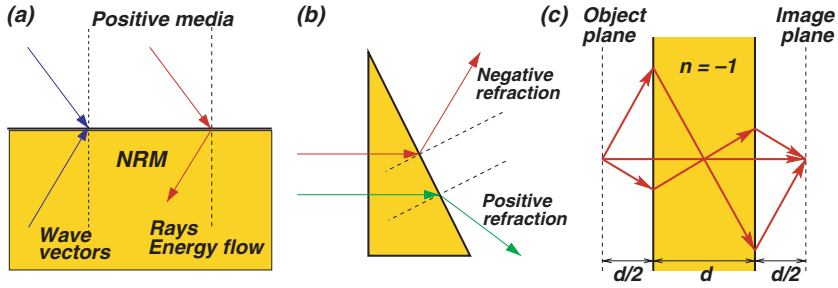

Figure 15. (*a*) Schematic depiction of the negative refraction at an interface between a positive medium and an NRM. The energy flow and the phase vectors are in opposite directions in the NRM. (*b*) The negative refraction effect through a prism. (*c*) The Veselago lens consisting of a slab of NRM that can focus a point source from one side of the slab to the other side.

flow corresponding to the refracted wave should now lie on the other side of the normal as shown in figure 15(*a*). This *negative* angle can also be intuitively inferred from Snell's law,

$$n_+ \sin\theta_+ = n_- \sin\theta_-, \tag{3.6}$$

where $n_- < 0 \Rightarrow \theta_- < 0$. The modification of the Snell's law is counter to a very fundamental concept in optics of isotropic media that, depending on how dense the second medium is, the refracted wave can bend as close to the normal as possible, but never cross it. In this case, the refracted beam actually emerges on the other side of the normal[5]. Note, however, that the angle of the reflected beam remains unaffected. Figure 15(*b*) shows the negative refraction through a prism which was used in the experiments of [5, 25].

As a direct consequence of this we have the result that a flat slab of an NRM[6] with $n = -1$ can focus a source as shown in figure 15(*c*). This lens is different from the usual optical lens with curved surfaces in that it does not focus rays from infinity to a point. These rays would simply pass through unaffected. On the other hand, rays emanating from a point source located at a distance d_1 on one side of the slab would be refocused to a point at a distance d_2 on the other side, provided that $d_1 + d_2 = d$, where d is the thickness of the slab. In fact, the total phase shift accumulated by any wave in going from the source point to the image point is zero as a consequence of the negative phase vector inside the NRM[7]. This is in contrast to the phase corrections that are made to different rays in a conventional lens. Consider now the behaviour of traditional curved lenses made of NRMs. Note that the phase accumulated due to traversal through the NRM is negative. Hence a convex lens causes a plane wave to diverge while a concave lens causes the plane wave to become convergent.

3.2.2. The reversed Doppler shift. Assume a moving source emitting radiation at a frequency ω in an NRM with a velocity $\boldsymbol{v}$ with respect to the medium. The frequency measured by a detector in the frame of the NRM is

$$\omega' = \gamma(\omega + \boldsymbol{k}\cdot\boldsymbol{v}), \tag{3.7}$$

where $\gamma = (1 - v^2/c^2)^{-1/2}$ is the relativistic factor. Noting that $|\boldsymbol{k}| = n\omega/c$, for emission along the direction of the motion of the source in the NRM (say, with $n = -1$)

$$\omega = \sqrt{\frac{c - v}{c + v}}, \tag{3.8}$$

[5] Note that negative refraction is possible in anisotropic media as well [108, 109].
[6] This is also called a Veselago lens today.
[7] In a sense, the phase unfolds inside the NRM and it is almost as if time runs backwards [110].

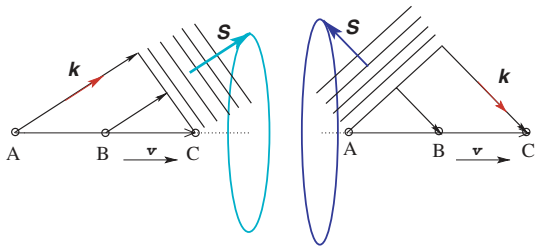

Figure 16. The Cerenkov radiation cone angle is modified for a reversed phase vector. There is constructive interference for emission only in one direction. The phases of the wavefront emitted by the particle at A, B and C have to be identical. The case on the left represents Cerenkov radiation in a positive medium with positive $\boldsymbol{k}$ while the figure on the right shows the emission in a medium with negative $\boldsymbol{k}$.

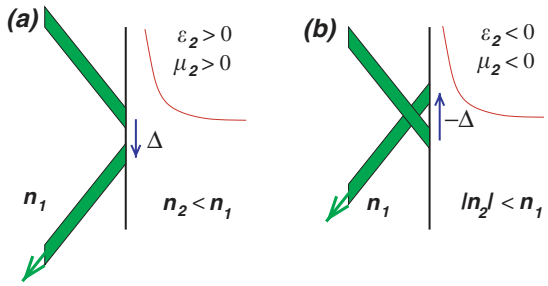

Figure 17. Schematic showing the transverse displacement of a beam of radiation undergoing total internal reflection. The GH shift is negative for reflection from NRMs.

i.e. the frequency measured by a detector would be smaller when the source is moving towards it! This is counter to the frequency increase that we would get in a normal medium. Again it is the reversed phase vector in NRMs that is responsible for this reversed Doppler shift.

3.2.3. An obtuse angle cone for Cerenkov radiation. A charged particle moving at relativistic speeds through a medium emits Cerenkov radiation in a cone of angles if its speed exceeds that of light in the medium. The angle of this cone is defined by the condition that the emitted radiation interferes constructively only in that direction while destructively interfering in all others. This condition is satisfied (see figure 16) along an acute angle defined by $\cos\theta = c/(nv)$. This angle, however, becomes obtuse for constructive interference in NRMs due to the reversed phase vector as is clear from figure 16, i.e. $\theta \to \pi - \theta$. In reality, due to the dispersion in the material parameters of the NRM, there will be Cerenkov radiation in both the forward and backward directions for different frequencies [111]. This modified cone for Cerenkov radiation has been numerically demonstrated for photonic crystals that exhibit the negative refraction effect [112].

3.2.4. Reversed Goos–Hänchen shift. When light is incident upon an optically rarer medium 2 from an optically denser medium 1 (the refractive indices $n_1 > n_2$), there is a critical angle of incidence, θ_c, given by

$$\sin\theta_c = \sqrt{\frac{\varepsilon_2\mu_2}{\varepsilon_1\mu_1}}, \tag{3.9}$$

beyond which the wave in medium 2 is evanescent and the radiation is completely reflected back into medium 1. For a beam of light with a finite transverse extent, this is also accompanied

by a shift of the beam in the transverse direction as shown in figure 17. This shift occurs usually along the parallel component of the wave-vector and was experimentally first demonstrated by Goos and Hänchen [113]. It turns out that the Goos–Hänchen (GH) shift is also negative for reflection from NRMs [114–117].

Artmann showed [118] that for angles of incidence sufficiently away from the critical angle and the grazing angle, the beam is displaced by

$$\delta_{gh} = -\frac{\partial \Phi_r}{\partial k_{x1}}, \tag{3.10}$$

where Φ_r is the phase shift for the reflected beam and k_{x1} is the parallel component of the wave-vector in medium 1. Now consider the reflection coefficient for p-polarized radiation:

$$r = \frac{k_{z1}\varepsilon_1 - k_{z2}\varepsilon_2}{k_{z1}/\varepsilon_1 + k_{z2}/\varepsilon_2}. \tag{3.11}$$

We note that for total internal reflection, $k_{z2} \to \mathrm{i}\kappa_z$ is imaginary. Now if we simultaneously make negative the signs of μ_2 and ε_2, κ_z remains unchanged. However the reflectivity from the NRM medium $r_- = 1/r_+ = \mathrm{e}^{-\mathrm{i}\Phi_r}$, where $r_+ = \mathrm{e}^{\mathrm{i}\Phi_r}$ is the coefficient of reflection from a medium with positive ε and μ. Clearly the GH shift will be negative. A similar analysis holds for the s-polarized radiation with μ replacing the corresponding ε in our analysis. Note that it is actually sufficient to make only $\varepsilon < 0$ for the p-polarization and $\mu < 0$ for the s-polarization to obtain a negative GH shift. It has been shown that the negative GH shift can be very large due to surface plasmon states [119], and negative GH shifts have also been shown for layered systems of positive and negative media [120]. The GH shift does not, however, violate causality, and a pulse would take a finite amount of time to undergo the transverse shift. This effect is primarily due to the evanescent fields in the second medium.

3.3. Phase velocity, group velocity and energy flow

The wave-vector $\boldsymbol{k}$ in an isotropic NRM points opposite to the direction of the Poynting vector $\boldsymbol{S} = \boldsymbol{E} \times \boldsymbol{H}$ which gives rise to the negative refraction effect. Thus it is clear that the phase velocity $\boldsymbol{v}_\phi = \boldsymbol{k}/\omega$ is negative. However, the energy flow is along the Poynting vector and away from a source. The group velocity, defined as $\boldsymbol{v}_g = \nabla_{\boldsymbol{k}}\omega(\boldsymbol{k})$, is usually along the direction of the Poynting vector for reasonably narrow-band pulses and thus should be oriented opposite to the phase velocity. We do note that the very concept of a group velocity can fail for broad-band pulses which can be distorted easily due to dispersion [121]. We note that the phase velocity and the Poynting vector do point in different directions in anisotropic media and they can also point in opposite directions in anisotropic media [108]. Hence this point need not surprise us greatly.

However, the negative refraction effect and the group velocity in an NRM have been the subject of some interesting debate [7,122]. Valanju *et al* [7] analysed the interference fronts of two waves with slightly differing frequencies and found that the interference fronts refracted in the positive sense (see figure 18). Misinterpreting the normal of these interference fronts to be along the group velocity, it was claimed that the refraction at an interface between a positive medium and an NRM was positive. First of all, the group velocity in a homogeneous isotropic medium can be expressed as [122]

$$\boldsymbol{v}_g = \nabla_{\boldsymbol{k}}\omega(k) = p\frac{\boldsymbol{k}}{k}\frac{\mathrm{d}\omega(k)}{\mathrm{d}k}, \tag{3.12}$$

where $p = \pm 1$, depending on the choice of sign of the square root as the frequency does not depend on the direction due to isotropy. This means that the group velocity can only be parallel

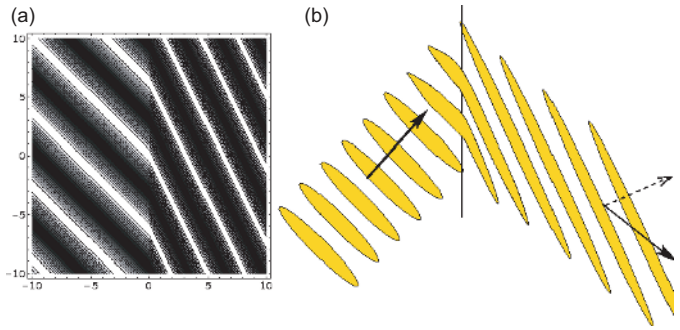

Figure 18. The interference patterns of two superimposed waves with slightly differing frequencies refracting at an interface between negative and positive refractive media. (*a*) The case of infinite plane waves when the interference fronts appear to refract positively. (*b*) A schematic picture of the refraction of beams with finite transverse size at slightly differing frequencies. Although the interference patterns appear to refract positively, the beams (energy flow) are seen to refract negatively. The sidewise motion of the interference fronts is not apparent in the case of infinitely extended plane waves.

(in a positive medium) or anti-parallel (in an NRM) to the phase velocity. The point is that the velocity of the interference fronts would coincide with the group velocity only if the waves have wave-vectors in the same direction with slightly differing magnitudes (frequencies). Due to dispersion in $\varepsilon(\omega)$ and $\mu(\omega)$ in the NRM, the two waves with differing frequencies would refract at slightly differing angles. Now the constitutive waves of the interference patterns in the NRM no longer point in the same direction and the corresponding interference front no longer propagates along the direction of the group velocity. In fact, a simulation using Gaussian beams [123] with slightly differing frequencies clearly showed that the beam suffers negative refraction while the normal of the interference fronts points in a completely different direction that would correspond to a positive angle of refraction. In fact this is true of any wave packet that is localized in the transverse direction [124, 125] and this motion is not apparent in the case of plane waves due to their infinite transverse extent. The numerical calculations of Caloz *et al* [126] showed that the refracted power in a waveguide bend filled with an NRM was along the angle for negative refraction. Pacheco *et al* [127] analytically calculated the Poynting vector for the refraction of a multi-frequency plane wave and found that the power flow was indeed along the angle for negative refraction. Interestingly an energy velocity $\boldsymbol{v}_{\mathrm{E}} = \boldsymbol{S}/u$ can be defined, where $\boldsymbol{S}$ is the Poynting vector and u is the average electromagnetic energy density. As pointed out, it is difficult to define u in a dispersive medium, and this quantity has not been well investigated for an NRM yet.

Foteinopoulou *et al* [128] have shown through numerical finite difference time domain (FDTD) calculations that the negative refraction of a beam experiences a long delay at the interface but the beam refracts in the NRM along the negative refraction angle. The FDTD calculations of Cummer [176] have also indicated that there is indeed a discontinuity in the phase front of the wave at the interface, but the phase discontinuity was shown to be causal. The group delay of a pulse propagating through a slab of NRM is also of great interest. For narrow-band pulses, the group delay time is $\tau_\phi = (\partial\phi)/(\partial\omega)|_{\omega_{\mathrm{c}}}$, where $\phi(\omega)$ is the phase of the transmission or reflection coefficient and ω_{c} is the carrier frequency of the pulse within the group velocity description. Dutta Gupta *et al* [129] have shown that the phase delay time for transmission across a slab of NRM is usually large (subluminal) and note interestingly that superluminal delay times can be obtained in the frequency region of plasma-like behaviour, $\omega_{\mathrm{m}} < \omega < \omega_{\mathrm{p}}$.

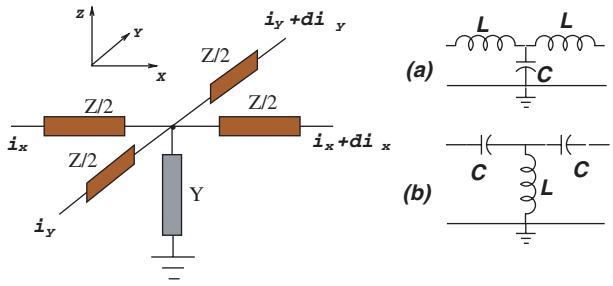

Figure 19. A transmission line network with distributed impedance and admittance. Choice of (*a*) for the inductances gives the usual transmission line with positive propagation constant, while (*b*) yields a backward wave structure in which the phase and group velocities are opposite.

3.4. Backward wave structures and transmission lines

There is another completely independent approach based on the theory of transmission lines to making NRMs [130–132]. This takes advantage of the fact that dielectric and magnetic materials can be modelled using distributed L–C networks. At radio-frequencies, this can be easily achieved by using lumped elements.

Consider the two-dimensional distributed network shown in figure 19. The system has an associated series impedance (Z) and shunt admittance (Y) per unit length. Concentrating on one section in the medium, one can write the equations for the potentials across the section,

$$\frac{\partial V}{\partial x} = ZI_x, \qquad \frac{\partial V}{\partial y} = ZI_y \tag{3.13}$$

and using Kirchoff's law, one can equate the currents in and out of the node,

$$\frac{\partial I_x}{\partial x} + \frac{\partial I_y}{\partial y} = YV. \tag{3.14}$$

Eliminating the currents, we obtain the Helmholtz equation:

$$\frac{\partial^2 V}{\partial x^2} + \frac{\partial^2 V}{\partial y^2} + \beta^2 V = 0, \tag{3.15}$$

where $\beta^2 = -ZY = -Z/Z'$, $Z' = Y$. As usual we have the same problem of a physical choice of the sign for the propagation constant, which will now depend on the impedances Z and Z'. Let us note that for a TE field (where the electric field E_z is perpendicular to the wave-vector) in a waveguide in the X–Y plane, we have the Maxwell's equations

$$\frac{\partial E_z}{\partial x} = -\mathrm{i}\omega\mu H_y, \qquad \frac{\partial E_z}{\partial y} = \mathrm{i}\omega\mu H_x, \tag{3.16}$$

$$\frac{\partial H_y}{\partial x} - \frac{\partial H_x}{\partial y} = -\mathrm{i}\omega\varepsilon E_z. \tag{3.17}$$

Mapping the voltage $V \to E_z$, the currents $I_x \to -H_y$ and $I_y \to H_x$, we identify the equivalent impedances of the material parameters

$$Z = -\mathrm{i}\omega\mu \qquad \text{and} \qquad Z' = \frac{1}{-\mathrm{i}\omega\varepsilon}. \tag{3.18}$$

If we choose $Z = -\mathrm{i}\omega L$ and $Z' = -1/\mathrm{i}\omega C$, where L and C are the inductance per unit length and capacitance per unit length as in figure 19(*a*), we obtain the propagation constant $\beta = \omega\sqrt{LC} = \omega\sqrt{\varepsilon\mu}$. The phase velocity for the wave in the distributed network is

$v_\phi = \omega/\beta = 1/\sqrt{LC} = 1/\sqrt{\varepsilon\mu}$ and the group velocity $v_g = (\partial\omega)/(\partial\beta)$ turns out to be the same. This is the case of usual positive media where the phase velocity and the group velocity are in the same direction. In fact $L = \mu_0$ and $C = \varepsilon_0$ yield us the equivalent circuit for vacuum with a characteristic impedance for the network of $Z_0 = \sqrt{\mu_0/\varepsilon_0} \simeq 377\,\Omega$.

This implies that the configuration in figure 19(*b*) has $Z = 1/-\mathrm{i}\omega C$ and $Z' = -\mathrm{i}\omega L$ and thereby the propagation constant is

$$\beta = -\frac{1}{\omega\sqrt{LC}}, \tag{3.19}$$

where the negative sign of the square root has been chosen. This is so that the group velocity (which is along the Poynting vector),

$$v_g = +\omega^2\sqrt{LC}, \tag{3.20}$$

is positive. Thus the phase velocity $v_\phi = -\omega^2\sqrt{LC}$ is opposite in this medium and we do have a backward wave in the distributed network. Thus the distributed LC network in the high-pass configuration behaves as a waveguide filled with an NRM.

Now we note that any practical implementation of such a backward wave structure would involve lumped L–C elements in a network, which would bring in its own associated length-scale, at which we periodically or randomly insert the lumped elements, and its corresponding band structure. To justify our assumption of a homogeneous medium we would require that the associated periodicity be much smaller than the wavelength of the radiation. The effective dielectric permittivity and the magnetic permeability at low frequencies for the periodically loaded medium can be approximated as [132]

$$\varepsilon_{\mathrm{eff}} = \varepsilon - \frac{1}{\omega^2 Ld}, \qquad \mu_{\mathrm{eff}} = \mu - \frac{1}{\omega^2 Cd}, \tag{3.21}$$

where ε and μ are due to the distributed capacitances and inductances due to the short interconnecting segments of length d between the lumped elements, acting as a host medium. At high frequencies, the propagation delays dominate and the medium is a positive index medium with $n = \sqrt{\varepsilon\mu}$. On the other hand, at low frequencies, the loading elements dominate and we have an NRM with a negative phase velocity and a refractive index of $1/\omega d\sqrt{LC}$.

Such backward wave structures show all the hallmarks of an NRM such as a modified Snell's law at an interface between a forward wave and backward structures. These have a great advantage of a large bandwidth.

3.5. Negative refraction effect in photonic crystals

Although photonic crystal and band-structure materials strictly cannot be considered to be homogeneous meta-materials, it has been pointed out that there is a very interesting negative refraction effect that can take place in photonic band-gap (PBG) media [36, 133]. The constituents of such a PBG medium are materials with positive refractive index, but a propagating ray incident on this medium appears to undergo negative refraction at the interface. This effect can usually be dismissed as a diffraction grating effect if it occurs only for certain wave-vectors. But there is a regime when this happens to all propagating waves within a certain frequency band, referred to as *all angle negative refraction* [36].

The secret to the all-angle negative refraction effect is that for strongly modulated PBG media the equifrequency surfaces in the k-space can become completely smooth convex surfaces around certain points of symmetry, for example the M point for a square lattice (see figure 20) for a band of frequencies. Such situations typically occur near the band edges, and the size of the convex equifrequency surface reduces with increasing frequency. This

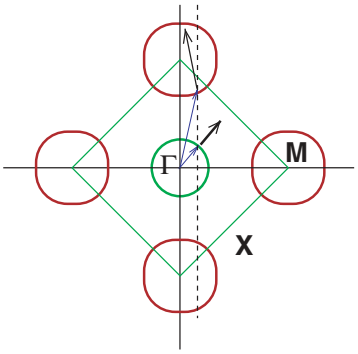

Figure 20. Schematic of the equifrequency surface for all-angle negative refraction for a square lattice. The dotted line is normal to the interface and shows the conservation of the parallel wave-vector. The thin lines show the wave-vector, while the thick lines which are the normals to the equifrequency surface denote the group velocities.

means that the group velocity is along the inward normal to these surfaces. If this situation results in the lowest photonic band, then the incoming wave couples to a single Bloch wave in the photonic crystal. The resulting diffraction will appear to be in the negative refraction sense. A schematic is shown in figure 20 for the *refraction* process in the case of a square lattice. The equifrequency surface is a convex surface around the M point and the incoming wave couples to a single Bloch wave in the negative refraction direction. There is a crucial condition that this equifrequency surface should be convex everywhere and have a larger size than a free space dispersion circle, so that every incoming wave couples to a Bloch wave. Note, however, that the group velocity and the phase velocity in the PBG medium are never anti-parallel as in the case of an isotropic NRM and $\boldsymbol{k} \cdot (\partial\omega)(\partial\boldsymbol{k}) \geqslant 0$ in the entire band. These frequency regions, however, do have a negative *effective mass*. Using a PBG medium of airholes in a dielectric, an all-angle negative refraction and a flat Veselago lens were demonstrated numerically by Luo *et al* in two dimensions [36] and three dimensions [134].

Note, however, that the equifrequency surface of the PBG medium need not be very spherical or circular. This leads to the fact that most of the radiation may couple mainly along one direction in photonic crystal (along [110] in figure 20). Thus the radiation might appear to stream along one direction [135, 136]. This would render the image that should be formed inside the NRM in the Veselago lens unobservable. Thus the negative refraction effect in the case of PBG materials can have an interpretation entirely in terms of band-structure effects without resorting to the idea of a negative refractive index. Further, although the concept of an effective refractive index might be useful near the band edges particularly with the lowest frequency bands, homogenization in the sense of meta-materials is difficult to achieve here. Although the free space wave-vector may be a few times larger than the unit cell of these PBG materials, the energy transport in these materials is still very sensitive to the periodicity and structural arrangements. Therefore, the propagation can be mainly considered as due to Bragg scattering, rather than due to a negative refractive index. But the PBG media which have all-angle negative refraction can be used to make unique photonic devices that can tailor the propagation.

3.6. Nonlinear effects in negative refractive media

One of the main aspects of the meta-materials is that the resonant nature of the effects makes the local microscopic fields in them highly inhomogeneous and fairly intense. There can

be immense enhancement of the local fields in these systems and the potential for nonlinear applications was pointed out in the very first paper on the SRR structure [3]. In fact, it is the intense magnetic fields in the vicinity of the wires in the case of the thin wire structures that makes them work as a low frequency plasma. SRRs also similarly concentrate the electric fields in the tiny capacitive gaps, and this leads to enormously enhanced local electric fields.

Consider the single ring SRR with two splits. The electric field across the capacitive gaps is $E_c = V_c/d_c$, where V_c is given by equation (2.37), yielding us

$$E_c(\omega_0) = \frac{\mu_0 \omega_p^2 r \tau_c}{2\gamma L_c}. \tag{3.22}$$

For the incident radiation, the energy is equally distributed between the electric and magnetic fields. Hence we obtain an enhancement factor of

$$\mathcal{Q} = \frac{1}{2}\frac{1/2\varepsilon_0|E_c(\omega_0)|^2}{1/2\mu_0|H_{ext}(\omega_0)|^2} = \frac{1}{8c^2}\left[\frac{r\tau_c\omega_p^2}{2\gamma L_c}\right]^2 \tag{3.23}$$

for the energy stored in the capacitive gaps at resonance, where the factor of 2 accounts for the fact that we have two gaps in our system. Typical numbers for this factor range from 10^4 to 10^6 [3, 28].

Regardless of the frequency of interest, the nonlinear Kerr effect in a dielectric is always possible [137]. This is a typical nonlinearity where the refractive index of the dielectric depends on the electromagnetic fields as

$$n = \sqrt{\varepsilon} = n_0 + n_2 I, \tag{3.24}$$

where $I = 1/2(\varepsilon/\mu)^2\varepsilon_0 c|E|^2$ is the intensity of light. The sign of n_2 can be positive or negative, and it is called a focusing or defocusing nonlinearity, respectively. Suppose the capacitive gap in the SRR is filled with a Kerr nonlinear dielectric; then large changes can be expected in response to the applied electromagnetic fields by virtue of the enhanced electric fields in the gaps. The capacitance of the SRR, and hence the resonant frequency, now becomes a function of the incident field strengths. Consider a meta-material of SRR with a nonlinear dielectric in the capacitive gaps. A relation between the incident field strength and the nonlinear resonance frequency can be obtained in a quasi-static calculation as [22, 138]

$$|H_{ext}|^2 = \frac{Z_d n^2 d_c^2}{4n_2 L_c^2 \omega_0^2}\frac{(1-x^2)[(x^2-\Omega^2)^2 + \Omega^2\Gamma'^2]}{\Omega^2 x^6}, \tag{3.25}$$

where $\Omega = \omega/\omega_0$, $x = \omega_{NL}/\omega_0$, $\Gamma' = \Gamma/\omega_0$, ω_0 is the resonance frequency for the SRR embedded in the linear material and ω_{NL} is the resonance frequency for the SRR imbedded in the nonlinear material. The plot of the nonlinear resonance frequency against the field strength is shown in figure 21 and the bistable behaviour is reasonably stable against dissipation. The material now switches between a negative magnetic medium ($\mu < 0$, $\varepsilon > 0$) with high reflectivity and a positive medium ($\mu > 0, \varepsilon > 0$) which can almost be transparent, depending on the incident intensity. Use of this mechanism to switch the behaviour of the meta-material of thin wires and SRR composites from a negative refractive index to a positive index or plasma-like behaviour has been suggested [138].

The intense field enhancements in meta-materials make this a very fertile ground for nonlinear optics. Phase matching conditions which are crucial in nonlinear optics can be met in a different manner in NRMs, leading to qualitative changes in the nonlinear responses. This has been pointed out in the context of second harmonic generation and stimulated Raman scattering [139]. The intense local field enhancements also make the SRR very sensitive to any absorbing molecular species in the regions of large fields, indicating the potential for use in molecular probes. Ultrashort pulse propagation in these media would be interesting in view of the very large dispersion in these media.

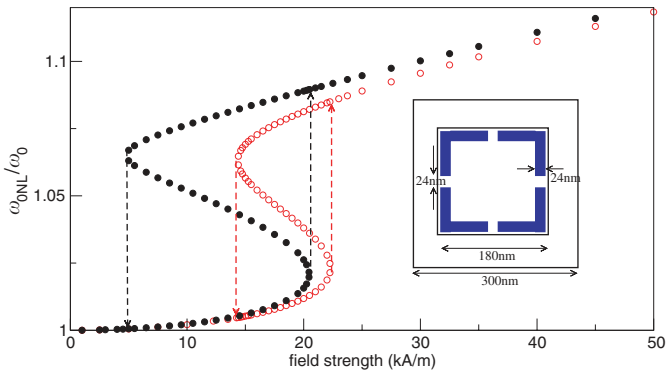

Figure 21. The nonlinear resonant frequency versus the field strength for two values of the dissipation rate: filled circles are for γ of silver and the open circles for 3γ. The inset shows the SRR structure with the relevant dimensions. The inner box shows the nonlinear medium just enclosing the SRR structure.

3.7. Surface electromagnetic modes in NRMs

Any material with a negative material permittivity and permeability permits the existence of surface modes on the interfaces with positive media. NRMs permit both p- and s-polarized surface modes, and this topic has received some attention recently [140–147].

Let us first examine the nature of the surface plasmons (for p-polarized incident light) at a single flat interface between semi-infinite positive and negative media. The condition for the existence of a surface plasmon at the interface is [32]

$$\frac{k_{z1}}{\varepsilon_+} + \frac{k_{z2}}{\varepsilon_-} = 0, \tag{3.26}$$

which gives the dispersion relation

$$k_x = \frac{\omega}{c}\left[\frac{\varepsilon_-(\varepsilon_- - \mu_-)}{\varepsilon_-^2 - 1}\right]^{1/2}, \tag{3.27}$$

assuming $\varepsilon_+ = 1$ and $\mu_+ = 1$ for the positive medium. For the sake of simplicity we will assume the causal plasma-like forms $\varepsilon_2 = 1 - \omega_p^2/\omega^2$ and $\mu_2 \simeq 1 - \omega_{mp}^2/\omega^2$ for the NRM. We omit dissipation to obtain the dispersion. The corresponding dispersion for the plasmon mode is plotted in figure 22. We can see that the plasmon dispersions take different forms for $\omega_{mp} > \omega_p$ (the upper curve) and $\omega_{mp} < \omega_p$ (the lower curve). At large k_x, the plasmon frequency tends to the electrostatic limit of $\omega_p/\sqrt{2}$ from either above ($\omega_{mp} > \omega_p$) or (below $\omega_{mp} < \omega_p$). At small k_x, the surface plasmon first appears at the light-line ($\omega = ck_x$). Note that the situation for the s-polarized mode is just the other way around: the lower curve would describe the s-polarized mode for $\omega_{mp} < \omega_p$ and the upper curve for $\omega_{mp} > \omega_p$. In both cases, the plasmon whose dispersion is given by the upper curve has a negative group velocity in the transverse direction. Similar results using a resonant form for the magnetic permeability have been obtained in [140, 143]. Then there are two branches to the p-polarized modes for $\omega_{mp} < \omega_p$, one below the magnetic resonant frequency when $\mu > 0$, $\varepsilon < 0$ and similarly one more above the magnetic plasma frequency.

Next let us examine the nature of the surface modes in a thin slab of NRM. As is well known, the two degenerate surface plasmons at the two interfaces get coupled for a thin slab and gives rise to coupled slab modes: a symmetric and an antisymmetric mode, also called slab

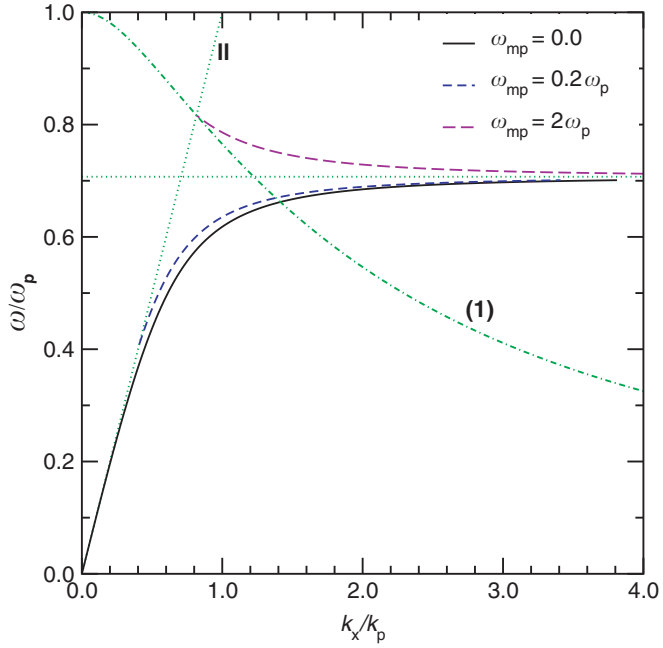

Figure 22. The dispersion for the surface plasmon at an interface between a negative medium and a positive medium when the effects of dispersion are included. The frequency axis is scaled with respect to the bulk plasmon frequency (ω_p) and the k_x axis is scaled with respect to $k_p = w_p/c$. The light line $\omega = ck_x$ and the $\omega = \omega_s = \omega_p/\sqrt{2}$ line are given by the dotted lines. The dispersion inside the infinite negative medium, $\omega = ck_x/\sqrt{\varepsilon_2\mu_2}$ with $\omega_{mp} = 2\omega_p$, is shown by the chain curve (1).

plasmon polariton modes. The condition for these resonances (for p-polarized light) are [32]

$$\tanh\left(\frac{k_z^{(2)}d}{2}\right) = -\frac{\varepsilon_2 k_z^{(1)}}{k_z^{(2)}}, \tag{3.28}$$

$$\coth\left(\frac{k_z^{(2)}d}{2}\right) = -\frac{\varepsilon_2 k_z^{(1)}}{k_z^{(2)}}, \tag{3.29}$$

where $k_z^{(j)} = \sqrt{k_x^2 - \varepsilon_j\mu_j\omega^2/c^2}$. Using the above conditions, the dispersion relation for the coupled surface modes can be obtained and we show them in figure 23, where again we have assumed the dispersive forms $\varepsilon(\omega) = 1 - \omega_p^2/\omega^2$ and $\mu_2 = 1 - \omega_{mp}^2/\omega^2$. We find that the finite frequency changes the dispersion from the electrostatic limit (where it is given by $\omega = \omega_p\sqrt{1 \pm \exp(-k_x d)/\sqrt{2}}$). The dispersion relations are qualitatively different for $\omega_{mp} < \omega_p$ (or $\mu_2(\omega_s) > -1$) and $\omega_{mp} > \omega_p$ (or $\mu_2(\omega_s) < -1$). Physically, the behaviour of both the symmetric and the antisymmetric modes, at large k_x, have to tend to the uncoupled plasmon dispersion for a single surface. Ruppin [141] has calculated the dispersions of these slab modes using a resonant form for μ and again obtained two branches. Interestingly we can also have waveguide modes in the slab when $\varepsilon < 0$, $\mu < 0$ and the refractive index of the slab is higher than that of vacuum as shown in figure 23. These new waveguide modes are absent in slabs with only one of ε or μ negative.

The surface plasmon resonances can have a great effect on the scattering properties of materials and on the radiation in the vicinity of these surfaces. The dispersion of the surface modes is a function of the geometry of the surface. Ruppin [144] has derived the Mie scattering

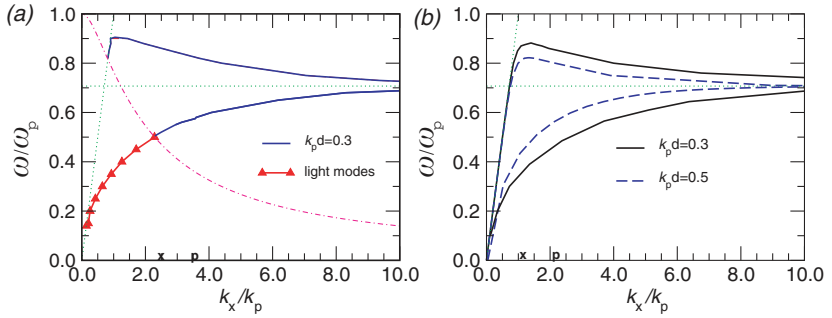

Figure 23. The dispersion for the coupled surface plasmons when the effects of retardation are included. The frequency axis is scaled with respect to the bulk plasmon frequency ($\omega_{\rm p}$) and the k_x axis is scaled with respect to $k_{\rm p} = w_{\rm p}/c$. The light-line $\omega = ck_x$ and the $\omega = \omega_{\rm p}/\sqrt{2}$ line are given by ($\cdots\cdots$). (*a*) $\mu = 1 - \omega_{\rm mp}^2/\omega^2$ with $\omega_{\rm mp} = 2\omega_{\rm p}$. The dispersion in the infinite negative medium, $\omega = ck_x/\sqrt{\varepsilon_2\mu_2}$, is shown by (— · —). The part of the lower branch with the $\diamond$ symbol shows the non-radiative light modes within the slab. (*b*) $\mu_2 = +1.0$.

coefficients for an NRM sphere and obtained new resonances corresponding to the negative magnetic permeability. Similarly the Mie scattering properties of a cylinder [148] made of an NRM have revealed the presence of new resonances in the NRM frequency band. Klimov [145] has also discussed the new TM scattering resonances due to a negative μ as well as the whispering gallery modes due to a negative refractive index in the scattering properties of an NRM sphere. The substantial changes to the spontaneous decay rates in the vicinity of an NRM has also been pointed out.

4. The perfect lens

One of the most debated consequences of negative refraction is the possibility of a perfect lens whose image resolution is not subject to the limitations of the traditional diffraction limit of a wavelength. Indeed the proposal for *a perfect lens* [6] has provoked heated debates and caught the imagination of the scientific community at large. It turns out that Veselago's flat slab of NRM with $\varepsilon = -1$ and $\mu = -1$ not only focuses the propagating radiations as shown by a ray picture, but also focuses the evanescent non-propagating components of radiation that are usually confined to the immediate vicinity of a source. The latter components are associated with the spatial features of the source at a sub-wavelength length-scale and the focusing action for the evanescent waves is accomplished through the surface states that reside on the NRM surfaces. This result has now been generalized to several configurations of NRMs [149]. It turns out that the focusing of the evanescent components is quite sensitive to imperfections in the NRM, and this does somewhat curtail the sub-wavelength focusing capabilities of the lens. Sub-wavelength image resolution, to quite some extent, is possible even with these imperfect lenses, which we will henceforth refer to as *super-lenses*. In this section, we will discuss this phenomenon of focusing the near-field components and will address several of the much-debated issues.

4.1. Near-field information and the diffraction limit

One principle that is taught in optics courses even at the freshman level is *the diffraction limit*, that we can never resolve features in an image to better than the order of a wavelength [35]. First let us re-examine it here. Consider an extended source that emits or scatters radiation.

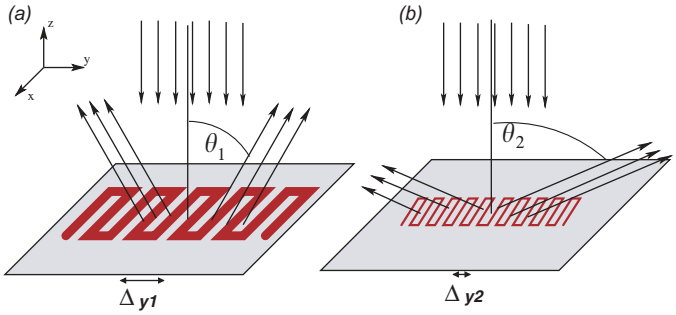

Figure 24. Radiation is scattered and emitted by an object. The angle at which light comes out depends on the spatial features of the source. A periodic object with large spatial period scatters the light through small angles (*a*), while the light comes out at large angles for a periodic object with small spatial periods (*b*).

For the time being assume it to be a planar object on the $z = 0$ plane and the optical axis for imaging along the z axis as shown in figure 24. Let $\boldsymbol{E}(x, y, 0)$ be the associated electric field. Now the electromagnetic fields over all space can be written down as

$$\boldsymbol{E}(x, y, z; t) = \left(\frac{1}{2\pi}\right)^2 \int_{k_x}\int_{k_y} \mathrm{d}k_x\, \mathrm{d}k_y \mathcal{E}(k_x, k_y) \exp[\mathrm{i}(k_x x + k_y y + k_z z - \omega t)], \tag{4.1}$$

where ω is the frequency of the radiation and

$$\mathcal{E}(k_x, k_y) = \int_x \int_y \mathrm{d}x\, \mathrm{d}y \boldsymbol{E}(x, y, 0) \exp[-\mathrm{i}(k_x x + k_y y)] \tag{4.2}$$

is the Fourier transform of the spatial variation of the source. The Maxwell equations impose the condition that

$$k_x^2 + k_y^2 + k_z^2 = \varepsilon_0 \mu_0 \frac{\omega^2}{c^2} = k_0^2 \tag{4.3}$$

in free space. Note that k_x and k_y represent the Fourier components of the spatial variation in the source in the corresponding directions.

Now $k_x = 2\pi/\Delta_x$ and $k_y = 2\pi/\Delta_y$, where Δ_x and Δ_y are some spatial periods of the variation. The source can have intensity or field variations over arbitrarily small distances. There is no restriction on that. As an example, consider the case of isolated molecules on a surface emitting radiation, in which case the $\Delta_{x,y}$ can literally be on atomic length-scales. The corresponding transverse wave-vectors k_x and k_y will then be very large, in which case the dispersion equation, equation (4.3), cannot be satisfied without making the associated k_z imaginary. Thus the waves with large $k_x > k_0$ and $k_y > k_0$ are evanescent and decay in amplitude exponentially away from the source $z = 0$ plane. These are the near-field modes of the radiation of the source and have a decay length of $1/k_{x,y} < \lambda/2\pi$. In conventional imaging systems, these modes are never detected as a consequence. Hence the corresponding source information about the fast varying features of the source is missing. The largest propagating wave-vector that contributes to the image is k_0 (assuming unit numerical aperture), and we obtain the corresponding spatial frequency of the wavelength, λ, to be the minimum limit on the spatial resolution in the image.

However note that this limitation can be side-stepped if the near-field modes of the source can be sampled. This is precisely what is done in near-field optical microscopy [150, 151], where a fine fibre tip is used to couple the near-field modes into the propagating modes in the fibre and detected. This does not violate any fundamental principle (such as the Heisenberg

uncertainty principle [152]). Although the transverse image resolution might be very small, the corresponding transverse component of the wave-vector is arbitrarily large. The essential higher dimensional (>1) nature of the problem makes this possible [153].

4.2. Pendry's proposal

Consider Veselago's lens consisting of a slab of NRM of thickness d with $\varepsilon = -1$ and $\mu = -1$ and surrounded by vacuum as shown in figure 25. Consider the source to be at $z = 0$ (the object plane): we wish to calculate the fields at $z = 2d$ (the image plane). First let us calculate the reflection and transmission coefficients for a plane wave incident on the NRM slab[8]: writing the solutions in terms of the partial reflection ($r_{jk}\ \forall j, k = 1, 2, 3$) and transmission coefficients ($t_{jk}\ \forall\ j, k = 1, 2, 3$) at the interfaces (see figure 25), we find

$$T = \frac{t_{21}t_{32}\,\mathrm{e}^{\mathrm{i}k_{z2}d}}{1 - r_{12}r_{21}\,\mathrm{e}^{2\mathrm{i}k_{z2}d}}, \tag{4.4}$$

$$R = \frac{r_{21} + r_{32}\,\mathrm{e}^{2\mathrm{i}k_{z2}d}}{1 - r_{12}r_{21}\,\mathrm{e}^{2\mathrm{i}k_{z2}d}}. \tag{4.5}$$

In this geometry, we have independent solutions for the p-polarized light (E field in the plane of reflection) and the s-polarized light (H field in the plane of polarization). The partial reflection and transmission Fresnel coefficients for the s-polarized light are

$$r_{21} = \frac{(k_{z1}/\mu_+) - (k_{z2}/\mu_-)}{(k_{z1}/\mu_+) + (k_{z2}/\mu_-)}, \qquad r_{12} = -r_{21}, \tag{4.6}$$

$$r_{32} = \frac{(k_{z2}/\mu_-) - (k_{z3}/\mu_+)}{(k_{z2}/\mu_-) + (k_{z3}/\mu_+)}, \tag{4.7}$$

$$t_{21} = \frac{2(k_{z1}/\mu_+)}{(k_{z1}/\mu_+) + (k_{z2}/\mu_-)}, \qquad t_{32} = \frac{2(k_{z2}/\mu_-)}{(k_{z2}/\mu_-) + (k_{z3}/\mu_+)}, \tag{4.8}$$

where μ_+ and μ_- are the permeability of free space and the NRM, respectively. Similarly, the partial reflection and transmission Fresnel coefficients for the p-polarized light are

$$r_{21} = \frac{(k_{z1}/\varepsilon_+) - (k_{z2}/\varepsilon_-)}{(k_{z1}/\varepsilon_+) + (k_{z2}/\varepsilon_-)}, \qquad r_{12} = -r_{21}, \tag{4.9}$$

$$r_{32} = \frac{(k_{z2}/\varepsilon_-) - (k_{z3}/\varepsilon_+)}{(k_{z2}/\varepsilon_-) + (k_{z3}/\varepsilon_+)}, \tag{4.10}$$

$$t_{21} = \frac{2(k_{z1}/\varepsilon_+)}{(k_{z1}/\varepsilon_+) + (k_{z2}/\varepsilon_-)}, \qquad t_{32} = \frac{2(k_{z2}/\varepsilon_-)}{(k_{z2}/\varepsilon_-) + (k_{z3}/\varepsilon_+)}, \tag{4.11}$$

where ε_+ and ε_- are the dielectric permittivity of free space and the NRM, respectively. The z-components of the wave-vector are

$$k_{z1} = \sqrt{\frac{\varepsilon_+\mu_+\omega^2}{c^2} - k_x^2 - k_y^2} = k_{z3}, \tag{4.12}$$

$$k_{z2} = \pm\sqrt{\frac{\varepsilon_-\mu_-\omega^2}{c^2} - k_x^2 - k_y^2}, \tag{4.13}$$

where we have to choose the component of the wave-vector k_{z2} in accordance with the arguments of section 3.1. For propagating waves we will choose the negative sign, and for evanescent waves we will choose the positive sign.

[8] This can be done in several ways: one can use partial reflections from the interfaces and sum them up. Or one can take the eigensolutions for the fields inside and outside the slab, and apply appropriate boundary conditions on the fields at the interfaces. The same solution results, irrespective of the manner of calculation.

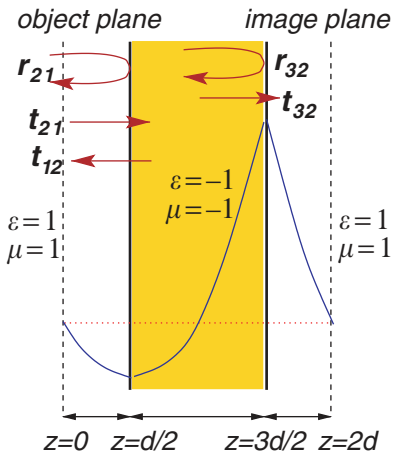

Figure 25. The perfect lens system consisting of a slab of NRM. The object, at a distance $d/2$ from the surface of the NRM, is focused on the other side of the slab. The restoration of the amplitude of an evanescent component is depicted schematically. The partial reflection/transmission coefficients across the boundaries are shown.

When the NRM has $\varepsilon_- = -\varepsilon_+ = -1$ and $\mu_- = \mu_+ = -1$, we obtain trivially for propagating waves that $k_{z2} = -k_{z1}$, and $t_{jk} = 1$ and $r_{jk} = 0$ due to the matched impedance. Hence for the slab

$$\lim_{\substack{\varepsilon_-\to-1\\ \mu_-\to-1}} T = \mathrm{e}^{-\mathrm{i}k_{z1}d}, \qquad \lim_{\substack{\varepsilon_-\to-1\\ \mu_-\to-1}} R = 0 \tag{4.14}$$

and this clearly shows that the total phase change for propagation from the object plane (at $z = 0$) to the image plane (at $z = 2d$) is zero. Thus we have the same results for the propagating waves as those yielded by a ray analysis.

Next consider the evanescent waves with $k_{z1} = \mathrm{i}\sqrt{k_x^2 + k_y^2 - \varepsilon_+\mu_+\omega^2/c^2} = \mathrm{i}\kappa_z$: then $k_{z2} = k_{z1}$ and the partial coefficients t_{jk} and r_{jk} diverge. However, the transmission and reflection coefficients for the slab are still well defined in this limit,

$$\lim_{\substack{\varepsilon_-\to-1\\ \mu_-\to-1}} T = \mathrm{e}^{+\kappa_z d}, \qquad \lim_{\substack{\varepsilon_-\to-1\\ \mu_-\to-1}} R = 0, \tag{4.15}$$

i.e. the slab actually increases exponentially the amplitude of the evanescent wave at the same rate by which it decays in free space. Thus the net amplitude change at the image plane (at $z = 2d$) from the object plane at $z = 0$ is zero (see figure 25. Thus we have that result the not only does the Veselago lens cancel the phase accumulation for the propagating waves, but it also restores the amplitudes of the evanescent components, bringing them both to a focus at the image plane. Further, the reflection is zero due to the impedance matching. Thus we have a lens that is unaffected by the diffraction limit as it includes all the components of the near-field too and hence it is a *perfect lens*. This result was demonstrated by Pendry in his now classic paper [6].

Note that the total transmission and reflection coefficients for the slab are well defined in spite of being the sum of a geometric series (of the partial waves [6]) whose terms can have magnitude greater than unity, and can even diverge in the case of evanescent waves. The calculation has been questioned on these grounds [154], but can be justified on grounds of analytic continuity: that the validity of the sum of an infinite series transcends the divergence of the series itself, provided that the sum was carried out to include all infinite terms and there

are no approximations [155]. In fact, we could have obtained the solution for the evanescent waves directly from that of the propagating waves by analytic continuation, $k_z \to \mathrm{i}\kappa_z$. Further note that the transfer matrix for the slab [35] is actually independent of the sign of the wave-vector. That means that the final solution is also independent of the sign of the wave-vector, but we choose the sign of the square root in accordance with section 3.1 for consistency.

The process of restoring the amplitudes of the evanescent components, henceforth called amplification by us[9] does not really involve any energy transport, as the Poynting vector associated with the evanescent waves in a lossless medium is strictly zero (see [156] for an elementary review). These are the steady state solutions of Maxwell's equations and give the field distributions essentially at infinite time. The large associated energy density in the NRM is obtained from the source itself and is built up over some time.

The perfect lens solutions are the exact conditions for the surface plasmons of both electric and magnetic nature on a surface of a semi-infinite NRM. The divergence of the partial reflection and transmission coefficients for the interfaces was just a manifestation of these resonances. The denominator of these coefficients going to zero is the condition for the homogeneous equation to have a non-trivial solution. It is these resonances that are responsible for the restoration or amplification of the evanescent near-fields of the source. This is a generic effect of a localized resonance for the Helmholtz equation—the transmission and reflection coefficients diverge. In fact, this amplification of the incident evanescent waves happens for the Schrödinger equation as well. Consider two identical separated localized potential wells (say a δ or a square well) in one dimension with the incident evanescent wave having the energy of one of the bound states of the wells. The evanescent wave amplifies in the region between the two potentials. It has been pointed out that the surface states on photonic band-gap media in the first Brillouin zone can also be used for the imaging of the near-fields [157].

In the limit of large wave-vectors ($k_x \to \infty$) the amplification of these evanescent waves leads to a divergence in the electromagnetic energy [8, 158]. This a manifestation of the pathological nature of the perfect lens and is because of the lack of a large momentum cutoff [159]. In principle, however, there is always a cutoff with meta-materials that corresponds to the inverse of the length-scale of the structure of the meta-material, $k_\mathrm{c} \sim 1/a$. The ideal lens conditions, $\varepsilon_- = -1$ and $\mu = -1$, are very singular. All calculations should be carried out by adding an infinitesimal $\mathrm{i}\delta$ to ω, and the limit $\delta \to 0$ should be taken to preserve causality. Thus, the unphysical divergences go away when one has even an infinitesimal level of absorption in the NRM, i.e. $\varepsilon_- = -1 + \mathrm{i}\delta$ and $\mu_- = -1 + \mathrm{i}\delta$, which essentially sets its own large momentum cutoff. This will be investigated in more detail in section 4.3. In fact, the absorption in the material limits the ability to amplify the evanescent waves, particularly those associated with large transverse wave-vectors and hence the resolving capabilities of the NRM lens [8, 160].

4.2.1. The quasi-static limit and the silver lens. We note that the perfect lens works when the conditions on both the permittivity and the permeability, $\varepsilon_- = -\varepsilon_+$ and $\mu_- = -\mu_+$, are satisfied. From our discussion in section 2, it is clear that to generate media with both ε and μ negative at the same frequency is quite difficult. Particularly at optical frequencies, this problem is more acute due to the lack of magnetic materials. It is in the optical and ultraviolet frequencies that the prospect of imaging the near-field modes becomes most exciting. Thus we would be severely handicapped by the lack of materials.

However, there is one great simplification that can be afforded, as pointed out by Pendry [6]. If we consider the case where all length-scales in the problem are much smaller than the

[9] Note that the solution amplifies with distance and not with time. This amplification is distinct from the more usual amplification related to laser gain or amplifiers in electronics, where there is an increase in energy.

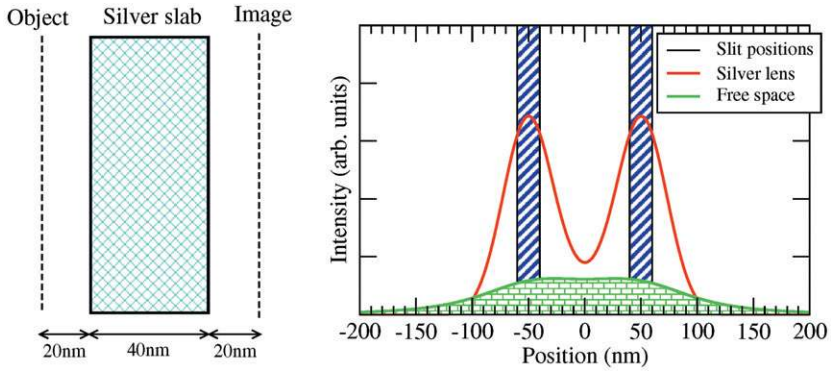

Figure 26. A thin film of silver can act as a near-field lens. The configuration used is shown on the left-hand side. The two slits, placed 100 nm apart (sub-wavelength distance), are clearly resolved by the lens while they cannot be resolved when at the same distance in vacuum. The calculations have been performed in the electrostatic limit, and a value of $\varepsilon_- = -1 + \mathrm{i}0.4$ has been used for silver.

wavelength, then we have $k_{x,y} \gg k_0 = \omega/c$ and $k_z \simeq k_x$ in both the positive and negative media. This is the *extreme near-field limit* or the *quasi-static limit*. In this limit, the Fresnel coefficients for the s-polarization given by equations (4.6)–(4.8) become independent of the dielectric constants and the Fresnel coefficients for the p-polarization given by equations (4.9)–(4.11) become independent of the magnetic permeabilities. Thus, a slab with negative magnetic permeability ($\mu_- = -\mu+$) would act as a near-field lens for the s-polarized waves. Similarly a slab with negative dielectric permittivity ($\varepsilon_- = -\varepsilon_+$) would act as a near-field lens for the p-polarized waves. Thus we can use a slab of metal as a near-field lens for the p-polarized radiation at a frequency when $\varepsilon_- = -1$. Noting that dissipation affects the capability to resolve large wave-vectors, one chooses a highly conducting metal such as silver. The image of two slits separated by a small distance imaged by a slab of silver is shown in figure 26 in this limit. The sub-wavelength resolution capabilities are clearly visible. The resolution is, however, limited by the large levels of dissipation in silver (at UV–visible frequencies, the dielectric permittivity of silver is reasonably described by $\varepsilon(\omega) \simeq 5.7 - 9^2/\omega^2 + \mathrm{i}0.4$, ω in electronvolts).

4.2.2. The role of surface plasmons. As has been pointed out, the role of the surface plasmons is crucial to the action of the perfect lens [6, 142, 158, 159]. The perfect lens conditions $\varepsilon_- = -\varepsilon_+$ are exactly the conditions for the surface plasmons on a metal surface and $\mu_- = -\mu_+$ are similarly the conditions for the s-polarized surface modes of a magnetic nature. In the special case when both these conditions are satisfied at a single frequency ω, the conditions for the surface modes on a semi-infinite NRM,

$$\frac{\sqrt{k_x^2 - \varepsilon_+\mu_+\omega^2/c^2}}{\varepsilon_+} + \frac{\sqrt{k_x^2 - \varepsilon_-\mu_-\omega^2/c^2}}{\varepsilon_-} = 0, \tag{4.16}$$

$$\frac{\sqrt{k_x^2 - \varepsilon_+\mu_+\omega^2/c^2}}{\mu_+} + \frac{\sqrt{k_x^2 - \varepsilon_-\mu_-\omega^2/c^2}}{\mu_-} = 0, \tag{4.17}$$

hold for all k_x and all the surface plasmon modes (of both polarizations) become degenerate at ω. These dispersionless modes have a zero group velocity along the surface. The total field can be written as a sum of the fields due to the source, and the fields of the surface mode

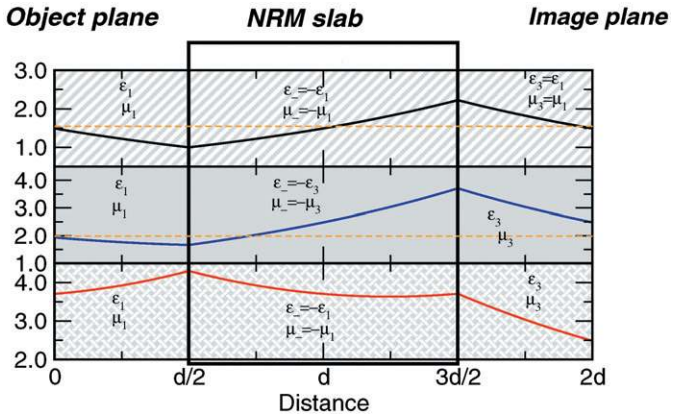

Figure 27. The asymmetric lens system consists of a slab of NRM with dielectric media with different ε on either side. The figure shows the three cases of (top panel) $\varepsilon_1 = \varepsilon_3 = -\varepsilon_2$—the perfect lens, (middle panel) matching the perfect lens conditions on the far-side, $\varepsilon_3 = -\varepsilon_2$ only, and (bottom panel) matching the perfect lens conditions on the near-side, $\varepsilon_1 = -\varepsilon_2$ only.

excitations for any wave vector $\mathrm{i}\kappa_z$,

$$E(z) = A\,\mathrm{e}^{-\kappa_z|z|} + B\,\mathrm{e}^{-\kappa_x|z-d_1|} + C\,\mathrm{e}^{-\kappa_z|z-d_2|}, \tag{4.18}$$

where $A = 1$ is the evanescent field of the source at $z = 0$, $B = -\mathrm{e}^{-\kappa_z d_1}$ is the contribution from the surface plasmon at the left surface $z = d_1$ and $C = \mathrm{e}^{-\kappa_z(d_2-2d)}$ is the field of the surface plasmon at the right surface $z = d_2$.[10] The presence of the other interface detunes the surface plasmon resonance on each interface so that they are excited to the correct degree so as to make the fields of the surface plasmon exactly cancel the incident fields for $z > d_1$. On the left side of the slab, the fields of the two surface plasmons again exactly cancel (for zero reflectivity). It is this coherent action of the surface plasmons that is responsible for the perfect lens action.

4.2.3. The asymmetric lens. It is actually not necessary that the perfect lens conditions of

$$\varepsilon_- = -\varepsilon_+, \qquad \mu_- = \mu_+ \tag{4.19}$$

be satisfied at both the interfaces to enable the amplification of evanescent waves. Consider the geometry shown in figure 27 with the negative medium between two positive media of different permittivity and permeability. It is sufficient if the plasmon conditions on both ε and μ are satisfied at either of the interfaces. In either case we have the transmission coefficient (for the p-polarization) through the slab to be

$$T = \frac{2(k_{z1}/\varepsilon_1)}{(k_{z3}/\varepsilon_3) + (k_{z1}/\varepsilon_1)} \exp(-\mathrm{i}k_{z2}d), \tag{4.20}$$

clearly showing the phase reversal for the propagating wave and amplification for the evanescent modes. In this asymmetric case, however, the field strength at the image plane differs from the object plane by a constant factor, and thus the image intensity is changed. Further, it is easily verified that wave-vectors with different k_x will refocus at slightly different positions except in the quasi-static limit $k_x \to \infty$. Thus there is no unique image plane and the focus of this lens is aberrated. There is also an impedance mismatch, and the reflection coefficient is clearly non-zero. Hence, we term the asymmetric slab *a near-perfect lens* [142].

[10] $d_1 = d/2$ and $d_2 = 3d/2$ in our case. But it is true as long as $d_2 + d_1 = 2d$.

A similar result holds for the s-polarized wave incident on the slab. We note that while the transmission is the same in both the cases, the spatial variation of the field is completely different as shown in figure 27. The reflection in the case of $\varepsilon_2 = -\varepsilon_1$ is also amplified.

The presence of a large reflectivity has serious consequences for the use of a lens for near-field imaging applications as it would disturb the object field. However, this idea does render the technology of making these lenses easier. Particularly in the case of the silver lens, it makes possible the use of a deposited silver thin film on a solid dielectric substrate, which is far preferable to a free-standing slab of silver with a sub-wavelength thickness. The technology for the deposition of these films on substrates is well established and the deposited film will certainly be more robust.

4.3. Limitations in real materials and imperfect NRMs

It should be emphasized that there is an inherent large momentum cutoff in all real materials, and an infinite resolution as our discussion above indicates is actually not possible. In meta-materials, it is clear that once the radiation can probe the structural details, effective medium parameters make no sense. Thus there is a natural cutoff on the transverse wave-vector of $k_x < k_c = 2\pi/a$, where a is the length-scale of periodicity of the meta-material structures. In the case of meta-materials, the boundaries of the slab are also indeterminate on the length-scale of a unit cell, which can also lead to some extra dispersion on the surface modes, thereby causing some degradation of the image [161]. Even with metals, the dielectric constant becomes dependent on the wave-vector at large wave-vectors and becomes spatially dispersive. For example, the Lindhard form [162] for the dielectric permittivity of a metal at small wave-vectors $k \ll k_F$ where k_F is the wave-vector at the Fermi surface, yields, within the random phase approximation (RPA),

$$\varepsilon(\omega, \boldsymbol{k}) = 1 - \frac{\omega_p^2}{\omega^2} \frac{1}{1 - 3/5(\boldsymbol{k} \cdot \boldsymbol{v}_f/\omega)^2}, \tag{4.21}$$

which shows a quadratic wavenumber dependence. Although the RPA holds until there is sufficient screening and is valid for a length-scale of a few atomic sizes, given the spatial dispersion, we would not be aiming to resolve atoms or small molecules with visible or IR light.

Much before this limit sets in, there are other mechanisms that limit the ability of this lens to focus the waves with large transverse wave-vectors. Foremost is the effect of absorption which is maximal in the regions of large electromagnetic fields. The exponential growth of the evanescent waves implies extremely large fields at the latter interface. The very large absorption that would occur implies that the source would no longer be able to maintain the energy supply and the amplification of the very large wave-vectors would not be possible. Thus absorption sets its own large wave-vector cutoff. The larger the absorption, the smaller the corresponding cutoff wave-vector. However, it does *not* imply that the amplification process would breakdown completely even in the presence of infinitesimal absorption as has been claimed [8].

In general, the perfect lens effect turns out to be rather sensitive to any deviations from the lens conditions $\varepsilon_- = -\varepsilon_+$ and $\mu_- = -\mu_+$ [15, 142, 163–167]. The effects of absorption can be included by including the imaginary part of ε_- and μ_- in the calculations. Thus they represent a deviation from these conditions in the imaginary parts. For the silver lens, this is even more acute as $\mu_- = 1$ represents a very large deviation from the perfect lens conditions. Consider the transmission coefficient for the p-polarized light across the slab,

$$T_p(k_x) = \frac{4(k_{z1}/\varepsilon_+)(k_{z2}/\varepsilon_-)\exp(ik_{z2}d)}{(k_{z1}/\varepsilon_+ + k_{z2}/\varepsilon_-)^2 - (k_{z1}/\varepsilon_+ - k_{z2}/\varepsilon_-)^2 \exp(2ik_{z2}d)}. \tag{4.22}$$

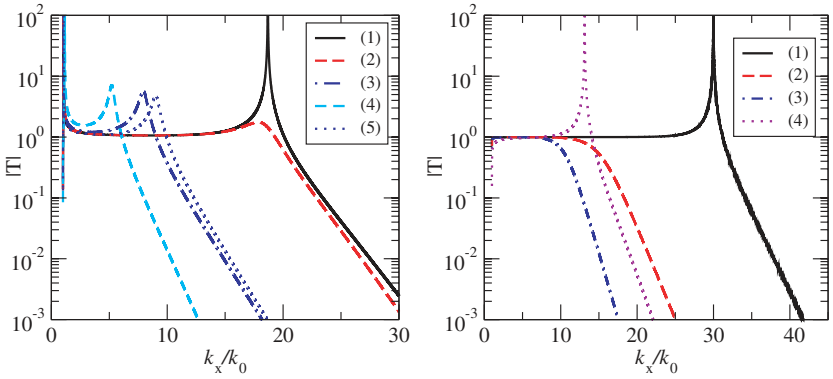

Figure 28. The absolute value of the transmitted field at the image plane $|T\exp(\mathrm{i}k_z^{(1)}d)|$, for the p-polarization as a function of k_x, showing the transmission resonances caused by the resonant excitations of the slab plasmon polaritons. On the left panel, $\mu = +1$ and (1) $\varepsilon = -1 + \mathrm{i}0.0$, $k_0d = 0.35$; (2) $\varepsilon = -1 + \mathrm{i}0.01$, $k_0d = 0.35$; (3) $\varepsilon = -0.9 + \mathrm{i}0.01$, $k_0d = 0.35$; (4) $\varepsilon = -0.9 + \mathrm{i}0.01$, $k_0d = 0.5$ and (5) $\varepsilon = -1.1 + \mathrm{i}0.01$, $k_0d = 0.35$. On the right panel, (1) $\mathrm{Re}\,\varepsilon = -1$ and (1) $\mathrm{Im}(\varepsilon) = 0$, $\mu = -1.1$, $k_0d = 0.35$; (2) $\mathrm{Im}(\varepsilon) = 0.01$, $\mu = -1.1$, $k_0d = 0.35$; (3) $\mathrm{Im}(\varepsilon) = 0.01$, $\mu = -1.1$, $k_0d = 0.5$; (4) $\mathrm{Im}(\varepsilon) = 0$, $\mu = -2$, $k_0d = 0.35$. The absorption broadens and softens the resonances. Deviations in ε affect the p-polarization more than the deviations in μ.

Under the perfect lens conditions, the first term in the denominator goes to zero for the evanescent waves and the exponential in the second term decays faster than the exponential in the numerator. However, if there was a mismatch of the material parameters ($\varepsilon_- = -1 + \delta\varepsilon$ and $\varepsilon_+ = +1$, say), then the first term is no longer zero. In the quasi-static limit ($k_x \gg \omega/c$) we find that the two terms in the denominator are approximately equal when

$$k_x d = -\ln\left|\frac{\delta\varepsilon}{2}\right|. \tag{4.23}$$

For larger wave vectors, the first term is larger than the second and hence the exponential decay in the numerator asserts itself. We can take this to be the largest wave-vector for which there is an effective amplification.

We can define the sub-wavelength resolution as the ratio of the optical wavelength to the linear size ($\Delta_{\min}$) of the smallest resolved feature, and we obtain

$$\mathrm{res} = \frac{\lambda}{\Delta_{\min}} = \frac{-\ln|\delta\varepsilon/2|}{2\pi}\frac{\lambda}{d}. \tag{4.24}$$

Thus the resolution depends logarithmically on the deviations of the material parameters and inversely with the width of the slab, implying that the perfect lens effect is very sensitive indeed to the material imperfections. The deviation, $\delta\varepsilon$, could be in the imaginary part also, with the same expression for the image resolution. Hence for our silver lens with a thickness of one-tenth the wavelength, we obtain a minimum resolved feature of about $\lambda/2.5$ from this expression. Some extra sub-wavelength information may be available from the smaller contributions at larger wave-vectors.

The detailed effects of absorption and the deviations in the real part of μ and ε which introduce retardation effects are, however, quite different. The absorption mainly causes an exponentially decaying transmission for large wave-vectors. The deviations in the real part on the other hand allow resonant excitations of the slab plasmon modes discussed in section 3.7. These resonant excitations of the slab would imply a very large transmission (for evanescent waves $T > 1$ is allowed) as shown in figure 28. The direct excitation of these surface modes for

imaging applications is undesirable, as these resonances will be disproportionately represented in the image; yet, the existence of these resonances is essential, as the recovery of the evanescent modes can be seen as the result of driving the surface plasmon far off-resonance. Absorption actually damps these transmission resonances and makes possible the very lensing action with some sub-wavelength resolution capabilities in the case of the silver lens with $\mu = +1$. The perfect lens solution in the absence of losses is very special, and can lead to paradoxical interpretations. The Poynting vector at the location of a point focus is strictly ill-defined. However, the presence of a small and finite absorption makes the focus a small blob instead and the Poynting vector also becomes well defined. In the case of the asymmetric lens, we note that the resolution works out to be

$$\text{res} = \frac{\lambda_0}{\lambda_{\min}} = -\frac{\ln|\varepsilon_2'/2\varepsilon_3|\lambda_0}{4\pi d} \tag{4.25}$$

(assuming $\varepsilon_3 \gg \varepsilon_2'$, and $\varepsilon_3 \gg \varepsilon_1$), in the favourable case of low reflection. In the limit of large ε_3 the resolution is actually enhanced [142].

Finally, one could ask if a finite aperture for the slab of the NRM would affect the near-field imaging process. To a first approximation, a slab with finite transverse width would prevent some propagating waves at large angles to the imaging axis from being lost. But the transport of the evanscent components will not be affected in the same manner and contribute substantially to the image. Thus some information is lost due to the loss of some propagating modes, but the near-field information is still preserved. The finite width of the slab, however, can have other effects. The very large density of states near the corners can distort the near-field image but will not affect it unless the transverse slab size becomes comparable with the size of the image features. The plasmons on the surface of the finitely wide slab can form standing waves along the transverse directions with the finite slab acting as a cavity [168] and significantly distort the image formation. But such cavity effects will be extremely limited in the presence of absorption.

4.4. Numerical simulations and time evolution

After the demonstration of the perfect lens effect by Pendry, there were several attempts to model this effect numerically. Some calculations obtained focusing [169, 170] while some others [30] did not show any focusing at all and yet others obtained focusing but not sub-wavelength image resolution [171, 172]. In view of the controversy surrounding the effect at that time, it was felt that some degree of numerical verification based on exact simulations of Maxwell's equations was necessary. On afterthought though, one was attempting to verify an exact analytical solution with numerical simulations which are necessarily approximate due to the finite differencing.

Cummer [173] pointed out that the discrete fields do not obey the same dispersion relations as the continuous fields do. For example, consider the discretization of the fields in the transfer matrix method [17, 70]. The dispersion for free space along one of the lattice directions (for a cubic lattice) for the discretized equations is

$$\omega^2(k_j) = \frac{c^2}{a^2} 4\sin^2\left(\frac{1}{2k_j a}\right) \simeq c^2 k_j^2 \left(1 + \frac{1}{2k_j^2 a^2}\right), \tag{4.26}$$

where $j = x, y, z$ and a here denotes the lattice spacing of the discretization grid. Evidently this converges to the continuum free space dispersion when $k_j a \ll 1$, i.e. when the discretization is indeed very small compared with the inverse wave-vector and they become identical only in the limit of the discrete intervals going to zero. Thus any discrete method has a wavenumber dependence and an inbuilt higher momentum cutoff that automatically precludes the perfect

focus. In the case of the perfect lens, as has been pointed out, the focusing is very sensitive to meeting the prescribed conditions on $\varepsilon = -1$ and $\mu = -1$. The different dispersion for the discrete fields is equivalent to having slightly different material parameters which thus leads to quite imperfect focusing as some have reported. Particularly for large wave-vectors, the different dispersion is acutely felt, and it was found to be only remedied by resorting to a larger degree of discretization [149]. The level of sub-wavelength focusing that can be obtained by a numerical calculation is a function of the finiteness of the differencing scheme even under the perfect conditions of no dissipation.

Cummer [173] also pointed out that the resonant surface plasmon modes at the interfaces for $n = -1$ are always excited by any causal incident wave or pulse with a finite bandwidth. In an FDTD calculation, these resonances at the two interfaces would ring indefinitely, and dissipation is always introduced into the material parameters in any such calculation to reach a steady state in a reasonable amount of time. This probably explains the report of [30], where it was found that the FDTD simulations never reached a steady behaviour for non-lossy NRMs. The loss also damps out the amplification for large wave-vectors, and the image resolution has been shown to be consistent with the estimate in section 4.3. These conclusions have been confirmed by FDTD calculations [174, 175] which used different boundary conditions to simulate evanescent waves.

As briefly noted before, the temporal evolution of the perfect focus is interesting as the focus refines in time, and under ideal conditions refines to a point focus at infinite time, which is what we obtain with the time-harmonic solutions. A calculation based on Laplace transform methods [163] indicated that for a source that is sharply switched on at $t = 0$, the lens forms a steady image only at times that are of the order of the absorption time ($t \sim 1/\mathrm{Im}(\varepsilon\mu)\omega$).

Gomez-Santos [158] has pointed out that the resonant excitation of the plasmons on the two surfaces is identical to the problem of coupled identical oscillators with an external force applied on one of the oscillators. The equations of motion for such a system of oscillators are

$$\ddot{x}_\mathrm{l} + \gamma\dot{x}_\mathrm{l}\omega_0^2 x_\mathrm{l} + k_\mathrm{c} x_\mathrm{r} = f(t), \tag{4.27}$$

$$\ddot{x}_\mathrm{r} + \gamma\dot{x}_\mathrm{r}\omega_0^2 x_\mathrm{r} + k_\mathrm{c} x_\mathrm{l} = 0, \tag{4.28}$$

where x_l and x_r are the amplitudes for the left and right oscillators and k_c is the coupling between them. First note that forcing the system at ω_0 with no damping makes only x_r non-zero in the steady state. The left oscillator does not move at all and all the excitation energy is passed on to the right oscillator. This corresponds to the zero reflection in our case. In the steady state the solutions for a time-harmonic excitation $f_0 \exp(-\mathrm{i}\omega t)$ are

$$x_\mathrm{l} = \frac{(\omega_0^2 - \omega^2 + \mathrm{i}\gamma\omega) f_0}{(\omega_0^2 - \omega^2 + \mathrm{i}\gamma\omega)^2 - k_\mathrm{c}^4}, \qquad x_\mathrm{r} = \frac{-k_\mathrm{c}^2 f_0}{(\omega_0^2 - \omega^2 + \mathrm{i}\gamma\omega)^2 - k_\mathrm{c}^4} \tag{4.29}$$

and it can be seen for the case of non-zero dissipation at resonance that the left oscillator is also excited. For large dissipation the right oscillator is no longer excited, which corresponds to the non-effective amplification in the case of the NRM slab. From this model we can further consider the temporal evolution of the imaging process by considering the rate at which energy is transferred between the two surfaces. Note that the slab plasmon polariton modes are decoupled from the singe plasmon frequency. Thus a source with a sharp onset has a frequency bandwidth and would excite them. The transmitted field across the lossless slab then has an amplitude [158]

$$E_t(t) = \Theta(t) A(t) \exp(-\mathrm{i}\omega_0 t) \exp(k_x d) \tag{4.30}$$

in the quasi-static limit and $A(t) \simeq 1/2(\Delta\omega_{kx} t)^2$, where $\Delta\omega_{kx}$ is the frequency spacing between the two slab plasmon polariton modes at a wave-vector k_x. As seen in section 3.7, the

spacing between the slab plasmon modes monotonically decreases and is exponentially small at k_x. Thus the large wave-vector components are very small at short times and a cutoff time can be defined by $\Delta\omega_{kx}t_{kx} \sim 1$ for every wave-vector k_x before which it does not appreciably contribute to the image formation. Thus the image is initially ill-defined and becomes better and better with the passage of time until it reaches the optimal resolution that is possible, given the levels of absorption in the system. Also note that without absorption, the slab plasmon polariton modes would ring indefinitely, never allowing the formation of a steady image.

5. Designing super-lenses

As discussed in the previous section, the perfect lens is in principle possible, if we had perfect negative refractive index materials with the specified material parameters. Inspite of the imperfect NRMs, sub-wavelength resolution is still possible to some extent, and we call such lenses with some degree of sub-wavelength image resolution *super-lenses*. It turns out that the flat slab lens of Veselago is only one lens of a whole class of perfect lenses or super-lenses that are possible. Negative refractive media are the optical analogues of anti-matter, in the sense that passage through NRMs nullifies the effect of passing through positive media with ε and μ of equal magnitude [149] for radiation. This concept of complementarity has led to the generalization of the Veselago lens to complementary media [13, 149] as well as other geometries including the cylindrical [177, 178] and the spherical [179] geometries. Interestingly, a change in the geometry enables magnification of even the near-field image. We will discuss these ideas in this section.

Any deviations from these lead to a drastic reduction in the possible sub-wavelength resolution of the lens. In fact, it is absorption that is the main culprit responsible for reducing the resolution, and as we saw in the case of the silver lens, we just obtain some sub-wavelength image information. Note that it is the ratio λ/d (wavelength to slab thickness) that dominates the resolution, the logarithm term being a relatively weakly varying function. For example, if $\lambda/d = 3$, we find that to achieve a resolution factor of 10, $\delta\varepsilon$ must be no greater than $\sim 10^{-11}$! However, for $\lambda/d = 10$, $\delta\varepsilon$ can be as large as ~ 0.002 and we can still achieve the same resolution. Thus, minimizing the effects of absorption is crucial in order to make these lenses work. Restructuring the lens to reduce these effects is possible and we first discuss some of the strategies that have been reported. But eventually it does appear that the composite structures should incorporate media with an active gain (as in a laser) in order to counter the dissipation [14, 180, 181].

5.1. Overcoming the limitations of real materials

The main limitation of the present day NRMs is the large amount of dissipation in them. The large amplification of the near-field modes causes large amounts of dissipation, which does not allow restoration of the near-field modes. As mentioned at the end of section 4.3, just by choosing the asymmetric configuration with a large dielectric constant on the side of the image we can increase the resolution of the slab lens [142]. Although it appears similar to the concept that is used in immersion lens near-field imaging [183], in this case it is more related to the fractional deviation from the perfect lens conditions that is reduced when the magnitude of the real part of the dielectric constant is very large. In fact, it has also been shown [142] that working at a slightly different frequency compared with when $\varepsilon = -1$ can lead to the resonant excitation of slab plasmons which can also help increase the maximum possible resolution. Solymar and co-workers [164] have considered that moving the image plane closer to the lens can actually compress the image.

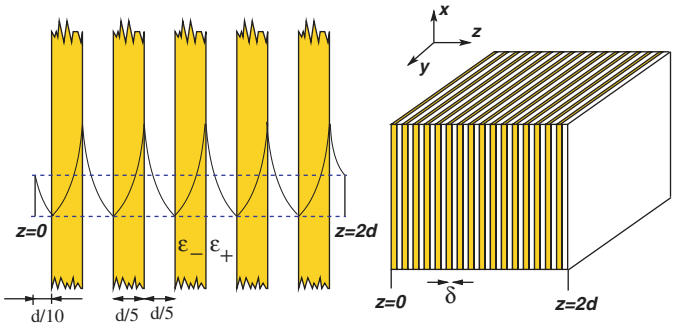

Figure 29. Chopping the slab of NRM into thin slices and distributing them around does not affect the image. The field distributions for a system of five such pieces is depicted. If this process of slicing into thinner and thinner layers is continued, we end up with a very unusual anisotropic effective medium as $\delta \to 0$.

One can reduce the effects of absorption by reducing the slab thickness. Then the evanescent fields amplify to much smaller extents, reducing the absorption and enhancing the image resolution. But then the distance over which we transfer the image is much smaller. We note that in the ideal lossless case, we can just take the original thick slab, chop it into thin layers and distribute it around between the source and image planes without affecting the result of perfect imaging [164, 182]. The perfect impedance matching makes this possible and the evanescent fields amplify within the NRM layers and decay in the positive layers as shown in figure 29. This does, however, make an enormous difference to the dissipation in the system. As the fields nowhere amplify to the same extent as they would have to in the single slab, the corresponding dissipation is much lower. We note that the source–lens edge and the lens edge–image plane distance have considerably reduced, and in the limit of the layer thickness becoming extremely small, the layered system merely transfers the image of the source from one edge to the other in the sense of an optical fibre bundle.

In the limit of a very small layer thickness and a large number of layers ($\delta \to 0$ as shown in figure 29(*b*)), the entire layered system may be regarded as an effective medium. If one considers the response of the system for an electric field applied parallel to the layers, one obtains

$$\langle D_x \rangle = \frac{\varepsilon_0}{2}(\varepsilon_+ E_x + \varepsilon_- E_x) = \varepsilon_0 \varepsilon_{xx} E_x, \tag{5.1}$$

where the tangential component of the $\boldsymbol{E}$ field is used. Similarly, considering the response of a field applied normal to the layers,

$$\langle E_z \rangle = \frac{1}{2\varepsilon_0}(\varepsilon_+^{-1} D_z + \varepsilon_-^{-1} D_z) = (\varepsilon_0 \varepsilon_{zz})^{-1} D_z, \tag{5.2}$$

where the continuity of the normal component of the $\boldsymbol{D}$ field is implied. Under the perfect lens conditions, we have the effective medium dielectric permittivity components

$$\varepsilon_{xx} = \frac{(\varepsilon_+ + \varepsilon_-)}{2} \to 0, \tag{5.3}$$

$$\varepsilon_{zz} = \frac{2}{(\varepsilon_+^{-1} + \varepsilon_-^{-1})} \to \infty \tag{5.4}$$

and the effective medium is an unusually anisotropic medium. Similar relations can be derived for the magnetic permeability using the continuity of $\boldsymbol{H}_\parallel$ and $B_\perp$. Noting that the wave

propagation for the p-polarized radiation in such a uniaxially anisotropic medium has the dispersion

$$\frac{k_x^2 + k_y^2}{\varepsilon_{zz}} + \frac{k_z^2}{\varepsilon_{xx}} = \varepsilon_0 \mu_{yy} \frac{\omega^2}{c^2}, \tag{5.5}$$

we have $k_z = 0$ as the only solution. Thus every wave passes through this anisotropic material without a change in amplitude or phase [182]. This anisotropic material is equivalent to a system of perfectly conducting wires along the layer normal embedded a medium with $\varepsilon = 0$. In the static limit and no dissipation, this corresponds to infinitely thin wires connecting the two end faces point to point. Thus, it acts as an optical fibre bundle, but unlike a conventional optical fibre bundle, it also transfers the near-field information. When there is dissipation, it merely corresponds to a finite fibre thickness and, consequently, a finite resolution. A slab and layered structure of positive media and anisotropic media with indeterminate permittivity and permeability tensors (i.e. all the components do not have the same sign) has also been shown to work as a layered lens with partial refocusing [184, 185].

We can write the transmission through such a layered system of thickness $2d$ in the quasi-static limit as [182]

$$T_{\mathrm{p}} \simeq \frac{1}{\cos(\mathrm{i}\varepsilon''_{-} k_x d) + (1/2)(\varepsilon_+ + \varepsilon_+^{-1}) \sin(\mathrm{i}\varepsilon''_{-} k_x d)}, \tag{5.6}$$

where the dissipation (represented by $\varepsilon''_{-} = \mathrm{Im}(\varepsilon_-)$) in the NRM layers has been taken into account. Note now that the resolution of this layered lens is

$$\mathrm{res} = \frac{\lambda}{2\pi \varepsilon_{-''}} \tag{5.7}$$

and the resolution depends inversely on the absorption rather than the logarithm of $\delta\varepsilon$, which varies very slowly. Thus the scope for improvement here by making the NRM less dissipative is much higher.

We note here that the study of layered structures with alternating layers of positive media and NRMs has been of considerable interest. The anomalous tunnelling across such media has also been considered in [186]. Such stacks can have a new kind of band-gap which corresponds to a zero refractive index ($n_- d_- + n_+ d_+ = 0$) [187]. Note that such zero index band-gaps can also occur for large layer thicknesses and are not related to our effective medium theory, above which there is also a perfect impedance matching. In fact, the layers in the zero index band-gap material should not be impedance matched. Interestingly the band-gap of these zero index layered systems is independent of periodicity and is robust against disorder. Other interesting properties of such layered structures such as omni-directional and large band-gaps [188–190], defect modes [188, 191], Bragg reflectors [192] and beam shaping [193], among others, have been considered.

Ultimately the resolution of the layered lens is also limited by dissipation. The point is that we need to have a *super-metal* that shows no dissipation. Another approach would be to put in by optical amplification that which is lost by dissipation [180]. Consider the perfect lens conditions with a lossy NRM: we see the possibility that if

$$\mathrm{Im}(\varepsilon_-) > 0, \qquad \mathrm{Im}(\mu_-) > 0, \tag{5.8}$$

then the condition may still be satisfied, provided that

$$\mathrm{Im}(\varepsilon_+) < 0, \qquad \mathrm{Im}(\mu_+) < 0. \tag{5.9}$$

In other words, the positive medium should be optically amplifying (as in a laser gain medium) in order to counter the effects of absorption in the negative medium. Then the perfect lens

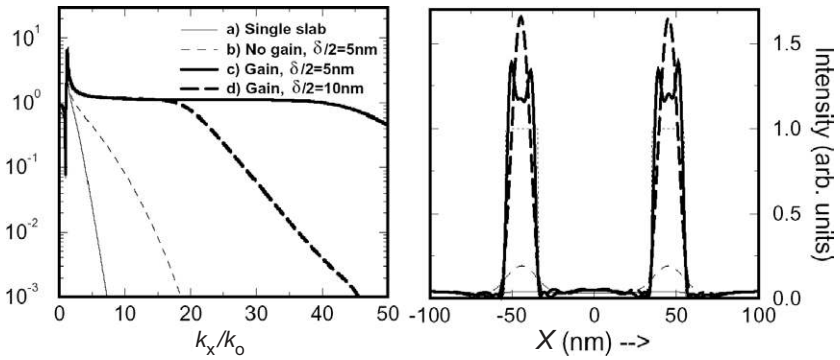

Figure 30. The transmission function (left) and the electromagnetic field intensity at the image plane (right) obtained (*a*) with a single slab of silver of 40 nm thickness, (*b*) when the slab is split into eight thin layers of $\delta/2 = 5$ nm thicknesses. (*c*) Layered silver-dielectric stack with optical gain and $\delta/2 = 5$ nm and (*d*) layered silver-dielectric stack with optical gain and $\delta/2 = 10$ nm. $\varepsilon_{\pm} = \pm 1 \mp \mathrm{i}0.4$ in (*c*) and (*d*).

conditions would be 'perfectly' met and the perfect image would result even with lossy NRM. Thus, the use of optical amplification is implied in the *perfect-lens condition* itself. Keeping with standard practice, we will subsume all the processes relating to the amplification (or absorption) of the electromagnetic wave into the negative (or positive) imaginary part of the dielectric constant.

More realistically, we can have optical amplification mainly for the electric dipole transitions. The incorporation of gain through the magnetic permeability would necessarily be through electronic amplifiers in the meta-materials for the microwave and rf frequencies. We will consider here the case of thin layers of silver with positive amplifying dielectric media in between. To satisfy the perfect lens conditions in both the real and the imaginary parts for the p-polarized light, we would require

$$\varepsilon_{+} = \varepsilon'_{+} - \mathrm{i}\varepsilon''_{+}, \qquad \varepsilon_{-} = -\varepsilon'_{+} + \mathrm{i}\varepsilon''_{+}. \tag{5.10}$$

Then the perfect lens conditions would be perfectly met and the perfect image would result, at least in the quasi-static limit. This can, for example, be accomplished by using a semiconductor laser material such as GaN or AlGaAs for the positive medium and silver for the negative medium. Using blue/ultraviolet (UV) light to pump the AlGaAs, one can make the AlGaAs now optically amplifying in the red region of the spectrum, where one can satisfy the perfect lens condition for the real parts of the dielectric constant. By adjusting the pump laser intensity, the imaginary part of the positive gain medium can be tuned. The imaging can now be carried out in the red. Of course, it would be possible to use other materials and correspondingly different wavelengths of light. Alternatively one could also use other high gain processes such as Raman gain for this purpose. As a note of caution, we note that in the presence of the intense field enhancements that are expected in this system the gain is likely to get saturated. The largest field enhancements will be for the largest transverse wave-vectors. If we make the layers very thin, the local field enhancements will not be as intense and the gain might not get completely bleached. In general, however, we do expect that the effective gain will be somewhat reduced and the corresponding enhancements of the image resolution will be smaller.

As a proof of the principle, the transmission function for the layered lens, with and without amplifications, and the images of two closely spaced sources as resolved by the respective lenses are shown in figure 30. For comparison, we also show the case of the original single slab of

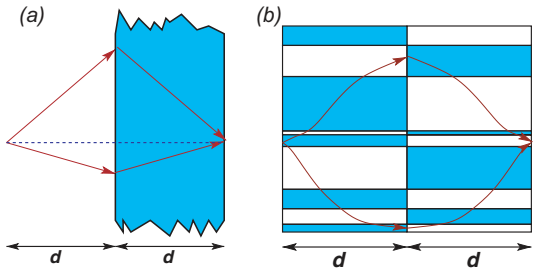

Figure 31. A pair of complementary media nullify the effect of each other for the passage of light. The light and dark regions indicate opposite refractive indices. The path for the propagating modes in the media will not be straight lines in general. The overall effect is as if the space of thickness $2d$ did not exist for an observer on the right-hand side.

silver as the lens (solid line and $\delta/2 = 40\,\text{nm}$) and a layered but gainless system. The two peaks in the image for the single slab can hardly be resolved, while they are clearly resolved in the case of the layered system with no gain. The improvement in the image resolution for the layered system with gain over the corresponding gainless systems is obvious, with the sharp edges of the slits becoming visible. Interestingly, the transmittance of the layered lens with gain does not decay rapidly with increase in the number of layers and a total stack thickness of even a few wavelengths [180]. Although the transmission function is not constant with the wave-vector due to the layer plasmon resonances, we emphasize that the high spatial frequency components are transferred across. Knowledge of the transmission function of the lens would therefore enable one to recover a clean image from the observed image.

5.2. The generalized perfect lens theorem

The negative refractive slab can also be considered as *optical anti-matter* for light in the sense it cancels out the effects of propagation through an equal amount of positive index media (see figure 31). This cancellation is applicable to the phase changes for propagating waves and the amplitude changes for the evanescent waves. Then it would appear for the world ahead of the slab that optically a thickness of $2d$ had been removed. In fact, the perfect focusing action occurs for more general conditions than a homogeneous slab with $n = -1$. It happens even when the dielectric permittivity and the magnetic permeability vary along the transverse directions, provided that the variation is just the same but with opposite signs:

$$\varepsilon_1 = +\varepsilon(x, y), \quad \mu_1 = +\mu(x, y), \qquad \forall 0 < z < d, \tag{5.11}$$

$$\varepsilon_2 = -\varepsilon(x, y), \quad \mu_2 = -\mu(x, y), \qquad \forall d < z < 2d, \tag{5.12}$$

where $\varepsilon(x, y)$ and $\mu(x, y)$ are some arbitrary functions of x and y and can take positive or negative values (see figure 31(b) for a schematic picture). This is the generalized lens theorem of [149] which we will merely state here and the proof of which we will give in appendix.

Consider the most general dielectric permittivity and magnetic permeability tensor for spatial region 1 ($0 < z < d$):

$$\tilde{\varepsilon}_1 = \begin{pmatrix} \varepsilon_{1xx} & \varepsilon_{1xy} & \varepsilon_{1xz} \\ \varepsilon_{1yx} & \varepsilon_{1yy} & \varepsilon_{1yz} \\ \varepsilon_{1zx} & \varepsilon_{1zy} & \varepsilon_{1zz} \end{pmatrix}, \qquad \tilde{\mu}_1 = \begin{pmatrix} \mu_{1xx} & \mu_{1xy} & \mu_{1xz} \\ \mu_{1yx} & \mu_{1yy} & \mu_{1yz} \\ \mu_{1zx} & \mu_{1zy} & \mu_{1zz} \end{pmatrix}. \tag{5.13}$$

Similarly, for region 2 ($d < z < 2d$)

$$\tilde{\varepsilon}_2 = \begin{pmatrix} \varepsilon_{2xx} & \varepsilon_{2xy} & \varepsilon_{2xz} \\ \varepsilon_{2yx} & \varepsilon_{2yy} & \varepsilon_{2yz} \\ \varepsilon_{2zx} & \varepsilon_{2zy} & \varepsilon_{2zz} \end{pmatrix}, \qquad \tilde{\mu}_2 = \begin{pmatrix} \mu_{2xx} & \mu_{2xy} & \mu_{2xz} \\ \mu_{2yx} & \mu_{2yy} & \mu_{2yz} \\ \mu_{2zx} & \mu_{2zy} & \mu_{2zz} \end{pmatrix}. \tag{5.14}$$

Note that the tensorial components can be specified functions of (x, y). It can be shown (see appendix for the proof) that the fields to the left and right of the interface between the two slabs are exactly identical but in opposite order as long as the two slabs have *complementary* material parameters:

$$\tilde{\varepsilon}_1 = \begin{pmatrix} \varepsilon_{1xx} & \varepsilon_{1xy} & \varepsilon_{1xz} \\ \varepsilon_{1yx} & \varepsilon_{1yy} & \varepsilon_{1yz} \\ \varepsilon_{1zx} & \varepsilon_{1zy} & \varepsilon_{1zz} \end{pmatrix}, \qquad \tilde{\mu}_1 = \begin{pmatrix} \mu_{1xx} & \mu_{1xy} & \mu_{1xz} \\ \mu_{1yx} & \mu_{1yy} & \mu_{1yz} \\ \mu_{1zx} & \mu_{1zy} & \mu_{1zz} \end{pmatrix} \tag{5.15}$$

and

$$\tilde{\varepsilon}_2 = \begin{pmatrix} -\varepsilon_{1xx} & -\varepsilon_{1xy} & +\varepsilon_{1xz} \\ -\varepsilon_{1yx} & -\varepsilon_{1yy} & +\varepsilon_{1yz} \\ +\varepsilon_{1zx} & +\varepsilon_{1zy} & -\varepsilon_{1zz} \end{pmatrix}, \qquad \tilde{\mu}_2 = \begin{pmatrix} -\mu_{1xx} & -\mu_{1xy} & +\mu_{1xz} \\ -\mu_{1yx} & -\mu_{1yy} & +\mu_{1yz} \\ +\mu_{1zx} & +\mu_{1zy} & -\mu_{1zz} \end{pmatrix}. \tag{5.16}$$

Then the two *complementary media* have an optical sum of zero. This result can be further generalized to any region that is mirror anti-symmetric about a given plane [149]. Such regions correspond to effectively optical null regions. These results have also been verified numerically by considering specific examples with spatially varying complementary media with mirror anti-symmetry [149].

This theorem, combined with the possibility of using co-ordinate transformations [194] to map the slab geometries into other geometries [149], allows us to generate a wide class of arrangements, all of which will exhibit the property of transferring images of sources in a perfect sense.

5.3. The perfect lens in other geometries

Traditionally lenses have been used to project images and more importantly magnify or demagnify the image of a source. The slab of NRM that is a perfect lens maps every point on the object plane to another point on the image plane. But the size of the image is identical to that of the source. This is due to the invariance in the transverse direction, and the transverse wavevector (k_x, k_y) is preserved in the refraction process. The curved surfaces of a conventional lens break this translational symmetry in the transverse direction and enable the change in the size of the image. In general, to obtain magnification and demagnification of the images, the translational symmetry would have to be broken and curved surfaces will need to be employed. The perfect lens action in the case of the NRM slab was crucially dependent on the near-degeneracy of the surface plasmons in the case of the slab, and curved surfaces, in general, have a completely different dispersion for the surface plasmons. Only in the quasi-static limit does a cylindrical surface with negative, homogeneous ε have a nearly degenerate plasmon dispersion, and a cylindrical shell in two dimensions with $\varepsilon = -1$ was shown to act as a lens, transferring in and out the image of a source [177]. In fact, the use of conformal mapping on the solutions to the Laplace equation (in the quasi-static limit) for the slab was shown to yield an entire class of near-field lenses in two dimensions. In the more general case, one uses the technique of co-ordinate transformations to map the solutions of the slab geometry into other geometries. Note that a distortion of space results in a change of the ε and μ tensors in general. Thus in many cases, the transformed geometry would involve spatially varying (heterogeneous) medium parameters. Here we will present three cases of a cylindrical lens,

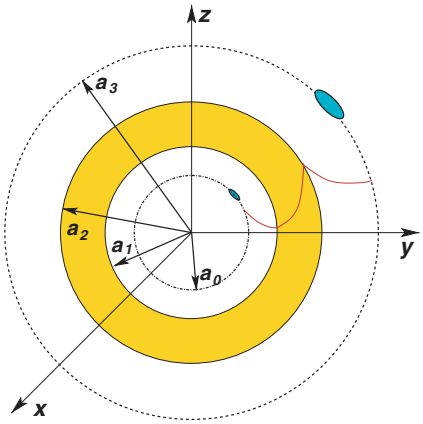

Figure 32. A spherical shell with negative $\varepsilon_-(r) \sim -1/r$ and $\mu_-(r) \sim -1/r$ images a source located inside the shell into the external region. The media outside have a positive refractive index, but $\varepsilon_-(r) \sim 1/r$ and $\mu_-(r) \sim 1/r$. The amplification inside the spherical shell of the otherwise decaying field is schematically shown.

a spherical lens and a corner-lens which focuses the source back on itself. The lenses in the curved geometries result in a magnification of the image including the near-field evanescent modes and the corner-lens is interesting as an open resonator.

5.3.1. Cylindrical lenses. The conformal transformation

$$z' = \ln z \tag{5.17}$$

was shown [177] to map the NRM slab into a cylindrical shell (see figure 32 and ignore the dependence along the Z axis). Note that the conformal transformation is valid for the Laplace equation and the solutions valid in the extreme near-field approximation. In general we can transform Maxwell's equations for the slab lens of an NRM, into a cylindrical shell with $\varepsilon_-(r)$ and $\mu_-(r)$ whose inner and outer radii are a_1 and a_2, embedded in a positive medium. As it has been shown [194], if we define the new coordinates $q_1(x, y, z)$, $q_2(x, y, z)$ and $q_3(x, y, z)$, then in the new frame, the material parameters and fields are given by

$$\tilde{\varepsilon}_i = \varepsilon_i \frac{Q_1 Q_2 Q_3}{Q_i^2}, \qquad \tilde{\mu}_i = \mu_i \frac{Q_1 Q_2 Q_3}{Q_i^2}, \tag{5.18}$$

$$\tilde{E}_i = Q_i E_i, \qquad \tilde{H}_i = Q_i H_i, \tag{5.19}$$

where

$$Q_i^2 = \left(\frac{\partial x}{\partial q_i}\right)^2 + \left(\frac{\partial y}{\partial q_i}\right)^2 + \left(\frac{\partial z}{\partial q_i}\right)^2. \tag{5.20}$$

Now consider the transformation to cylindrical co-ordinates

$$x = r_0 \, \mathrm{e}^{\ell/\ell_0} \cos\phi, \qquad y = r_0 \, \mathrm{e}^{\ell/\ell_0} \sin\phi, \qquad z = Z, \tag{5.21}$$

so that

$$Q_\ell = \frac{r_0}{\ell_0} \mathrm{e}^{\ell/\ell_0}, \qquad Q_\phi = r_0 \, \mathrm{e}^{\ell/\ell_0}, \qquad Q_Z = 1. \tag{5.22}$$

We obtain the transformed dielectric permittivity and magnetic permeability to be

$$\tilde{\varepsilon}_\ell = \ell_0 \varepsilon_\ell, \qquad \tilde{\varepsilon}_\phi = \ell_0^{-1} \varepsilon_\phi, \qquad \tilde{\varepsilon}_Z = \frac{r_0^2}{\ell_0} \exp\left(\frac{2\ell}{\ell_0}\right) \varepsilon_z, \tag{5.23}$$

$$\tilde{\mu}_\ell = \ell_0 \mu_\ell, \qquad \tilde{\mu}_\phi = \ell_0^{-1} \mu_\phi, \qquad \tilde{\mu}_Z = \frac{r_0^2}{\ell_0} \exp\left(\frac{2\ell}{\ell_0}\right) \mu_z. \tag{5.24}$$

Choosing the scale factor $\ell_0 = 1$ and

$$\varepsilon_r = \mu_r = +1, \quad \varepsilon_\phi = \mu_\phi = +1, \quad \varepsilon_z = \mu_z = +\frac{1}{r^2}, \qquad \forall\, r < a_1, \tag{5.25}$$

$$\varepsilon_r = \mu_r = -1, \quad \varepsilon_\phi = \mu_\phi = -1, \quad \varepsilon_z = \mu_z = -\frac{1}{r^2}, \qquad \forall\, a_1 < r < a_2, \tag{5.26}$$

$$\varepsilon_r = \mu_r = +1, \quad \varepsilon_\phi = \mu_\phi = +1, \quad \varepsilon_z = \mu_z = +\frac{1}{r^2}, \qquad \forall\, a_2 < r, \tag{5.27}$$

where $r = r_0 \exp(\ell)$, we obtain

$$\tilde{\varepsilon}_\ell = \tilde{\mu}_\ell = +1, \quad \tilde{\varepsilon}_\phi = \tilde{\mu}_\phi = +1, \quad \tilde{\varepsilon}_z = \tilde{\mu}_z = +1, \qquad \forall \ell < \ell_0 \ln\left(\frac{a_1}{r_0}\right), \tag{5.28}$$

$$\tilde{\varepsilon}_\ell = \tilde{\mu}_\ell = -1, \quad \tilde{\varepsilon}_\phi = \tilde{\mu}_\phi = -1, \quad \tilde{\varepsilon}_z = \tilde{\mu}_Z = -1, \quad \forall\, \ell_0 \ln\left(\frac{a_1}{r_0}\right) < \ell < \ell_0 \ln\left(\frac{a_2}{r_0}\right), \tag{5.29}$$

$$\tilde{\varepsilon}_\ell = \tilde{\mu}_\ell = +1, \quad \tilde{\varepsilon}_\phi = \tilde{\mu}_\phi = +1,$$
$$\tilde{\varepsilon}_z = \tilde{\mu}_Z = +1, \qquad \forall\, \ell_0 \ln\left(\frac{a_2}{r_0}\right) < \ell \tag{5.30}$$

in the ℓ, ϕ, Z plane, which is identical to the situation of the Veselago lens. Hence the new system must accordingly act as a cylindrical lens and transfer images in and out of the cylindrical lens. The image will be formed on the surface $a_3 = a_0(a_2/a_1)^2$ and there will be a magnification of the image by the factor

$$\mathcal{M} = \left(\frac{a_2}{a_1}\right)^2. \tag{5.31}$$

Note that these cylindrical lens are also short-sighted in the same manner as the slab lens. They can focus sources from inside to the outside only when $a_1^2/a_2 < r < a_1$, and the other way around from outside to the inner world, when the source is located in $a_2 < r < a_2^2/a_1$. They cannot focus outside this region. Further note that for the optical axis along the ℓ direction, the generalized lens theorem predicts that the variations in the transverse ϕ, Z directions are irrelevant. Hence the medium parameters in general could also be arbitrary functions of ϕ and Z.

In general, a whole class of lenses can be generated in two dimensions using the transformation techniques [177, 178].

5.3.2. A spherical lens. The transformation technique can be similarly used to map the slab lens into spherical co-ordinates $(r = r_0\, \mathrm{e}^{\ell/\ell_0}, \theta, \phi)$, and using the generalized lens theorem, a spherical shell of NRM with $\varepsilon_-(r) \sim -1/r$ and $\mu_-(r) \sim -1/r$ embedded in a positive medium with $\varepsilon_+(r) \sim +1/r$ and $\mu_+(r) \sim +1/r$ will act as a spherical lens projecting sources in and out of the shell [149]. For this specific case, we will present a more conventional proof in terms of the TE and TM modes in the spherical geometry [179].

Consider the spherically symmetric system shown in figure 32. Under the circumstances of spherical symmetry, it is sufficient to specify the quantities $(\boldsymbol{r}\cdot\boldsymbol{E})$ and $(\boldsymbol{r}\cdot\boldsymbol{H})$, which will constitute a full solution to the problem. Consider now the TM polarized modes $\boldsymbol{r}\cdot\boldsymbol{H}=0$, implying that only the electric fields have a radial component E_r. Operating on Maxwell's equation with ∇,

$$\nabla\times\nabla\times\boldsymbol{E}=\mathrm{i}\omega\mu_0\nabla\times[\mu(\boldsymbol{r})\boldsymbol{H}]=\frac{\omega^2}{c^2}\mu(\boldsymbol{r})\varepsilon(\boldsymbol{r})\boldsymbol{E}+\mathrm{i}\omega\frac{\nabla\mu(\boldsymbol{r})}{\mu(\boldsymbol{r})}\times\nabla\times\boldsymbol{E} \tag{5.32}$$

and we have

$$\nabla\cdot\boldsymbol{D}=\nabla\cdot[\varepsilon(\boldsymbol{r})\boldsymbol{E}]=\nabla\varepsilon(\boldsymbol{r})\cdot\boldsymbol{E}+\varepsilon(\boldsymbol{r})\nabla\cdot\boldsymbol{E}=0. \tag{5.33}$$

And if we assume $\varepsilon(\boldsymbol{r})=\varepsilon(r)$ and $\mu(\boldsymbol{r})=\mu(r)$, we have

$$\nabla\cdot\boldsymbol{E}=-\frac{\varepsilon'(r)}{r\varepsilon(r)}\boldsymbol{r}\cdot\boldsymbol{E}=-\frac{\varepsilon'(r)}{r\varepsilon(r)}(rE_r). \tag{5.34}$$

We note the following identities for later use:

$$\nabla\times\nabla\times\boldsymbol{E}=\nabla(\nabla\cdot\boldsymbol{E})-\nabla^2\boldsymbol{E}, \tag{5.35}$$

$$\nabla^2(\boldsymbol{r}\cdot\boldsymbol{E})=\boldsymbol{r}\cdot\nabla^2\boldsymbol{E}+2\nabla\cdot\boldsymbol{E}. \tag{5.36}$$

Using the fact that ε only depends on r, we also note that

$$\boldsymbol{r}\cdot\nabla(\nabla\cdot\boldsymbol{E})=-\frac{\partial}{\partial r}\left(\frac{\varepsilon'(r)}{\varepsilon(r)}(rE_r)\right)+\left(\frac{\varepsilon'(r)}{\varepsilon(r)}E_r\right). \tag{5.37}$$

Using the above four equations, we can obtain the equation for E,

$$\nabla^2(rE_r)+\frac{\partial}{\partial r}\left[\frac{\varepsilon'(r)}{\varepsilon(r)}(rE_r)\right]+\frac{\varepsilon'(r)}{r\varepsilon(r)}(rE_r)+\varepsilon(r)\mu(r)\frac{\omega^2}{c^2}(rE_r)=0, \tag{5.38}$$

which is separable, and the spherical harmonics are a solution to the angular part. Hence the solution is $(rE_r)=U(r)Y_{lm}(\theta,\phi)$, where the radial part, $U(r)$, satisfies

$$\frac{1}{r^2}\frac{\partial}{\partial r}\left(r^2\frac{\partial U}{\partial r}\right)-\frac{l(l+1)}{r^2}U+\frac{\partial}{\partial r}\left[\frac{\varepsilon'(r)}{\varepsilon(r)}U\right]+\frac{\varepsilon'(r)}{r\varepsilon(r)}U+\varepsilon(r)\mu(r)\frac{\omega^2}{c^2}U=0. \tag{5.39}$$

If we choose $\varepsilon(r)=\alpha r^p$ and $\mu(r)=\beta r^q$, we can have a solution $U(r)\sim r^n$ and we get

$$[n(n+1)-l(l+1)+p(n-1)+p]r^{n-2}+\frac{\alpha\beta\omega^2}{c^2r^{p+q+n}}=0, \tag{5.40}$$

implying $p+q=-2$ and

$$n_\pm=\frac{1}{2}\left[-(p+1)\pm\sqrt{(p+1)^2+4l(l+1)-\frac{4\alpha\beta\omega^2}{c^2}}\right]. \tag{5.41}$$

Hence the general solution can be written as

$$E_r(\boldsymbol{r})=\sum_{l,m}[n_+A_{lm}r^{n_+-1}+n_-B_{lm}r^{n_--1}]Y_{lm}(\theta,\phi) \tag{5.42}$$

and a similar solution can be obtained for the TE modes with $\boldsymbol{r}\cdot\boldsymbol{E}=0$.

Now assuming an arbitrary source at $r=a_0$, we can now write down the electric fields of the TM modes in the different regions for the negative spherical shell of figure 2 as

$$\boldsymbol{E}^{(1)}(\boldsymbol{r})=\sum_{l,m}[n_+A^{(1)}_{lm}r^{n_+-1}+n_-B^{(1)}_{lm}r^{n_--1}]Y_{lm}(\theta,\phi),\quad a_0<r<a_1, \tag{5.43}$$

$$\boldsymbol{E}^{(2)}(\boldsymbol{r})=\sum_{l,m}[n_+A^{(2)}_{lm}r^{n_+-1}+n_-B^{(2)}_{lm}r^{n_--1}]Y_{lm}(\theta,\phi),\quad a_1<r<a_2, \tag{5.44}$$

$$\boldsymbol{E}^{(3)}(\boldsymbol{r})=\sum_{l,m}[n_+A^{(3)}_{lm}r^{n_+-1}+n_-B^{(3)}_{lm}r^{n_--1}]Y_{lm}(\theta,\phi),\quad a_2<r<\infty \tag{5.45}$$

and similarly for the magnetic fields. Note that $B_{lm}^{(1)}$ correspond to the field components of the source located at $r = a_0$. For causal solutions $A_{lm}^{(3)} = 0$. Now the tangential components of the magnetic fields and the normal components of the displacement fields have to be continuous across the interfaces. Under the conditions $p = -1$, $q = -1$, $\varepsilon_+(a_1) = -\varepsilon_-(a_1)$ and $\varepsilon_+(a_2) = -\varepsilon_-(a_2)$, we have

$$A_{lm}^{(1)} = 0, \tag{5.46}$$

$$A_{lm}^{(2)} = \left(\frac{1}{a_1^2}\right)^{\sqrt{l(l+1)-\alpha\beta\omega^2/c^2}} B_{lm}^{(1)}, \qquad B_{lm}^{(2)} = 0, \tag{5.47}$$

$$B_{lm}^{(3)} = \left(\frac{a_2^2}{a_1^2}\right)^{\sqrt{l(l+1)-\alpha\beta\omega^2/c^2}} B_{lm}^{(1)}. \tag{5.48}$$

The lens-like property of the system becomes clear by writing the field outside the spherical shell as

$$E_r^{(3)} = \frac{1}{r}\left[\frac{a_2^2}{a_1^2} r\right]^{\sqrt{l(l+1)-\alpha\beta\omega^2/c^2}} B_{lm}^{(1)} Y_{lm}(\theta, \phi). \tag{5.49}$$

Hence, apart from a scaling factor of $1/r$, the fields on the sphere $r = a_3 = (a_2^2/a_1^2)a_0$ are identical to the fields on the sphere $r = a_0$. We also have a spatial magnification in the image by a factor of a_2^2/a_1^2. As with the cylindrical lens, this spherical lens will be able to image sources which are also located only within in a finite distance of the spherical layer. Note that the positive medium outside the shell is also required to have spatially varying material parameters $\sim 1/r$. In the presence of finite dissipation, using the ideas of the asymmetric lens [142], we can terminate the spatially varying media at some finite but large distance. Let us note a couple of points about the above perfect lens solutions in the spherical geometry. First, for $r > a_3$, i.e. points outside the image surface, the fields appear as if the source were located on the spherical image surface ($r = a_3$). However, this is not true for points $a_2 < r < a_3$ within the image surface. Second, note that our imaging direction is along r, and ε and μ can now be arbitrary functions of θ and ϕ, with only the condition of complementarity between the negative and positive regions. Third, given that $\varepsilon_-(a_2) = -\varepsilon_+(a_2)$, we have the perfect lens solutions if and only if $n_+ = -n_-$, which implies that $p = -1$ in equation (5.41). Although the solutions given by equation (5.42) occur in any medium with $\varepsilon\mu \sim 1/r^2$, the perfect lens solutions only occur for $\varepsilon \sim \mu \sim 1/r$. Here we have written down the solutions for the TM modes. The solutions for the TE modes can be similarly obtained.

Again there is a considerable simplification that is possible in the extreme near-field limit [179]. Then the imaging for the TM modes becomes independent of μ and only requires $\varepsilon_- \sim -1/r^2$. Similarly the TE modes become independent of ε, and the only condition is that $\mu_- \sim -1/r^2$. Further the constraint that the positive media outside also be spatially varying can be dropped. In this limit it can be shown that the largest multipole that can be resolved is again limited by the dissipation in the NRM and is approximately [179]

$$l_{\max} \simeq \frac{\ln\{3\varepsilon_1\varepsilon_3/[\varepsilon_i(a_1)\varepsilon_i(a_2)]\}}{2\ln(a_2/a_1)}, \tag{5.50}$$

where $\varepsilon_1 = -\mathrm{Re}(\varepsilon_-(a_1))$ and $\varepsilon_3 = -\mathrm{Re}(\varepsilon_-(a_2))$ for the perfect lens conditions and $\varepsilon_{\mathrm{i}}(r) \sim 1/r^2$ is the imaginary part of the permittivity for the negative medium shell.

5.3.3. A perfect two-dimensional corner lens. Consider an infinitely extended corner of NRM with $n = -1$ as shown in figure 33(a). A ray diagram shows that a source located in the

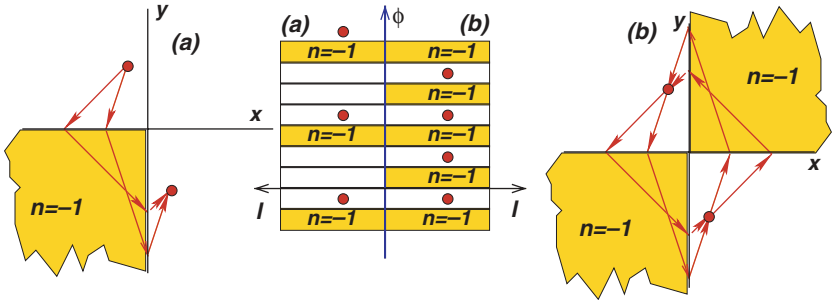

Figure 33. (*a*) A corner of NRM with $n = -1$ refocuses a source. This corner lens can be shown to be perfect by mapping it to a periodic layered stack. (*b*) A double corner of NRM refocuses the source back onto itself and creates an image in the diagonally opposite quadrant. This focus is also perfect in that it includes the near-field components and can be shown by the mapping into a periodically layered stack as shown.

second quadrant can be focused into the fourth quadrant. In fact combining two such corners as shown in figure 33(*b*) makes it even more exotic: classical rays emanating from a source placed in any one of the quadrants are returned to the source point [195]. Using the generalized lens theorem, a more rigorous result can be proved, namely that the focusing with these corner lenses is true for the evanescent components as well and is perfect!

Consider the periodic arrangements of slabs shown beside the corners with material parameters

$$\varepsilon(\phi) = \mu(\phi) = \begin{cases} +1 & -\dfrac{\pi}{2} < \phi < \pi, \\ -1 & -\pi < \phi < -\dfrac{\pi}{2} \end{cases} \tag{5.51}$$

in the first case (a) of a single corner and

$$\varepsilon(\phi) = \mu(\phi) = \begin{cases} +1 & -\dfrac{\pi}{2} < \phi < 0 \quad \text{and} \quad \dfrac{\pi}{2} < \phi < \pi, \\ -1 & -\pi < \phi < -\dfrac{\pi}{2} \quad \text{and} \quad 0 < \phi < \dfrac{\pi}{2} \end{cases} \tag{5.52}$$

in the second case (b) of the double corner lens. Using the transformation as in the case of the cylindrical lens,

$$x = r_0\, \mathrm{e}^{\ell/\ell_0} \cos\phi, \qquad y = r_0\, \mathrm{e}^{\ell/\ell_0} \sin\phi, \qquad z = Z, \tag{5.53}$$

gives us

$$\tilde{\varepsilon}_\ell = \tilde{\mu}_\ell = \tilde{\varepsilon}_\phi = \tilde{\mu}_\phi = \begin{cases} +1 & \tilde{\varepsilon}_Z = \tilde{\mu}_Z = r_0^2\, \mathrm{e}^{2\ell/\ell_0} \\ -1 & \tilde{\varepsilon}_Z = \tilde{\mu}_Z = -r_0^2\, \mathrm{e}^{2\ell/\ell_0} \end{cases} \tag{5.54}$$

in the respective positive and negative quadrants. The conditions of complementarity are satisfied. The dependence along the r axis is irrelevant as it is orthogonal to the imaging axis along ϕ. Hence we conclude that the images in both the cases of the single corner (a) and the double corner (b) will be perfect.

Note that case (b) is unusually singular as each source images on each other and the fields grow indefinitely in time. It has also been shown that all the surface modes of this system are degenerate and the density of modes at the double corner is very large [149]. Such a system can form a very interesting open resonator in which light can be trapped for long times.

6. Experimental evidence for NRMs and super-lenses

This field has been one in which theoretical developments have led the experimental activities. NRMs had been predicted by Veselago in 1967. It was the theoretical recipes of Pendry *et al* [2, 3, 43] for designing negative material parameters that made the real developments possible. But the main catalyst for the sudden increase in the interest in NRMs came from the experimental demonstration of NRMs by the San Diego group in 2000 [4, 5]. These have now been followed up by several experimental groups. But on the whole, the growth of experimental activity has been rather slow compared with the almost frenetic pace in the theoretical studies. Part of the reason could be that the experimental samples are not easy to fabricate, particularly the microstructures for high frequency operation. This is also possibly the reason why most of the experiments have been performed at microwave frequencies. But there is enough experimental evidence to place many of the theoretical ideas on a very safe footing. In this section,we will briefly cover the main experimental activities.

6.1. Experiments on negative refractive index

The first experiments on the plasmonic nature of thin wire arrays were reported in [43], where the thin wire arrays were made using spark chamber technology. These consisted of sheets of polysterene rohacell sheets with 20 μm gold-plated tungsten wires laid on them with a 5 mm spacing, and these sheets were stacked up, with alternate sheets rotated by 90°. This stack would be expected to have two diagonal components of the dielectric tensor negative below the plasma frequency. The measured reflectivity and transmission of these samples indicated a plasma frequency of about 9 GHz, which could be reduced to 6 GHz by diluting the density of the wires by half, thus confirming the theoretical prediction of a low frequency plasmonic medium. Other experiments [196] have used a loop-like structure to increase the inductance of thicker wires and obtained a low frequency cutoff medium.

There have been several experimental efforts at obtaining negative magnetic materials after the San Diego experiments [4] brought them into the limelight. There have been studies of the single scatterer response of these SRR media [62]. There have been attempts at producing isotropic SRR media by combining three orthogonal SRRs into a single three-dimensional scatterer [63]. Marqués *et al* [198] have implemented a modified SRR structure where the two planar split rings are capacitively coupled not through their edges but through the broadside by depositing equal sized split rings on either side of an insulating board. This ameliorates the bianisotropy of the SRRs as well. Wiltshire *et al* [23, 24] have experimentally implemented the Swiss roll design for operation at radio-frequencies. The dispersion of $\mu(\omega)$ has been measured and found to match accurately with the theoretical predictions. By using the large effective magnetic permeability of these Swiss rolls at frequencies just below the resonance frequency, these media have been used as effective flux tubes for the radio-frequency magnetic fields and the potential for MRI has been demonstrated. Very recently the magnetic properties of microscale SRRs has been demonstrated at terahertz frequencies [27].

The San Diego experiments [4, 5] combined the planar SRRs and the thin wire arrays to make the world's first NRM (see figure 12). Transmission experiments were first carried out on uniaxial SRR media, which consisted of planar SRRs of copper rings printed on circuit boards, placed in a microwave guide, and showed a low transmission band for radiation with the magnetic field along the SRR axis. This could be attributed to the negative μ at frequencies above the LC resonance of the SRRs. Combining this with 0.8 mm wires placed symmetrically between the SRRs with the electric field along the thin wire resulted in an

enhanced transmission within the negative μ band compared with the transmission of the bare wire media, indicating a pass-band due to a negative refractive index. A prism made with a similar two-dimensional isotropic NRM was shown to exhibit the negative refraction effect [5]. These experiments have, however, been criticized for the low transmittivity of the samples [9]. Several reasons can qualitatively account for the low transmittivity including the dissipation in the circuit boards, the large wire diameter and the corresponding large impedance mismatch. But it certainly does not negate the conclusion of a negative refractive index.

The experiments of Parazzoli *et al* [25,26] have provided decisive experimental evidence of a negative refractive index in composite samples of thin wire arrays and SRRs. These experiments used large sized three-dimensional isotropic samples and were conducted in free space rather than in waveguides. These experiments used thin wires of 0.25 mm thickness and a low absorption substrate (Rogers 5880) and measured both the reflected and transmitted power. The insertion loss was shown to be smaller (about $-1\,\mathrm{dB\,cm^{-1}}$) [26] and the contribution of the conduction losses in the SRRs appears to dominate. The issue of loss in these NRM is complex, and a clear verdict on the exact level of losses is yet to emerge. A prism made of this medium was shown to again refract microwaves negatively [25], where it was also numerically shown that the angle of refraction was insensitive to the degree of absorption in the sample. The transmission pass-band for the composite SRR and thin wire medium has also been obtained experimentally by other groups [197]. Marqués *et al* [90] have shown that placing SRRs within a waveguide operating below the cutoff also creates a pass-band below the cutoff frequency which can be attributed to a negative refractive index.

Loaded L–C backward wave transmission lines have been implemented by Eleftheriades *et al* [131, 132] and Liu *et al* [130]. The transmission line approach has shown that NRM structures with a low loss and wide bandwidth are possible, particularly at microwave frequencies, something that the other resonant structures are not capable of. Eleftheriades *et al* experimentally implemented two-dimensional loaded L–C backward transmission lines and have demonstrated the negative refraction effect [131]. They demonstrated that an image placed in a positive medium near an interface with the NRM would create an image inside the NRM in the sense of the Veselago lens. Liu *et al* [130] have demonstrated the feasibility of a forward microwave coupler between two backward wave structures using a very short coupling length. This becomes possible due to the inverse dependence of the wave-vector on the frequency ($\beta = -1/(\omega\sqrt{LC})$). This idea has also been extended to coupling between ordinary transmission lines and backward wave transmission lines [199].

6.2. Photonic crystals and the Veselago flat lens

There has been extensive activity on the negative refraction effect with photonic crystals. Cubukcu *et al* [200] have shown the negative refraction effect in such media by using the reversed transverse shift a beam undergoes upon oblique transmission through a slab compared with normal media. Using a two-dimensional array of alumina rods, a Gaussian beam of microwaves at about 15 GHz was shown to undergo a reversed transverse shift. Parimi *et al* [201] have demonstrated the flat lens imaging, again with a two-dimensional photonic crystal of cylindrical alumina rods, at about 9 GHz. More recently this effect has been demonstrated at telecommunications infrared frequencies using even a low contrast two-dimensional photonic crystal [202]. These measurements are consistent with the theoretical predictions of Luo *et al* [36]. The imaging with a flat lens has also been extended to sonic

waves, and phononic crystals have also been shown to focus sound in a similar manner [203]. The complete generality of this effect becomes clear in the recent flat lens imaging by liquid surface waves where a two-dimensional lattice of rigid rods was used to act as a crystal for the surface waves.

6.3. Demonstrating super-lenses

By super-lenses, we mean lenses with sub-wavelength resolution enabled by NRMs. Super-lenses and sub-wavelength focusing capabilities have enormous implications for near-field imaging and near-field optical lithography. The interest in it has been enormous. The sub-wavelength resolving capabilities of the super-lenses stem from the way the evanescent near-field components are transmitted across it: these components are amplified in magnitude. There is now definite experimental evidence to confirm the essentials of the theory of super-lenses. But more refined measurements are expected in the near future.

Grbic and Eleftheriades [205] have experimentally noted super-lens behaviour with a planar NRM lens made out of two-dimensional transmission lines. Sub-wavelength image resolutions at about 1 GHz were clearly measured with the capacitively loaded transmission grid kept between the source and detector, compared with the case of diffraction limited patterns. The measured electric fields also clearly showed the amplification of the evanescent waves across the slab. The sub-wavelength image resolution was limited only by the levels of absorption in the NRM. Thus, most of the elementary features of the theory have been clearly verified.

Liu *et al* [204] used a reversed attenuated total reflection (RATR) experiment to directly measure the transmitted fields across thin films of silver. Using the surface roughness to linearly couple a propagating mode into evanescent surface modes on a silver surface, the transmitted evanescent fields of the surface plasmon modes were coupled out using a hemisphere on the other side of the silver film. The measured transmittance increased exponentially with film thickness up to some maximum and then decayed quickly with a further increase in thickness which was caused by the increased dissipation in the film. The behaviour of the transmittance was quantitatively predicted by Pendry's expressions and the material parameters of silver [71] and has offered indirect evidence of the capability for super-lensing of the silver lens. More recently, sub-micron imaging using the silver slab lens has also been demonstrated [206] in the context of optical lithography. The images were obtained using a 120 nm thick slab of silver which, however, precluded the possibility of sub-wavelength image resolution due to losses and retardation. The images with lower resolution were obtained which, however, were demonstrated to be superior to the traditional proximity imaging techniques. At the time of writing, sub-wavelength image resolution at optical frequencies using the silver lens is yet to be demonstrated.

7. Conclusions

In conclusion, we have reviewed the recent developments in the area of negative refractive index materials. Although predicted a long time ago, in 1967, the practical creation of these materials had to wait for recipes to selectively make materials with a negative dielectric permittivity and magnetic permeability. We have examined the problem of making materials with negative material parameters which are mostly structured composites. The design of meta-materials that show a negative refractive index is an extreme form of electromagnetic engineering. The negative material parameters mostly result from an over-screened, under-damped response due to the structural resonances. A negative refractive index is obtained by interleaving two structures that individually show a negative ε or negative μ. It should be noted that the sizes of

the structures in these materials are usually much smaller than the wavelength of radiation that enables them to be treated effectively as homogeneous media. The simplification that results is considerable as the complex internal microscopical fast varying fields become irrelevant and need not concern us anymore. There are still very significant issues of non-local fields, bianisotropy and homogenization that need to be carefully looked at. There is now sufficient experimental evidence for a negative refractive index and the associated effects. The high degree of absorption in these materials, primarily arising due to conduction losses in the metallic structures, is a cause for concern, and one of the main challenges remaining in this area is developing new designs for meta-materials with smaller losses. But on the whole NRMs have to be accepted as today's reality. They are very dispersive and dissipative, but very real nevertheless. Calculations indicate that scaling to high frequencies, up to the near-infrared and perhaps even the optical frequencies, is possible. The fundamental limitation comes from the finite electronic mass as real currents have to flow in these structures.

Several new effects that are possible in NRMs have been discussed. The immensely dispersive nature of these materials can create many new surprises. These materials can support a host of surface modes and have a large potential in the newly developing area of plasmonics. The resonances in the meta-materials can cause intense local field enhancements. This makes it a new fertile ground for nonlinear phenomena. The study of nonlinear meta-materials is only starting now, but surprises will almost certainly abound. We have discussed the backward wave structures using transmission lines that can act as NRMs at microwave frequencies and radio-frequencies and the photonic band-gap materials that can show the negative refraction effect. There are considerable problems of homogenization in the photonic band-gap materials, and they are perhaps better described by the band theory than by homogeneous negative material parameters. But these PBG materials that show the all-angle negative refraction have a tremendous technological potential due to the low degree of absorption in them, and some of the earliest technical innovations and applications will possibly occur using them.

The perfect lens that can be made from a slab of NRM is perhaps the most dramatic of the new effects that are possible. We have discussed in detail this effect where both the propagating and the evanescent near-field modes participate in the image formation. We have considered how the excitation of surface plasmon modes on the surface of the NRMs are crucial to restoration of the amplitudes of the evanescent modes. The dissipative and dispersive nature of the NRM, however, spoils the perfect focus and imposes limits on the maximum extent of sub-wavelength image resolution that we can obtain. We have discussed the generalization of this effect to spatially varying media and the concept of optically complementary media that behave in a sense like *optical antimatter*. This generalization, along with a method of co-ordinate transformations, enables us to generate classes of surfaces with degenerate surface plasmons and perfect lenses in different geometries. Several new configurations of the super-lenses that include the near-field have been presented. The immense potential of the perfect lens effect for near-field imaging, electromagnetic couplers and waveguides in photonic devices cannot be underemphasized. NRM enable us to manipulate the near-field radiation which up to now was untouchable.

The developments in the past few years have only offered us a glimpse of what is possible. NRM are new electromagnetic materials with no conventional analogues in many cases. Many of the intuitions of conventional electromagnetism fail here and one needs to develop new physical intuition here. Further developments will crucially depend on our ability to make better quality NRM, particularly from the point of view of low losses and large bandwidths. NRM can enable new near-field technologies when coupled with innovations in antennae, integrated circuits, waveguide technology and photonic circuits that can outperform their conventional counterparts.

Acknowledgments

I would like to acknowledge with thanks Professor John Pendry for encouragement and enlightening discussions. I would also like to thank him and Imperial College London, and Professor N Kumar and the Raman Research Institute, Bangalore, for hospitality during part of the time when this review was written. Much of my knowledge of negative index materials has come from discussions with Olivier Martin, David Smith, N Kumar, Stephen O'Brien, Mike Wiltshire, Martin McCall and Sebastien Guenneau. I would like to thank Harshawardhan Wanare and Wayne Williams for critically reading the manuscript.

Appendix. Proof of the generalized perfect lens theorem

Here we present the proof of section 5.2, that two media with complementary optical behaviour amount effectively to an optical null space as shown in figure 31. Consider the two slabs with the spatially varying dielectric permittivity tensors and magnetic permeability tensors described by equations (5.13) and (5.14), respectively. Now the electromagnetic fields have to satisfy Maxwell's equations:

$$\nabla \times \boldsymbol{E} = \mathrm{i}\omega\mu_0\tilde{\mu}\boldsymbol{H}, \qquad \nabla \times \boldsymbol{H} = -\mathrm{i}\omega\varepsilon_0\tilde{\varepsilon}\boldsymbol{E}. \tag{A1}$$

Now decomposing the fields into the Fourier components in the two slabs,

$$\boldsymbol{E}_1(x, y, z) = \exp(\mathrm{i}k_{1z}z)\sum_{k_x,k_y}\exp[\mathrm{i}(k_x x + k_y y)]\begin{pmatrix}E_{1x}(k_x, k_y)\\ E_{1y}(k_x, k_y)\\ E_{1z}(k_x, k_y)\end{pmatrix}, \tag{A2}$$

$$\boldsymbol{E}_2(x, y, z) = \exp(\mathrm{i}k_{2z}z)\sum_{k_x,k_y}\exp[\mathrm{i}(k_x x + k_y y)]\begin{pmatrix}E_{2x}(k_x, k_y)\\ E_{2y}(k_x, k_y)\\ E_{2z}(k_x, k_y)\end{pmatrix}, \tag{A3}$$

where the Bloch conditions can be assumed. Substituting these fields into Maxwell's equations and separating the components, we have

$$\begin{aligned}k_y E_{1z}(k_x, k_y) - k_{1z}E_{1y}(k_x, k_y) = -\omega\mu_0\sum_{k'_x,k'_y}[&\mu_{1xx}(k_x, k_y; k'_x, k'_y)H_{1x}(k'_x, k'_y)\\ &+\mu_{1xy}(k_x, k_y; k'_x, k'_y)H_{1y}(k'_x, k'_y) + \mu_{1xz}(k_x, k_y; k'_x, k'_y)H_{1z}(k'_x, k'_y)],\end{aligned} \tag{A4}$$

$$\begin{aligned}k_{1z}E_{1x}(k_x, k_y) - k_x E_{1z}(k_x, k_y) = -\omega\mu_0\sum_{k'_x,k'_y}[&\mu_{1yx}(k_x, k_y; k'_x, k'_y)H_{1x}(k'_x, k'_y)\\ &+\mu_{1yy}(k_x, k_y; k'_x, k'_y)H_{1y}(k'_x, k'_y) + \mu_{1yz}(k_x, k_y; k'_x, k'_y)H_{1z}(k'_x, k'_y)],\end{aligned} \tag{A5}$$

$$\begin{aligned}k_x E_{1y}(k_x, k_y) - k_y E_{1x}(k_x, k_y) = -\omega\mu_0\sum_{k'_x,k'_y}[&\mu_{1zx}(k_x, k_y; k'_x, k'_y)H_{1x}(k'_x, k'_y)\\ &+\mu_{1zy}(k_x, k_y; k'_x, k'_y)H_{1y}(k'_x, k'_y) + \mu_{1zz}(k_x, k_y; k'_x, k'_y)H_{1z}(k'_x, k'_y)]\end{aligned} \tag{A6}$$

and

$$\begin{aligned}k_y H_{1z}(k_x, k_y) - k_{1z}H_{1y}(k_x, k_y) = \omega\varepsilon_0\sum_{k'_x,k'_y}[&\varepsilon_{1xx}(k_x, k_y; k'_x, k'_y)E_{1x}(k'_x, k'_y)\\ &+\varepsilon_{1xy}(k_x, k_y; k'_x, k'_y)E_{1y}(k'_x, k'_y) + \varepsilon_{1xz}(k_x, k_y; k'_x, k'_y)E_{1z}(k'_x, k'_y)],\end{aligned} \tag{A7}$$

$$k_{1z}H_{1x}(k_x,k_y)-k_xH_{1z}(k_x,k_y)=\omega\varepsilon_0\sum_{k'_x,k'_y}[\varepsilon_{1yx}(k_x,k_y;k'_x,k'_y)E_{1x}(k'_x,k'_y)$$
$$+\varepsilon_{1yy}(k_x,k_y;k'_x,k'_y)E_{1y}(k'_x,k'_y)+\varepsilon_{1yz}(k_x,k_y;k'_x,k'_y)E_{1z}(k'_x,k'_y)], \tag{A8}$$

$$k_xH_{1y}(k_x,k_y)-k_yH_{1x}(k_x,k_y)=\omega\varepsilon_0\sum_{k'_x,k'_y}[\varepsilon_{1zx}(k_x,k_y;k'_x,k'_y)E_{1x}(k'_x,k'_y)$$
$$+\varepsilon_{1zy}(k_x,k_y;k'_x,k'_y)E_{1y}(k'_x,k'_y)+\varepsilon_{1zz}(k_x,k_y;k'_x,k'_y)E_{1z}(k'_x,k'_y)]. \tag{A9}$$

Now consider the substitution

$$E_{2x}(k_x,k_y)=E_{1x}(k_x,k_y),\qquad E_{2y}(k_x,k_y)=E_{1y}(k_x,k_y),\qquad E_{2z}(k_x,k_y)=-E_{1z}(k_x,k_y), \tag{A10}$$

$$H_{2x}(k_x,k_y)=H_{1x}(k_x,k_y),\qquad H_{2y}(k_x,k_y)=H_{1y}(k_x,k_y),\qquad H_{2z}(k_x,k_y)=-H_{1z}(k_x,k_y) \tag{A11}$$

and

$$k_{2z}=-k_{1z}, \tag{A12}$$

$$\tilde{\varepsilon}_2(k_x,k_y;k'_x,k'_y)=\begin{pmatrix}-\varepsilon_{1xx}(k_x,k_y;k'_x,k'_y) & -\varepsilon_{1xy}(k_x,k_y;k'_x,k'_y) & +\varepsilon_{1xz}(k_x,k_y;k'_x,k'_y)\\ -\varepsilon_{1yx}(k_x,k_y;k'_x,k'_y) & -\varepsilon_{1yy}(k_x,k_y;k'_x,k'_y) & +\varepsilon_{1yz}(k_x,k_y;k'_x,k'_y)\\ +\varepsilon_{1zx}(k_x,k_y;k'_x,k'_y) & +\varepsilon_{1zy}(k_x,k_y;k'_x,k'_y) & -\varepsilon_{1zz}(k_x,k_y;k'_x,k'_y)\end{pmatrix}, \tag{A13}$$

$$\tilde{\mu}_2(k_x,k_y;k'_x,k'_y)=\begin{pmatrix}-\mu_{1xx}(k_x,k_y;k'_x,k'_y) & -\mu_{1xy}(k_x,k_y;k'_x,k'_y) & +\mu_{1xz}(k_x,k_y;k'_x,k'_y)\\ -\mu_{1yx}(k_x,k_y;k'_x,k'_y) & -\mu_{1yy}(k_x,k_y;k'_x,k'_y) & +\mu_{1yz}(k_x,k_y;k'_x,k'_y)\\ +\mu_{1zx}(k_x,k_y;k'_x,k'_y) & +\mu_{1zy}(k_x,k_y;k'_x,k'_y) & -\mu_{1zz}(k_x,k_y;k'_x,k'_y)\end{pmatrix} \tag{A14}$$

which solves Maxwell's equations in region 2 inside the slab and also matches the fields across the boundaries of the slabs. Hence we have the field

$$E(x,y,z=2d)=E(x,y)\exp(-\mathrm{i}k_zd)=E(z,y,z=0). \tag{A15}$$

Thus the fields are exactly repeated in region 2 but in exactly the opposite order. This completes the proof of the theorem.

References

[1] Veselago V G 1967 *Usp. Fiz. Nauk* **92** 517
Veselago V G 1968 *Sov. Phys.—Usp.* **10** 509
[2] Pendry J B, Holden A J, Stewart W J and Youngs I 1996 *Phys. Rev. Lett.* **76** 4773
[3] Pendry J B, Holden A J, Robbins D J and Stewart W J 1999 *IEEE Trans. Microwave Theory Tech.* **47** 2075
[4] Smith D R, Padilla W J, Vier D C, Nemat-Nasser S C and Schultz S 2000 *Phys. Rev. Lett.* **84** 4184
[5] Shelby R A, Smith D R and Schultz S 2001 *Science* **292** 77
[6] Pendry J B 2000 *Phys. Rev. Lett.* **85** 3966
[7] Valanju P M, Walser R M and Valanju A P 2002 *Phys. Rev. Lett.* **88** 187401
[8] Garcia N and Nieto-Vesperinas M 2002 *Phys. Rev. Lett.* **88** 207403
[9] Garcia N and Nieto-Vesperinas M 2002 *Opt. Lett.* **27** 885
[10] McCall M, Weiglhoffer W S and Lakhtakia A 2002 *Eur. J. Phys.* **23** 353
[11] Markos P and Soukoulis C M *Preprint* cond-mat/0212136
[12] Shen J Q 2004 *Preprint* cond-mat/0402213
[13] Pendry J B 2004 *Contemp. Phys.* **45** 191

[14] Pendry J B and Smith D R 2004 *Phys. Today* **57** 37
[15] Shen J T and Platzmann P M 2002 *Appl. Phys. Lett.* **80** 3286
[16] Yablonovitch E 1987 *Phys. Rev. Lett.* **58** 2059
Yablonovitch E 1993 *J. Phys.: Condens. Matter* **5** 2443
[17] Pendry J B 1996 *J. Phys.: Condens. Matter* **8** 1085
[18] Jackson J D 1999 *Classical Electrodynamics* (Singapore: Wiley)
[19] Landau L D, Lifschitz E M and Pitaevskii L P 1984 *Electrodynamics of Continuous Media* 2nd edn (Oxford: Pergamon)
[20] Kotthaus J P and Jaccarino V 1972 *Phys. Rev. Lett.* **28** 1649
Grunberg P and Metawe F 1977 *Phys. Rev. Lett.* **39** 1561
Sandercock J R and Wettling W 1979 *J. Appl. Phys.* **50** 7784
Camley R E and Mills D L 1982 *Phys. Rev.* B **26** 1280
Remer L, Luthi B, Sauer H, Geick R and Camley R E 1986 *Phys. Rev. Lett.* **56** 2752
Dumelow T, Camley R E, Abraha K and Tilley D R 1998 *Phys. Rev.* B **58** 897
[21] Pendry J B and O'Brien S 2002 *J. Phys.: Condens. Matter* **14** 7409
[22] O'Brien S, MacPeake D, Ramakrishna S A and Pendry J B 2004 *Phys. Rev.* B **69** 241101
[23] Wiltshire M C K, Pendry J B, Young I R, Larkman D J, Gilderdale D J and Hajnal J V 2001 *Science* **291** 848
[24] Wiltshire M C K, Hajnal J V, Pendry J B and Edwards D J 2003 *Opt. Express* **11** 709
[25] Parazzoli C G, Greegor R B, Li K, Kontenbah B E C and Tanielian M H 2003 *Phys. Rev. Lett.* **90** 107401
[26] Li K, McLean S J, Greegor R B, Parazzoli C G and Tanielian M H 2003 *Appl. Phys. Lett.* **82** 2535
[27] Yen T J, Padilla W J, Fang N, Vier D C, Smith D R, Pendry J B, Basov D N and Zhang X 2004 *Science* **303** 1494
[28] O'Brien S and Pendry J B 2002 *J. Phys.: Condens. Matter* **14** 6383
[29] Lindell I V, Tretyakov S A, Nikoskinen K I and Ilvonen S 2001 *Microwave Opt. Tech. Lett.* **31** 129
[30] Ziolkowski R W and Heyman E 2001 *Phys. Rev.* E **64** 056625
[31] Ritchie R H 1957 *Phys. Rev.* **106** 874
[32] Raether H 1980 *Excitation of Plasmons and Interband Transitions by Electrons* (Berlin: Springer)
[33] Pendry J B 2001 *Proc. NATO Advanced Study Inst. (Crete, NATO ASI Series)* ed C M Soukoulis (Dordrecht: Kluwer)
[34] Barnes W L, Dereux A and Ebbesen T W 2003 *Nature* **424** 824
[35] Born M and Wolf E 1989 *Principles of Optics* (Oxford: Pergamon)
[36] Luo C, Johnson S G, Joannopoulos J D and Pendry J B 2002 *Phys. Rev.* B **65** 201104
[37] Pines D and Bohm D 1952 *Phys. Rev* **85** 338
Bohm D and Pines D 1953 *Phys. Rev.* **92** 609
[38] Ebbesen T W, Lezec H J, Ghaemi H F, Thio T and Wolff P A 1998 *Nature* **391** 667
Martin-Moreno L *et al* 2004 *Phys. Rev. Lett.* **86** 1114
Martin-Moreno L, Garcia-Vidal F J, Lezec H J, Degiron A and Ebbesen T W 2003 *Phys. Rev. Lett.* **90** 167401
[39] Harris S E, Field J E and Imamoglu A 1990 *Phys. Rev. Lett.* **64** 1107
Scully M O 1992 *Phys. Rep.* **219** 191
Harris S E 1997 *Phys. Today* **50** 36
[40] Scully M O and Zubairy M S 1997 *Quantum Optics* (Cambridge: Cambridge University Press)
[41] Sarychev A K and Shalaev V M 2000 *Phys. Rep.* **335** 275
[42] Lagarkov A N and Sarychev A K 1996 *Phys. Rev.* B **53** 6318
Matitsine S M, Hock K M, Liu L, Gan Y B, Lagarkov A N and Rozanov K N 2003 *J. Appl. Phys.* **94** 1146
[43] Pendry J B, Holden A J, Robbins D J and Steward W J 1998 *J. Phys.: Condens. Matter* **10** 4785
[44] Sievenpiper D F, Sickmiller M E and Yablonovitch E 1996 *Phys. Rev. Lett.* **76** 2480
[45] Maslovsky S I, Tretyakov S A and Belov P A 2002 *Microwave Opt. Tech. Lett.* **35** 47
[46] Belov P A, Marqueś R, Maslovski S I, Nefedov I S, Silveirinha M, Simovski C R and Tretyakov S A 2003 *Phys. Rev.* B **67** 13103
[47] Mikhailov S A 1997 *Phys. Rev. Lett.* **78** 4135
[48] Pendry J B 1997 *Phys. Rev. Lett.* **78** 4136
[49] Walser R M, Valanju A P and Valanju P M 2001 *Phys. Rev. Lett.* **87** 119701
[50] Pendry J B 2002 private communication
[51] van Coeverden D V, Sprik R, Tip A and Lagendijk A 1996 *Phys. Rev. Lett.* **77** 2412
[52] Koschny T, Markos P, Smith D R and Soukoulis C M 2003 *Phys. Rev.* E **68** 065602
[53] Makhnovsky D P and Panina L V 2003 *J. Appl. Phys.* **93** 4120
[54] Simovsky C R and He S 2003 *Phys. Lett.* A **311** 254
[55] Rotman W 1962 *IRE Trans. Antennas Propagat.* **AP10** 82
[56] King R J, Thiel D V and Park K S 1983 *IEEE Trans. Antennas Propag.* **AP-31** 471

[57] Brown J 1960 *Prog. Dielectr.* **2** 195
[58] Pitarke J M, Garcia-Vidal F J and Pendry J B 1998 *Phys. Rev.* B **57** 15261
[59] Takeda H and Yoshino K 2003 *Phys. Rev.* B **67** 245109
[60] Anderson P W 1963 *Phys. Rev.* **130** 439
[61] Kittel C, Fahy S and Louie S G 1988 *Phys. Rev.* B **37** 642
[62] Gay-Balmaz P and Martin O J F 2002 *J. Appl. Phys.* **92** 2929
[63] Gay-Balmaz P and Martin O J F 2002 *Appl. Phys. Lett.* **81** 939
[64] Hsu A c, Cheng Y K, Chen K H, Chern J L, Wu S C, Chen C F, Chang H, Lien Y H and Shy J T 2004 *Japan. J. Appl. Phys.* **43** L176
[65] Markos P and Soukoulis C M 2002 *Phys. Rev.* B **65** 033401
[66] Huang Y C, Hsu Y-J, Lih J S and Chern J L 2004 *Japan. J. Appl. Phys.* **43** L190
[67] Sievenpiper D, Zhang L, Braos R F J, Alexópolous N G and Yablonovitch E 1999 *IEEE Trans. Microwave Theory Tech.* **47** 2059
[68] Broas R F J, Sievenpiper D and Yablonovitch E 2001 *IEEE Trans. Microwave Theory Tech.* **49** 1262
[69] Enoch S, Tayeb G and Maystre D 1999 *Opt. Commun.* **161** 171
Gralak B, Enoch S and Tayeb G 2000 *J. Opt. Soc. Am.* **17** 1012
[70] Pendry J B and MacKinnon A 1992 *Phys. Rev. Lett.* **69** 2772
Pendry J B 1994 *J. Mod. Opt.* **41** 209
[71] Johnson P B and Christy R W 1972 *Phys. Rev.* B **6** 4370
[72] Smith D R, Schultz S, Markos P and Soukoulis C M 2002 *Phys. Rev.* B **65** 195104
[73] Kumar N 2003 *Proc. Asia Academic Seminar (Hyderabad)* ed P R Rao *et al* (International Advanced Research Centre for Powder Metallurgy & New Materials and Japan Society for Promotion of Science) p 33
[74] Dimmock J O 2003 *Opt. Express* **11** 2397
[75] Panoiu N C and Osgood R M 2003 *Opt. Commun.* A **223** 331
[76] Panina L V, Grigorenko A N and Makhnovskiy D P 2002 *Phys. Rev.* B **66** 155411
[77] Hrabar S, Eres Z and Bartolic J 2002 *Proc. Eur. Micowave Conf. (Milan)* pp 327–30
[78] Shamonina E, Kalinin V A, Ringhofer K H and Solymar L 2002 *J. Appl. Phys.* **92** 6252
[79] Shamonin M, Shamonina E, Kalinin V and Solymar L 2004 *J. Appl. Phys.* **95** 3778
[80] Kong J A 1990 *Electromagnetic Wave Theory* (New York: Wiley-Interscience)
[81] Saadoun M M I and Engheta N 1992 *Microwave Opt. Tech. Lett.* **5** 184
[82] Marques R, Medina F and Rafii-El-Idrissi R 2002 *Phys. Rev.* B **65** 144440
[83] O'Brien S and Pendry J B 2002 *J. Phys.: Condens. Matter* **14** 4035
[84] Shelby R A, Smith D R, Nemat-Nasser S C and Schultz S 2001 *Appl. Phys. Lett.* **78** 489
[85] Markos P and Soukoulis C M 2002 *Phys. Rev.* E **65** 036622
[86] Pokrovsky A L and Efros A L 2002 *Phys. Rev. Lett.* **89** 093901
[87] Marqués R and Smith D R 2004 *Phys. Rev. Lett.* **92** 059401
[88] Simovski C R, Belov P A and He S 2004 *IEEE Trans. Antennas Propag.* **51** 2582
[89] Simovski C R and Sauviac B 2004 *Preprint* cond-mat/0403047
[90] Marqués R, Martel J, Medina F and Mesa F 2002 *Phys. Rev. Lett.* **89** 183901
[91] Bergman D J and Stroud D 1992 *Solid State Phys.* **46** 147
[92] Stroud D 1975 *Phys. Rev.* **12** 3368
[93] Hunderi O 1973 *Phys. Rev.* B **7** 3419
[94] Milton G W 2002 *The Theory of Composites* (Cambridge: Cambridge University Press)
[95] Kramers H A 1929 *Phys. Z.* **30** 522
de Kronig R 1942 *Natuurk* **9** 402
[96] Kircheva P P and Hadjichristov G B 1994 *J. Phys. B: At. Mol. Opt. Phys.* **27** 3781
[97] Tokunaga E, Terasaki A and Kobayashi T 1993 *Phys. Rev.* A **47** R4581
[98] Peiponnen K E, Vartiainen E M and Saarinen J J 2004 *Phys. Rev.* A **69** 043818
[99] Ginzburg V L and Meiman N N 1964 *Sov. Phys.—JETP* **19** 169
[100] Diener G 1997 *Phys. Lett.* A **235** 118
[101] Glasgow S, Ware M and Peatross J 2001 *Phys. Rev.* E **64** 046610
[102] Smith D R and Kroll N 2000 *Phys. Rev. Lett.* **85** 2933
[103] Pokrovsky A L and Efros A L 2002 *Solid State Commun.* **124** 283
[104] Ramakrishna S A and Martin O J F 2004 *Preprint* cond-mat/0402570
[105] Depine R A and Lakhtakia A 2004 *Microwave Opt. Tech. Lett.* **41** 315
[106] Wang J and Lakhtakia A 2002 *Microwave Opt. Tech. Lett.* **33** 465
[107] Loudon R 2002 *J. Mod. Opt.* **49** 821
[108] Lakhtakia A and McCall M W 2004 *Preprint* cond-mat/0402001

[109] Zhang Y, Fleugel B and Mascarenhas A 2003 *Phys. Rev. Lett.* **91** 157404
[110] Pendry J B 2000 *Phys. World* **13** 27
[111] Lu J, Grzegorczyk T M, Zhang Y, Pacheco J, Wu B, Kong J A and Chen M 2003 *Opt. Express* **11** 723
[112] Luo C, Ibanescu M, Johnson S G and Joannopoulos J D 2003 *Science* **299** 368
[113] Goos F and Hänchen H 1947 *Ann. Phys. Lpz.* **1** 333
[114] Kong J A, Wu B I and Zhang Y 2002 *Appl. Phys. Lett.* **80** 2084
[115] Berman P R 2002 *Phys. Rev.* E **66** 067603
[116] Lakhtakia A 2002 *Electromagnetics* **23** 71
Lakhtakia A 2002 *Preprint* cond-mat/0305133
[117] Ziolkowski R W 2003 *Opt. Express* **11** 662
[118] Artmann K 1948 *Ann. Phys. Lpz.* **2** 87
[119] Shadrivov I V, Sokhorukov A A and Kivshar Y S 2003 *Appl. Phys. Lett.* **82** 3820
[120] Shadrivov I V, Zharov A A and Kivshar Y S 2003 *Appl. Phys. Lett.* **83** 2713
[121] Landauer R and Martin Th 1994 *Rev. Mod. Phys.* **66** 217
[122] Pendry J B and Smith D R 2003 *Phys. Rev. Lett.* **90** 029703
[123] Smith D R, Schurig D and Pendry J B 2002 *Appl. Phys. Lett.* **81** 2713
[124] Lu W T, Sokoloff J B and Sridhar S 2002 *Preprint* cond-mat/0207689
[125] Lu W T, Sokoloff J B and Sridhar S 2004 *Phys. Rev.* E **69** 026604
[126] Caloz C, Chang C C and Itoh T 2001 *J. Appl. Phys.* **90** 5483
[127] Pacheco J, Grzegorczyk T M, Wu B I, Zhang Y and Kong J A 2002 *Phys. Rev. Lett.* **89** 257401
[128] Foteinopoulou S, Economou E N and Soukoulis C M 2003 *Phys. Rev. Lett.* **90** 107402
[129] Dutta Gupta S, Arun R and Agarwal G S 2004 *Phys. Rev.* B **69** 113104
[130] Liu L, Caloz C, Chang C-C and Itoh T 2002 *J. Appl. Phys.* **92** 5560
[131] Eleftheriades G V, Iyer A K and Kremer P C 2002 *IEEE Trans. Microwave Theory Tech.* **50** 2702
[132] Grbic A and Eleftheriades G V 2002 *J. Appl. Phys.* **92** 5930
[133] Notomi M 2000 *Phys. Rev.* B **62** 10696
[134] Luo C, Johnson S G and Joannopoulos J D 2002 *Appl. Phys. Lett.* **81** 2352
[135] Chien H-T, Tang H-T, Kuo C-H, Chen C-C and Ye Z 2003 *Preprint* cond-mat/0312582
[136] Kuo C-H and Ye Z 2003 *Preprint* cond-mat/0310423
Kuo C-H and Ye Z 2003 *Preprint* cond-mat/0312288
[137] Shen Y R 1984 *The Principles of Non-Linear Optics* (New York: Wiley)
[138] Zharov A A, Shadrivov I V and Kivshar Y S 2003 *Phys. Rev. Lett.* **91** 037401
[139] Agranovich V M, Shen Y R, Baughman R H and Zakhidov A A 2004 *Phys. Rev.* B **69** 165112
[140] Ruppin R 2000 *Phys. Lett.* A **277** 61
[141] Ruppin R 2001 *J. Phys.: Condens. Matter* **13** 1811
[142] Ramakrishna S A, Pendry J B, Smith D R, Schurig D and Schultz S 2002 *J. Mod. Opt.* **49** 1747
[143] Darmanyan S A, Neviére M and Zakhidov A A 2003 *Opt. Commun.* **225** 233
[144] Ruppin R 2000 *Solid State Commun.* **116** 411
[145] Klimov V V 2002 *Opt. Commun.* **211** 183
[146] Cory H and Barger A 2003 *Microwave Opt. Tech. Lett.* **38** 392
[147] Alu A and Engheta N 2002 *Microwave Opt. Tech. Lett.* **35** 460
[148] Kuzmiak V and Maradudin A A 2002 *Phys. Rev.* B **66** 045116
[149] Pendry J B and Ramakrishna S A 2003 *J. Phys.: Condens. Matter* **15** 6345
[150] Greffet J J and Carminati R 1997 *Prog. Surf. Sci.* **56** 133
[151] Pohl D and Courjon D 1993 *Near-Field Optics* (Dordrecht: Kluwer)
[152] Williams J M 2001 *Phys. Rev. Lett.* **87** 249703
[153] Pendry J B 2001 *Phys. Rev. Lett.* **87** 249704
[154] 't Hooft G W 2001 *Phys. Rev. Lett.* **87** 249701
[155] Pendry J B *Phys. Rev. Lett.* **87** 249702
[156] Ramakrishna S A and Armour A D 2003 *Am. J. Phys.* **71** 562
[157] Luo C, Johnson S G, Joannopoulos J D and Pendry J B 2003 *Phys. Rev.* B **68** 045115
[158] Gomez-Santos G 2003 *Phys. Rev. Lett.* **90** 077401
[159] Haldane F D M *Preprint* cond-mat/0206420
[160] Pendry J B 2003 *Phys. Rev. Lett.* **91** 099701
[161] Feise M W, Bevelacqua P J and Schneider J B 2002 *Phys. Rev.* B **66** 035113
[162] Ashcroft N W and Merimin N D 1976 *Solid State Physics* (Philadelphia: Saunders College)
[163] Smith D R, Schurig D, Rosenbluth M, Schultz S, Ramakrishna S A and Pendry J B 2003 *Appl. Phys. Lett.* **82** 1506

[164] Shamonina E, Kalinin V A, Ringhofer K H and Solymar L 2001 *Electron. Lett.* **37** 1243
[165] Fang N and Zhang X 2003 *Appl. Phys. Lett.* **82** 161
[166] Ye Z 2003 *Phys. Rev.* B **67** 193106
[167] Merlin R 2004 *Appl. Phys. Lett.* **84** 1290
[168] Chen L, He S and Shen L 2004 *Phys. Rev. Lett.* **92** 107404
[169] Paul J, Christopoulos C and Thomas D W P 2001 *Electron. Lett.* **37** 912
[170] Kolinko P and Smith D R 2003 *Opt. Express* **11** 640
[171] Loschialpo P F, Smith D L, Forester D W, Rachford F J and Schelleng J 2003 *Phys. Rev.* E **67** 025602
[172] Kärkäinnen M K and Maslovski S A 2002 *Microwave Opt. Tech. Lett.* **37** 4
[173] Cummer S A 2002 *Appl. Phys. Lett.* **82** 1503
[174] Rao X S and Ong C K 2003 *Phys. Rev.* B **68** 113103
[175] Rao X S and Ong C K 2003 *Phys. Rev.* E **68** 067601
[176] Cummer S A 2003 *Appl. Phys. Lett.* **82** 2008
[177] Pendry J B and Ramakrishna S A 2002 *J. Phys.: Condens. Matter* **14** 8463
[178] Pendry J B 2003 *Opt. Express* **11** 755
[179] Ramakrishna S A and Pendry J B 2004 *Phys. Rev.* B **69** 115115
[180] Ramakrishna S A and Pendry J B 2003 *Phys. Rev.* B **67** 201101
[181] Tretyakov S A 2001 *Microwave Opt. Tech. Lett.* **31** 169
[182] Ramakrishna S A, Pendry J B, Wiltshire M C K and Stewart W J 2003 *J. Mod. Opt.* **50** 1419
[183] Mansfield S M and Kino G S 1990 *Appl. Phys. Lett.* **57** 2615
[184] Smith D R and Schurig D 2003 *Phys. Rev. Lett.* **90** 077405
[185] Smith D R, Schurig D, Mock J J, Kolinko P and Rye P 2004 *Appl. Phys. Lett.* **84** 2244
[186] Zhang Z M and Fu C J 2002 *Appl. Phys. Lett.* **80** 1097
[187] Li J, Zhou L, Chan C T and Sheng P 2003 *Phys. Rev. Lett.* **90** 083901
[188] Jian H, Chen H, Li H, Zhang Y and Zhu S 2003 *Appl. Phys. Lett.* **83** 5386
[189] Bria D, Djafari-Rouhani B, Akjouj A, Dobrzynski L, Vigneron J P, El Boudouti E H and Nougaoui A 2004 *Phys. Rev.* E **69** 066613
[190] Nefedov I S and Tretyakov S A 2002 *Phys. Rev.* E **66** 036611
[191] Feise M W, Shadrivov I S and Kivshar Y S 2004 *Preprint* cond-mat/0402087
[192] Ruppin R 2003 *Microwave Opt. Technol. Lett.* **38** 494
[193] Shadrivov I S, Sukhorukov A A and Kivshar Y S 2003 *Appl. Phys. Lett.* **82** 3820
[194] Ward A J and Pendry J B 1996 *J. Mod. Opt.* **43** 773
[195] Notomi M 2002 *Opt. Quant. Electron* **34** 133
[196] Smith D R, Vier D C, Padilla W, Nemat-Nasser S C and Schultz S 1999 *Appl. Phys. Lett.* **75** 1425
[197] Ozbay E, Aydin K, Cubukcu E and Bayindir M 2003 *IEEE Trans. Antennas Propag.* **51** 2592
[198] Marqués R, Mesa F, Martel J and Medina F 2003 *IEEE Trans. Antennas Propag.* **51** 2572
[199] Caloz C and Itoh T 2004 *IEEE Microwave Wirel. Components Lett.* **14** 31
[200] Cubukcu E, Aydin K, Ozbay E, Foteinopoulou S and Soukoulis C M 2003 *Nature* **423** 604
[201] Parimi P V, Lu W T, Vodo P and Sridhar S 2003 *Nature* **426** 404
[202] Berrier A, Mulot M, Swillo M, Qiu M, Thylen L, Talneau A and Anand S 2004 *Phys. Rev. Lett.* **93** 073902
[203] Yang S, Page J H, Liu Z, Cowan M L, Chan C T and Sheng P 2004 *Phys. Rev. Lett.* **93** 024301
[204] Liu Z, Fang N, Yen T-J and Zhang X 2003 *Appl. Phys. Lett.* **83** 5184
[205] Grbic A and Eleftheriades G V 2004 *Phys. Rev. Lett.* **92** 117403
[206] Melville D O S, Blaikie R J and Wolf C R 2004 *Appl. Phys. Lett.* **84** 4403